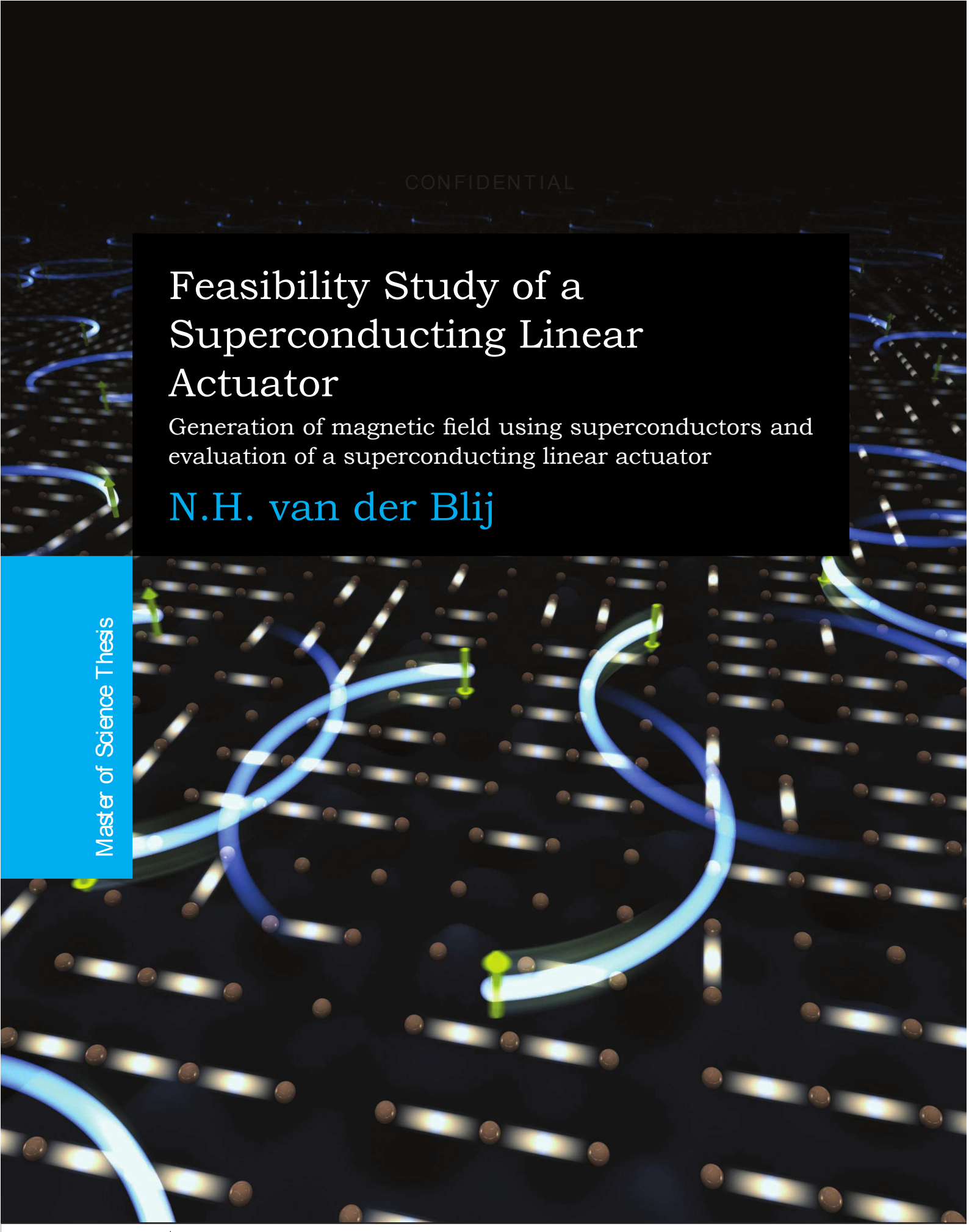

Feasibility Study of a Superconducting Linear Actuator

Generation of magnetic field using superconductors and evaluation of a superconducting linear actuator

N.H. van der Blij

Master of Science Thesis

TU Delft Delft University of Technology

PHILIPS
sense and simplicity

Technical University Delft

Feasibility Study of a Superconducting Linear Actuator

Generation of magnetic field using superconductors and evaluation of a superconducting linear actuator

In collaboration with Philips Innovation Services

Author:
N.H. van der Blij

Supervisor:
Dr. Ir. H. Polinder

May 15, 2013

Preface

This thesis is written in assignment of the Electrical Power Processing department of the TU Delft. It is a final assessment for the completion of the master Electrical Engineering (track Electrical Power Engineering).

The research was done in a period of 8 months at the department of Mechatronics Technologies at Philips Innovation Services. The design of high precision system's linear actuators is one of the competences of this department.

The main focus of the study is to assess the feasibility of using superconductors in a linear actuator. Throughout the period of 8 months various aspects of superconductivity were investigated.

First, the theoretical background of superconductivity was researched. Second, the achievable magnetic fields using commercially available superconducting bulk and superconducting wire were determined. Third, the performance of a superconducting actuator and a reference permanent magnet actuator were evaluated. Last the electromechanical, thermal and commercial feasibility were determined.

My eternal gratitude to the following persons who have had considerable contributions to the research and this master thesis:

- Dr. Ir. Henk Polinder
- Dr. Ir. Funda Sahin
- Dr. Ir. Gert-Jan P. Nijsse
- Dr. Ir. Marcel J. M. Renkens

Abstract

High precision systems have an ever increasing demand on the throughput. To accommodate the higher throughput demand the acceleration of the actuators must be increased. The acceleration can either be increased by increasing the magnetic field at the armature or the armature current density.

In this thesis the feasibility of using superconductors to generate a magnetic field in an actuator is studied. The first objective of the thesis is to determine the achievable magnetic fields with commercially available superconductors. Second a superconducting actuator and its cryostat are designed. Finally the superconducting actuator is evaluated on its electromechanical, thermal and commercial feasibility.

As approach to the first goal a method is developed to determine the maximum achievable fields using the critical characteristics. For high (77 and 65 K) and low (20 and 4 K) temperatures coil designs are made and the maximum achievable fields are determined. Additionally bulk superconductors are also considered as magnets.

Several design options for the cryostat and actuator topologies are provided throughout this thesis. The stator magnets, the armature and the cryostat of a superconducting linear actuator are designed.

Provided a comparable high performance permanent magnet actuator the superconducting linear actuator is evaluated electromechanically. The thermal load of the cryostat and the costs of both actuators are also assessed.

For superconducting coils at 20 K, the magnetic field at the armature is increased with a factor of 9. Furthermore the acceleration of the actuator is increased by a factor of 8.

A cryostat is designed which only envelops the superconducting magnets. The heat load is calculated and compared to the available cooling power evaluating the thermal feasibility.

The cost of both the superconducting and the permanent magnet actuator is determined. The price per performance ($ per N/kg) of superconducting coils is about a factor of 10 higher than the cost per performance of permanent magnets.

It is found that superconductors can be feasible in linear actuators. However it is only feasible for certain applications where high performance is the primary concern and the cost is less important.

Contents

Glossary

Anisotropic	Characteristics are directionally dependent
BCS theory	Theory on the electron-phonon interaction by Bardeen, Schrieffer and Cooper
Coherence length	Length over which superconductive properties cannot change
Cooper pair	A pair of electrons bound by a weak attractive force
Critical Temperature	Temperature after which a material loses its superconductive properties
Cryogen	A liquid that boils at a temperature below 110 K
Cryostat	A stable environment at cryogenic temperatures
FEM	Finite Element Modeling
Fluxon	Quantized amount of flux
GdBCO	Material consisting of Gadolinium, Barium, Copper and Oxygen
High Temperature Superconductor	Superconductor not sufficiently described by the BCS theory
Liquefaction	Proces of condensation of a gas
Low Temperature Superconductor	Superconductor sufficiently described by the BCS theory
Nb3Sn	Material consisting of Niobium and Tin
NbTi	Material consisting of Niobium and Titanium
Perfect Conductor	Material without resistivity
Quench	The loss of superconductive properties
SmBCO	Material consisting of Samarium, Barium, Copper and Oxygen
TFM	Trapped field magnet
YBCO	Material consisting of Yttrium, Barium, Copper and Oxygen

List of Figures

List of Tables

Chapter 1

Introduction

Contents

This chapter focuses on the background of the thesis. First the motivation of researching superconductivity is explained in section 1.1. Second the scope and the goals of the thesis are explained in section 1.2. Last the layout of the thesis is discussed in section 1.3.

1.1 Motivation

Linear actuators are used for many applications in present time. A linear actuator, in contrast to a rotational actuator, creates a motion in a straight line.

Currently Philips Innovation Services' Mechatronics Technologies department designs high precision linear synchronous machines for assembly equipment, wafer scanners, inspection equipment and many other applications.

These high precision system stages mostly use multiple stages to keep the accuracy high while the acceleration requirements increase. Long- and short-stroke linear actuators are utilized to achieve high precision. These actuators can either be planar or linear motors. An example of a high precision stage is shown in Figure 1.1.

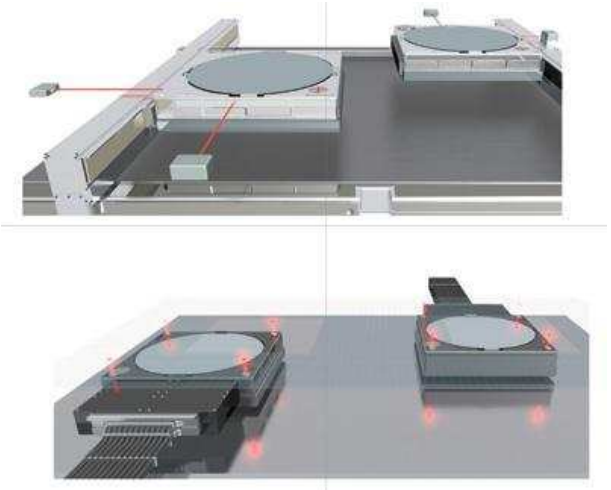

Figure 1.1: Planar actuator implemented in an ASML lithography machine

The stator in a linear synchronous machine consists of either a one-sided or two-sided plate with permanent magnets. This configuration can also make use of a back iron or a Halbach magnet array to further enhance the magnetic field.

The mover in this application consists of a three-phase armature. The armature windings are generally concentrated copper (or aluminum) windings.

The acceleration requirements of the linear actuators continually rise with a higher throughput demand of high precision systems. By Newtons second law the acceleration is proportional to the force density (N/kg) or equivalently, for a fixed armature design, the force.

The force generated in these linear actuators can, in general, be simplified to be dependent on both the field generated by the stator and the current flowing in the armature. Consequently the force can be approximated by Equation 1.1.

$$F \approx K_m B_a I_a \tag{1.1}$$

Where K_m is a machine constant, B_a is the magnetic field at the armature and I_a is the current flowing in the armature.

From Equation 1.1 it becomes clear the performance of the linear actuator can be increased either by increasing the current in the armature or the field generated by the magnets.

The maximum current that can flow through the copper armature windings is heavily dependent on the cooling of these windings. In the armature heat is generated by resistive losses (Joule heating). This heat needs to be transported elsewhere to prevent the armature from overheating and eventually melting. Generally water is used to cool the copper windings. Using an extensive water cooling system a maximum current density of 50 A/mm^2 can be achieved in copper armatures.

Employing permanent magnets in the stator severely limits the maximum magnetic field achievable at the armature. The maximum field achievable at the surface of a permanent magnet usually lies around 1.5 T. Mainly due to the air gap the maximum field achievable at the armature is realistically around 0.7 T.

With current technology the limitations are reached for the current density in copper and the magnetic field generated by permanent magnets. Possible successors of these technologies are superconductors. The main merits of superconductors are that they have virtually no resistance and can carry high current densities.

In the armature superconductors may provide means to increase the maximum achievable armature current. The superconductors can also be used to generate a magnetic field. Therefore the feasibility of the employment of superconductors in a linear actuator is investigated.

1.2 Thesis scope and goals

The previous section explained the motivation to study the feasibility of using superconductors in linear actuators.

To fully understand superconductors and thoroughly design an actuator using superconductivity extensive knowledge of physics, thermal engineering and mechanical engineering is required. The time and resources to acquire this knowledge is very limited however. Therefore it is important to define a clear scope and clear goals of the thesis.

The scope of the thesis is limited on three aspects of designing a superconducting linear actuator.

First, **AC operation of superconductors is not considered**. AC operation of superconductors differs greatly of the DC operation. When a superconductor carries a DC current no loss mechanisms are present in the superconductor. However when a superconductor carries an AC current a loss mechanism exists (similar to the hysteresis losses in iron). The analysis of this loss mechanism can be very extensive and is therefore be disregarded.

Superconductors can either be used in the armature or be used to generate magnetic fields. The scope of the thesis is however limited to the DC operation of superconductors. Therefore the use of superconductors in the armature is not considered.

Second, **extensive mechanical and thermal calculations are omitted**. A complete design of an actuator using any form of superconductors requires extensive thermal and mechanical engineering. The scope of the thesis however does not envelop the thermal and mechanical part of the design process.

An electromechanical design is made. Additionally the thermal feasibility of the actuator is investigated. However the extensive calculations necessary to evaluate mechanical strengths and local temperatures in the actuator are not done.

Third, **several specifications for the linear actuator are given**. The stroke length of the actuator is chosen to be 40 cm.

Additionally the most important specification of the actuator is the force density (N/kg). The often used steepness parameter (N^2/W) is less important in this case, as power efficiency is less crucial. The force density is determined by dividing the force of the armature by the mass of the armature copper. The mass of an actual mover is about 5 to 6 times higher. However the total mass of the mover is irrelevant as the superconducting actuator is evaluated by comparing it to a high performance permanent magnet actuator with a similar mover.

Moreover the weight and volume of the stator are considered unimportant as these do not influence the force density.

The maximum current density in the armature coils is assumed to be 50 A/mm^2. This current density is reasonable for an extensively water cooled copper armature.

The goals of the thesis can be split up in three separate parts:

- Determine the achievable magnetic fields with commercially available superconductors.
- Make a basic design of a superconducting linear actuator including the magnets, armature and cryostat.
- Evaluate the electromechanical, thermal and commercial feasibility of the designed superconducting linear actuator.

1.3 Layout of the thesis

The previous section discussed the scope and the goals of the thesis. In this section the several chapters and their contents are enumerated.

Chapter 2 - The thesis first discusses the history of superconductivity and the history of the extraction of helium. The discovery of superconductivity and the history of the various theories regarding superconductivity are discussed.

Chapter 3 - In Chapter 3 the theory necessary to understand the several aspects of superconductivity is reviewed. The theoretical physics background is discussed. Furthermore the characteristics, their implications and the classification of superconductors are explained.

Chapter 4 - Chapter 4 discusses the maximum achievable fields at high temperature (77 and 65 K). Coil and trapped field (bulk) magnets are considered. The achievable magnetic field inside and outside these magnets are determined.

Chapter 5 - Again the maximum achievable fields are determined in Chapter 5 but now at low temperatures (4 and 20 K). In this chapter the maximum achievable field inside and outside coil magnets are calculated.

Chapter 6 - In Chapter 6 the several thermal aspects of the cryostat are discussed. The equations to calculate the heat load for a cryostat are reviewed. Additionally several cryostat systems are considered.

Chapter 7 - Chapter 7 discusses several possible linear actuator topologies. Conventional and unconventional machines are discussed.

Chapter 8 - A basic design is made for a superconducting linear actuator in Chapter 8. Several design choices are made with respect to topology, magnet, cryostat and operating conditions. Additionally a superconducting coil magnet and an armature is designed.

Chapter 9 - Chapter 9 analyzes the designed superconducting linear actuator in accordance to electromechanical performance, thermal feasibility and cost. Moreover a high performance permanent magnet machine is introduced as reference.

Chapter 10 - In Chapter 10 the results of the thesis are recapped and recommendations are given for future research.

Appendix A - The first Appendix of the thesis contains the Opera2D FEM models used for the several computations in the thesis. Additionally the field distribution are shown for some models.

Appendix B - Appendix B contains a paper written using the thesis as a basis. This paper can be freely published when the confidentiality embargo has been lifted.

Chapter 2

History of superconductivity

Contents

Before going into technical details in Chapter 3 and onwards it is important to outline the history of superconductivity theories.

Section 2.1 first discusses the discovery and production of liquid helium in the early days of cryogenics. After this the discovery and history of superconductivity are reviewed in sections 2.2 and 2.3 respectively.

2.1 Liquefaction of helium

The liquefaction of helium starts at Heike Kamerlingh Onnes in Leiden. When Onnes was appointed as professor at the University of Leiden in 1882 he urged the board of governors to renovate the physics laboratorium to be able to keep up with other universities (and fit to his personal research agenda). During the following years many important discoveries in cryogenics were made such as the production of liquid oxygen (1892) and the discovery of helium (1895).

Working to prove the theory of his compatriot J.D. van der Waals by measuring 'permanent' gasses over a wide range of temperatures Onnes used his new (cryogenics) laboratorium, which consisted of mostly home brew equipment, to successfully liquefy helium in 1908. He did so using a Joule-Thompson expansion of the helium after it was precooled by liquid hydrogen.

At this time the procurement of helium itself was quite complicated and time-consuming. Helium could only be obtained by isolating it from monazite sand. For the extraction of one cubic meter of helium gas one ton of monazite sand was necessary. This complication was worsened by the fact that this sand was only readily available in America. In 1909 an alternative had presented itself to Onnes when the Welsbach firm offered him a trade. The company produced thorianite mantles for gas lamps for which they processed large quantities of thorianite also producing helium as a waste product (thorianite contains a small amount of helium). In return for flasks of helium Onnes would send the monazite sand waste (still containing thorium) which would otherwise be discarded. [1, 2, 3, 4]

At present time helium is mainly extracted from natural gas using fractional distillation which enables semi-large scale use. The helium extraction takes place in three stages namely the removal of large impurities, extraction of high-molecular-weight hydrocarbons and finally cryogenic processing after which crude helium (50-70%) is obtained. It is also possible to extract helium from the atmosphere although this is often not economically viable. [5]

2.2 Discovery of superconductivity

Due to the progress made by Onnes temperatures as low as 1 K were available for various research areas. Heike Kamerlingh Onnes himself was studying the resistance of metals at temperatures nearing 0 K. On this topic different theories emerged. Kelvin believed that the electrons would freeze in place and no conduction could take place (leading to infinite resistivity). Matthiessen thought that the resistance would eventually decline to a certain value depending on the impurity of the sample. Dewar on the other hand believed the decline of resistivity would continue eventually leading up to zero resistivity. [1, 2] The three theories are illustrated in Figure 2.1.

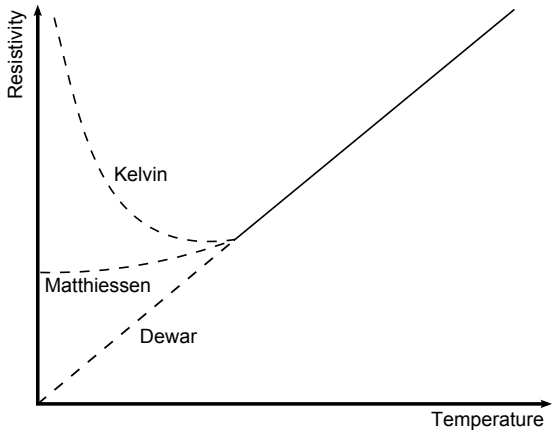

Figure 2.1: Theories on resistance at temperatures near 0 K

Onnes set out to measure samples of gold and silver. The results of these measurements were in favor of Matthiessens theory, the resistance remained constant after a certain temperature. As Onnes was keen on studying even purer metals and his research team had considerable experience purifying mercury their next experiment involved distilled mercury. [2]

During the purified mercury experiment Onnes wrote in his notebook 'kwik nagenoeg nul' [6] meaning mercury nearly zero. Further experiments resulted in the graph shown in Figure 2.2.

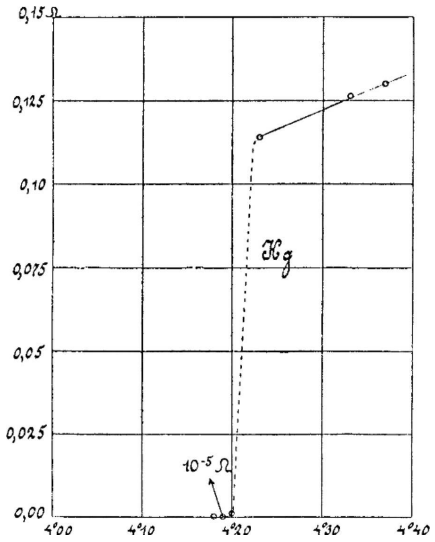

Figure 2.2: Resistance of mercury nearing 0 K [7]

The results of the experiments had proved the existence of superconductivity, a state where the resistance is zero. More interestingly the transition from the resistive to the superconductive state is not gradual but abrupt as the material is cooled down below a certain 'critical' temperature as seen in Figure 2.2. Onnes proved shortly after that impure mercury exhibits the same characteristics implying none of his colleagues' theories were correct.

Soon the desire to use superconductivity to obtain strong magnetic fields emerged. Onnes quickly encountered that a relatively low magnetic field would 'quench' (extinguish) the superconductive properties of the sample. [2]

It was not until 1933 that significant progress was made in the field of superconductivity. Meissner and Ochsenfeld reported superconducting materials having an additional characteristic besides the zero resistivity. Superconducting material exhibits, what would later be called 'the Meissner effect', an expulsion of magnetic field. The Meissner effect is shown in Figure 2.3.

According to Meissner applying sufficient magnetic field forces the magnetic field to re-enter the sample cancelling superconductive properties, much like the results of Onnes. Furthermore, decreasing the field subsequently results in a reinstatement of the superconductive properties implying a thermodynamic equilibrium. [8]

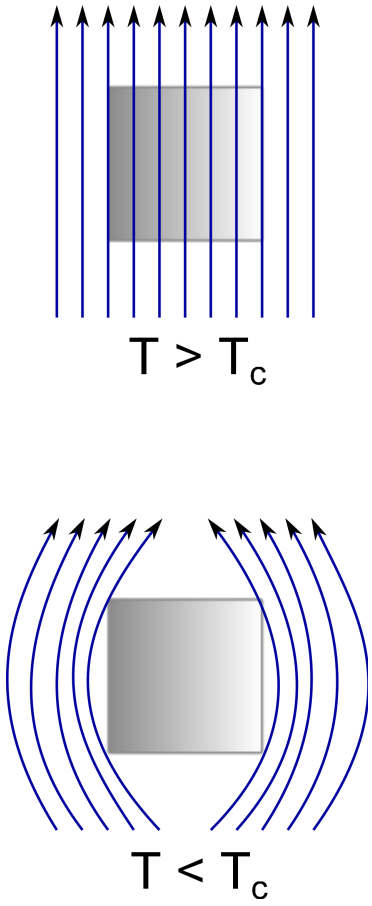

Figure 2.3: The expulsion of magnetic field below the critical temperature

2.3 Superconductivity theories history

In 1934 F. London described, with his brother H. London, the electrodynamics of superconductivity in an attempt understand the Meissner effect. Later, in 1938, F. London was the first to propose that superconductivity had correlations with a Bose-Einstein condensation. In 1950 he described the phenomenon in his pair of books explaining the relation between magnetic field and the current in superconductors (Unlike Ohm's law relating the current to the electric field).

According to F. London current flowing in a superconductor flows in an outer shell that effectively screens any magnetic field. Due to this effect the current density and magnetic field decay over a short depth inside the superconductor as shown in Figure 2.4. This would later be known as the 'London penetration depth λ'. [9]

In the same year F. London published his books Ginzburg and Landau published their theory which largely explained macroscopic properties of superconductors and would lead to Abrikosov predicting the existence of two types of superconductors (now known as type I and type II).

Not long after, Bardeen and Schrieffer argued their microscopic theories on the Meissner effect and paired electrons respectively. In collaboration with Schrieffer they combined and published their theories in 1957 which would later be known as 'the BCS theory'.

According to the BCS theory, when the temperature is sufficiently low, electrons form Cooper pairs (by lattice phonon interaction) and condense into a Bose-Einstein condensate (The topic of Cooper pairs is elaborated in Chapter 3). [10]

The formation of Cooper pairs was not deemed possible at temperatures above 30 K until Bednorz and Müller published their discovery of (high temperature) superconductivity at 35 K in 1986. The discovery questioned the validity of the BCS theory (for these 'high temperature superconductors') as lattice phonon interactions are believed to be overcome by thermal lattice vibrations at temperatures above 30 K. [11]

The search for an alternative mechanism causing the formation of Cooper pairs began. Ever since many theories have arisen yet none have been proved...

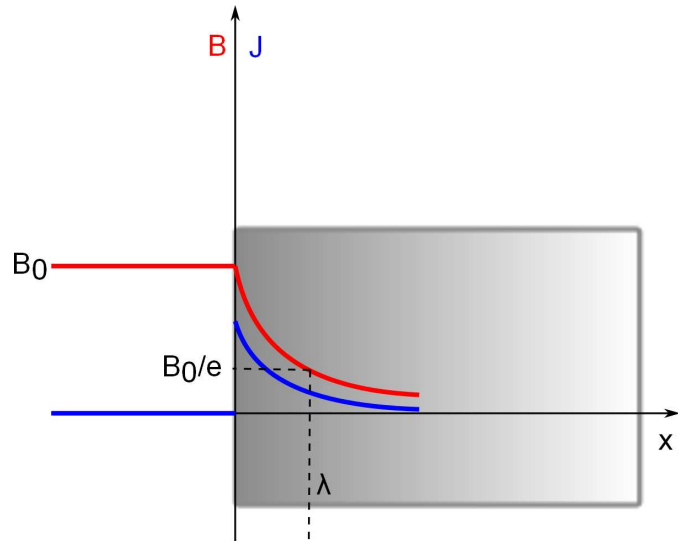

Figure 2.4: Magnetic field inside a superconductor

Chapter 3

Superconductivity theory

Contents

Chapter 2 presented several concepts and theories of superconductivity and their respective discoveries. This chapter discusses the theory necessary to comprehend the limitations and the design of the superconducting linear machine in the following chapters.

First the origin of superconductivity is discussed in detail in section 3.1. Second basic characteristics of superconductors are reviewed in section 3.2. Subsequently the different classifications and the critical characteristics of superconductors are considered in sections 3.3 and 3.4 respectively. Last different superconductive materials are discussed in section 3.5.

3.1 Superconductivity physics

This section discusses the theoretical physics behind superconductivity. If this background poses no interest to the reader this section can be skipped. The basic characteristics are reviewed in section 3.2.

The origin of the characteristics of superconductivity can only be explained by describing superconductivity both microscopically and macroscopically. The BCS theory is used to describe the superconductivity phenomenon on microscopic scale while the macroscopic behavior is described by starting with the London equations.

3.1.1 Microscopic physics

The equations of Bardeen, Schrieffer and Cooper are beyond the scope and necessity of this study and thus their theory are only conceptually evaluated.

Essential for the properties of superconductivity is the formation of so called *Cooper pairs*. These Cooper pairs are formed when two electrons are mutually attracted by a weak force at low temperatures. [13]

In conventional (LTS) superconductors the attractive force between the electrons is caused by electron-phonon interaction. This interaction can be explained by an electron moving through a lattice as shown in Figure 3.1. The electron attracts the local positively charged ions deforming the lattice creating a local concentration of positive charge. The local concentration of positive charge attracts another electron and if this attraction is not overcome by thermal lattice vibration (at temperatures below the so called *critical temperature*) or Coulomb repulsion a Cooper pair is formed. [13, 14]

In unconventional (HTS) superconductors the attraction is said to be caused by magnetic interaction or one of the many other possible mechanisms but none have been proved. [15]

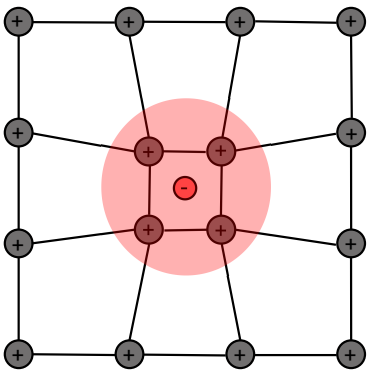

Figure 3.1: Electron interaction with a lattice

The average maximum distance between the electrons of a Cooper pair is called the *coherence length* and is denoted by ξ. The coherence length can also be seen as the length long enough so the Coulomb repulsion has sufficiently been screened but still small enough for phonon interaction to facilitate the formation of a Cooper pair. [14]

Care must be given to not address the Cooper pairs as two mutually exclusive paired electrons. Electrons go in and out of the bound states and pair with other electrons.

Electrons in a Cooper pair have a spin of $^1/_2$ or $^{-1}/_2$. Consequently a Cooper pair has a spin of 0,1 or -1 (depending on the pairing mechanism). As Cooper pairs have integer spin they are Bose particles (quasi-bosons) which do not obey the Pauli exclusion principle. Consequently these Cooper pairs condense into a Bose-Einstein condensate possessing a wave function with identical phase for all pairs (phase coherence). [15]

The coherence of the pairs results in a resilience to split even a single Cooper pair of the condensate. This leads to a finite amount of energy required to break up one pair of the condensate. The required energy at 0 K is given by:

$$2\Delta(0) = 3.5 k_B T_c \tag{3.1}$$

Where k_B is the Boltzmann constant and T_c is the critical temperature. [10, 14, 15]

Resistance in normal metals is caused by scattering of the electrons which happens at any infinitesimal small amount of energy. But as the electrons in a superconductor are bound in a Cooper pair they cannot be scattered unless the energy is higher than the energy gap $2\Delta(0)$ removing them from the condensate and breaking the pair. It was already discussed that at sufficient low temperatures the thermal scattering energy due to lattice vibration is insufficient to break a Cooper pair. As there are no other scattering mechanisms able to break a Cooper pair this leads to the zero resistivity of a superconductor. [14]

3.1.2 Macroscopic physics [9, 15]

The origin of the Bose-Einstein condensate and consequently the phase coherence and zero resistivity of superconductors have been illustrated. The macroscopic consequences are now proved using general formulae and the London equations. This subsection uses Gaussian units for the derivations.

Assuming current flows with no dissipation the equation for the current density is given by:

$$j_s = n_s e v_s \tag{3.2}$$

Where n_s is the density of superconductive electrons, v_s their velocity and e is their charge.

As this current is non-dissipative it contributes to the kinetic energy of superconducting electrons. The total free energy is a sum of the kinetic energy of superconducting electrons and the magnetic energy:

$$F = \int \left(\frac{n_s m v_s^2}{2} + \frac{H^2}{8\pi} \right) \mathrm{d}V = \int \left(\frac{m j_s^2}{2 n_s e^2} + \frac{H^2}{8\pi} \right) \mathrm{d}V \tag{3.3}$$

Using the Maxwell Equation 3.4 and a small enough volume we arrive at Equation 3.5.

$$j_s = \frac{c}{4\pi} \nabla \times H \tag{3.4}$$

$$F = \frac{1}{8\pi} \int \mathrm{d}V \big(H^2 + \lambda_L^2 (\nabla \times H)^2 \big) \tag{3.5}$$

Where λ_L is the London penetration depth given by:

$$\lambda_L = \left(\frac{m c^2}{4\pi n_s e^2} \right)^{\frac{1}{2}} \tag{3.6}$$

It can be shown that variation with respect to the magnetic field (using vector identities) gives:

$$\delta F = \frac{1}{4\pi} \int \mathrm{d}V \big(H + \lambda_L^2 \nabla \times \nabla \times H \big) \delta H \tag{3.7}$$

From this it can be seen that for the minimization of the free energy F the following equation has to be solved:

$$H + \lambda_L^2 \nabla \times \nabla \times H = H - \lambda_L^2 \nabla^2 H = 0 \tag{3.8}$$

$$H = \lambda_L^2 \nabla^2 H \tag{3.9}$$

With Equation 3.9 derived using the London theory one can prove the Meissner effect in a superconductor. Suppose the situation in Figure 2.4 where a superconductors border is at $x = 0$ and suppose a magnetic field perpendicular to this border. Using Equation 3.9 we start at:

$$H_x = \lambda_L^2 \frac{\mathrm{d}^2}{\mathrm{d}x^2} H_x \tag{3.10}$$

Which has the following solution:

$$H_x = H_x(0) e^{-\frac{x}{\lambda_L}} \tag{3.11}$$

This means that after the penetration depth the field has decreased significantly and the magnetic field in the bulk of the material is zero, the Meissner effect.

The quantum-mechanical expression for the momentum per unit volume is given by:

$$j_m = \hbar |\phi|^2 \nabla \chi \tag{3.12}$$

Where ϕ is the wave function of all the superconducting electrons , χ their phase and $\hbar$ is the Dirac constant. This equation implies that $\hbar \nabla \chi$ is the canonical momentum P of a condensate particle. For charged particles the momentum is given by:

$$p = P - \left(\frac{2e}{c}\right) A = \hbar \nabla \chi - \left(\frac{2e}{c}\right) A \tag{3.13}$$

Where a charge of 2e is used as a Cooper pair contains two electrons and A is the vector potential of the magnetic field. Using this equation the velocity and current density of a superconducting electron become:

$$v_s = \frac{\hbar}{2m} \left(\nabla \chi - \frac{2e}{\hbar c} A \right) \tag{3.14}$$

$$j_s = n_s e v_s = -\frac{e^2 n_s}{mc} \left(A - \frac{\hbar c}{2e} \nabla \chi \right) \tag{3.15}$$

Now consider a closed contour fully inside a superconductor around a non-superconductive region (E.G. inside the ring and around the center of the ring in Figure 3.4) we evaluate the contour integral:

$$-\frac{mc}{e^2 n_s} \oint j_s \, \mathrm{d}l = \oint \left(A - \frac{\hbar c}{2e} \nabla \chi \right) \mathrm{d}l = \int \nabla \times A \, \mathrm{d}S - \frac{\hbar c}{2e} \Delta \chi = \Phi - \frac{\hbar c}{2e} 2\pi n \tag{3.16}$$

Where Φ is the flux through the contour and $\Delta \chi = 2\pi n$ because all the Cooper pairs have the same phase due to phase coherence. Also because there is no current inside the bulk of the superconductor the left-hand side of the equation is 0 resulting equation:

$$\Phi = \frac{\hbar c}{2e} 2\pi n = \frac{hc}{2e} n \tag{3.17}$$

This equation proves the fact that the flux through a superconducting closed contour must be an integer multiple of ϕ_0 (the quantization of flux) where:

$$\phi_0 = \frac{hc}{2e} \tag{3.18}$$

3.2 Superconductivity characteristics

A common misconception is that superconductivity is merely the absence of resistance in a compound. While it is one of the hallmarks of superconductivity superconductors exhibit additional characteristics besides zero resistivity. This section recaps the characteristics of superconductivity derived in the previous section.

3.2.1 Zero resistivity

Cooling down a pure metal to 0 K will result in a resistivity equal to zero. If the metal contains any impurities some residual resistance will be present at 0 K. [12] When a superconductor is cooled down below a certain temperature, the critical temperature, its resistivity abruptly drops to zero. These three different trajectories are shown in Figure 3.2

A conductor which has zero resistivity is called a *perfect conductor* this means both pure metals and superconductors are perfect conductors. This means all perfect conductors are not necessarily superconductors, even though it is true all superconductors are perfect conductors. Superconductors also exhibit the Meissner effect.

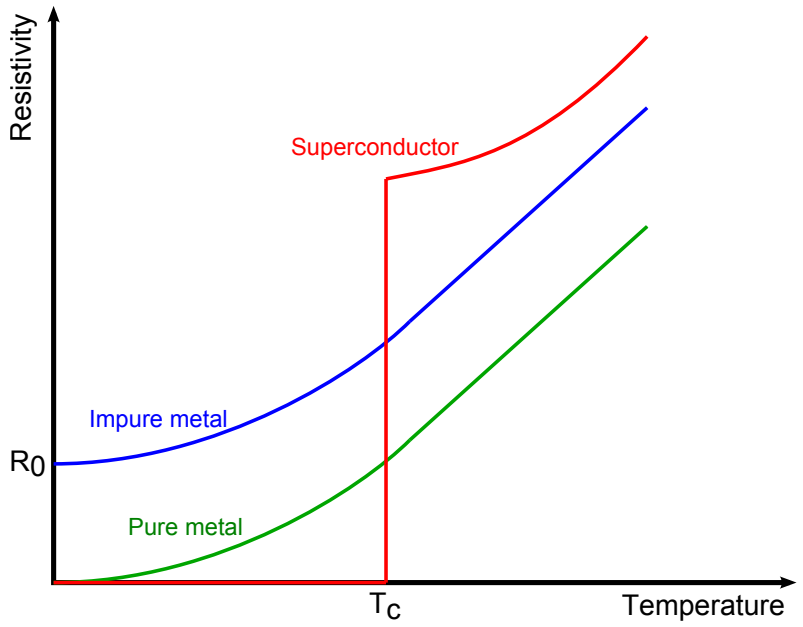

Figure 3.2: Resistance of different materials nearing 0 K

3.2.2 The Meissner effect

As previously discussed in Chapter 2 the Meissner effect is the expulsion of magnetic field in superconductors (Shown in Figure 2.3).

The difference between pure metal (perfect conductors) and superconductors is best explained using both materials in two situations. In the first situation the material is cooled down under zero magnetic field, when perfect conduction is achieved a magnetic field is applied to the material. In the second situation the material is cooled down to perfect conduction under a magnetic field. The result of such an experiment for a pure metal and a (type I) superconductor is shown in Figure 3.3.

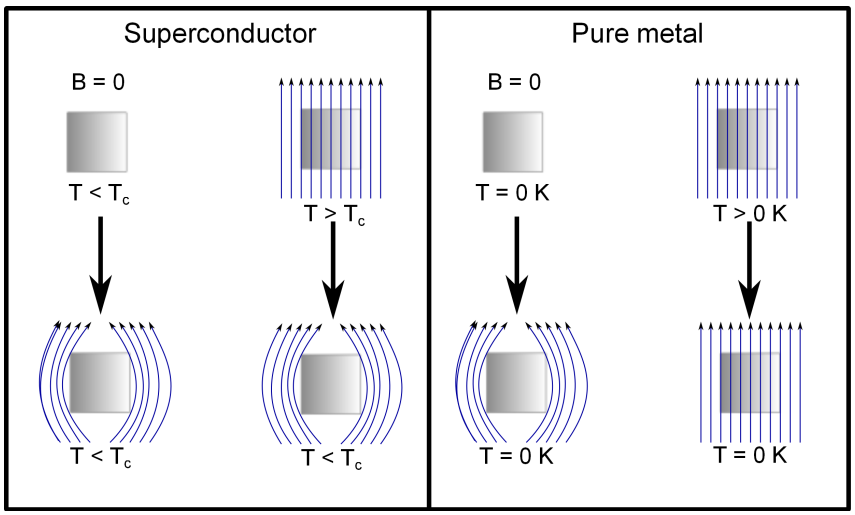

Figure 3.3: Field cooling and zero field cooling of (type I) superconductors and pure metals

As can be seen from Figure 3.3 a (type I) superconductor always expels the magnetic field and a pure metal conserves the magnetic field in which it was cooled. Furthermore if one would remove the magnetic field after the second situation the magnetic field around and inside the superconductor would be zero while the magnetic field inside the pure metal would be preserved.

3.2.3 Flux Quantization

The lesser known but not less important trait of superconductors is flux quantization. Flux quantization is best illustrated using a superconducting ring as shown in Figure 3.4.

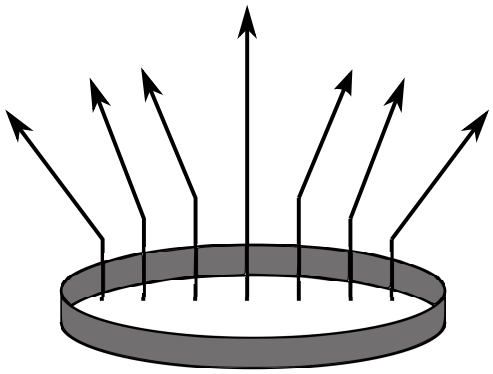

Figure 3.4: Superconducting ring in a magnetic field

The flux contained by the ring is quantized meaning it can only be integer multiples of a constant. This integer constant of flux is called a *fluxon* and is denoted by ϕ_0. The flux through the ring is then given by the following equations:

$$\Phi = \iint B\, n \,\mathrm{d}A = n\phi_0 \tag{3.19}$$

$$\phi_0 = \frac{hc}{2e} \tag{3.20}$$

Where A is the surface inside the ring, B is the magnetic field, h is Planck's constant, c is the speed of light and e is the elemental charge.

3.2.4 Preservation of flux

Zero resistivity causes currents flowing in superconductors to persist indefinitely. As a consequence of the persistent current the flux through a loop of superconductive material will remain constant. To prove this take the ring in Figure 3.4 and use Faraday's law of induction:

$$\oint E \,\mathrm{d}l = -\frac{\mathrm{d}}{\mathrm{d}t} \iint B\, n \,\mathrm{d}A \tag{3.21}$$

Assuming a homogeneous field B through the ring the equation for the induced voltage is:

$$u = Ri + L\frac{\mathrm{d}i}{\mathrm{d}t} = -\frac{\mathrm{d}}{\mathrm{d}t} B\, A \tag{3.22}$$

If we now assume zero resistivity for the superconductor we arrive at the following equation:

$$L\frac{\mathrm{d}i}{\mathrm{d}t} = -\frac{\mathrm{d}}{\mathrm{d}t} B\, A \tag{3.23}$$

Integrating both sides and rearranging the terms the following equations emerge:

$$L(i + i(0)) = -A(B + B(0)) \tag{3.24}$$

$$L\, i + A\, B = -A\, B(0) - L\, i(0) = Constant \tag{3.25}$$

This implies that the sum of the flux generated by the current of the ring ($L\, i$) and the flux generated by the external field ($B\, A$) is constant. The flux of the ring is kept constant by compensation. If the external field is changed an additional current is superimposed in the superconductor that opposes the change in order to preserve the initial flux.

3.3 Classification of superconductors

Having derived the characteristics of superconductors it is important to discuss the different methods of classification of superconductors. This section provides explanation of the classification to field behavior and the classification to temperature behavior.

3.3.1 Classification according to field behavior [12, 15]

In the previous sections the coherence length ξ and the London penetration depth λ_L have been introduced. These two parameters are material dependent and as a result their ratio differs. For the classification of superconductors it is important to introduce this ratio, also called the Ginzberg-Landau parameter, κ, and is given by:

$$\kappa = \frac{\lambda_L}{\xi} \tag{3.26}$$

Using κ, superconductors can be classified in either type I or type II superconductors.

For type I superconductors the following is true:

$$\kappa < \frac{1}{\sqrt{2}} \tag{3.27}$$

As the coherence length is the average maximum distance of the Cooper pairs it can also be seen as the minimum distance over which the superconductive properties can change. This is of

course due to the fact that either both or neither of the electrons in a single pair are part of the condensate.

The magnetic field on the other hand is considered to be insignificant after a length of $\sqrt{2}\lambda_L$ (after which it has less than a quarter of its initial value).

As such in a type I superconductor any magnetic field is unable to change the superconductive state of the material locally as the magnetic field deteriorates to less than a quarter of its initial value over the coherence length.

For type II superconductors the following is true:

$$\kappa > \frac{1}{\sqrt{2}} \tag{3.28}$$

In this case as the magnetic field is able to penetrate far enough into the material to be able to locally change the superconductive state of the superconductor. This means that if the magnetic field rises above a certain value resistive regions start to form in the superconductor.

This results in Type I and type II superconductors behaving considerably different to magnetic fields. Type I superconductors completely expel external magnetic fields (exhibiting the Meissner effect) up to a critical field B_c. At fields higher than the critical field the material loses its superconductive properties.

Type II superconductors exhibit the Meissner effect up to a much lower critical field B_{c1}. At higher fields than B_{c1} regions of normal conductivity start to form inside the superconductor, these regions of normal conductivity allow penetration of the magnetic field. This is illustrated in Figure 3.5. Only when the field is above B_{c2}, which is normally much higher than B_c of a type I superconductor, does the type II superconductor lose its superconductive properties.

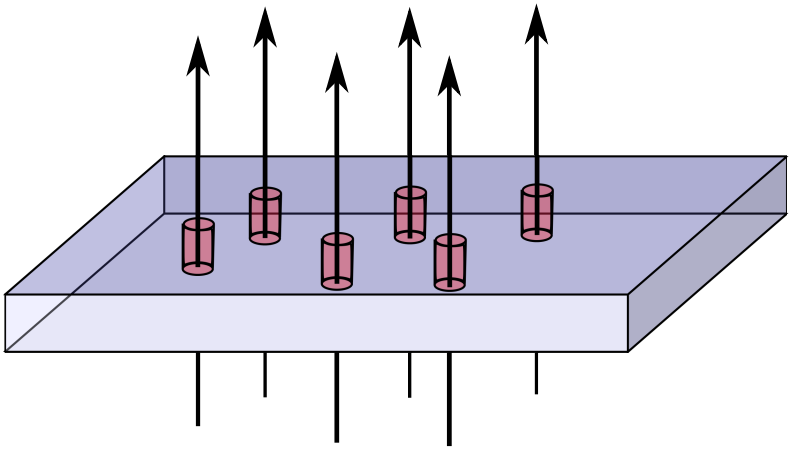

Figure 3.5: Flux penetrating resistive regions of a type II superconductor

3.3.2 Classification according to temperature behavior

Superconductors are not only classified by their reaction to magnetic field but also classified by their reaction to temperature. Superconductors are either called *low temperature superconductors* (LTS) or *high temperature superconductors* (HTS).

Low temperature superconductors are considered to be sufficiently described by the BCS theory and Cooper pairs are considered to be formed by means of lattice-phonon interaction.

In high temperature superconductors the formation of Cooper pairs is not considered to be sufficiently described by lattice-phonon interaction and a different mechanism is required. This is due to the fact that lattice-phonon interaction is believed to be overcome by thermal lattice vibration at temperatures higher than 30 K. [11]

As a side note, most HTS materials are type II while this is not necessarily true vice versa.

3.4 Critical parameters

When the temperature of a superconductor is increased above the critical temperature the superconductive properties disappear. As discussed in the previous section the superconductivity properties can also disappear under influence of a magnetic field. This disappearance of superconductive properties is in both cases due to the available energy in the superconductor becoming higher than the energy gap keeping the condensate and Cooper pairs together. This gives rise to the notion of critical parameters. These indicate when the superconductive properties are preserved and when the superconductor loses its superconductive properties. [12]

One can also deduce that the available energy can be an addition of both the magnetic field and thermal energy. Furthermore the magnetic field can be subdivided in self-generated field and external field. Resulting is a 3D 'critical surface' which indicates under what conditions of current, external field and temperature a material is superconducting. An example of such a three dimensional plot is given in Figure 3.6.

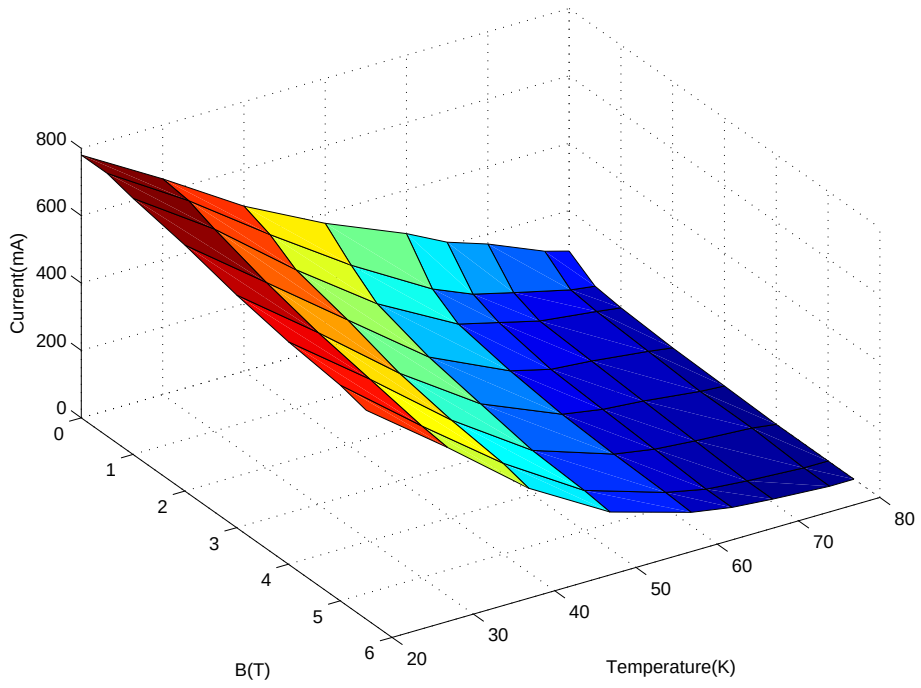

Figure 3.6: 3D plot of a critical surface

3.5 Superconducting materials

Since the discovery of superconductivity many superconductive materials have been found with varying properties. Very few have practical characteristics and have matured enough to be viable in practical applications.

Re-BCO, MgB_2, NbTi and Nb_3Sn are the most matured superconductive materials that are commercially available and are for this reason the only materials considered.

3.5.1 Re-BCO

Re-BCO superconductors are the most commonly used HTS materials and are type II superconductors. A Re-BCO superconductor is a ceramic comprised of a rare-earth material (E.G. yttrium), barium, copper and oxygen. The critical temperatures of most Re-BCO superconductors are achievable with liquid nitrogen which makes it clear why these materials are so popular.

For superconductive wires *YBCO* is the most common. YBCO has a critical temperature of around 90 K (depending on the exact composition and treatment of the material).

YBCO wire is often called 2^{nd} generation HTS wire. The 1^{st} generation wire was a wire of BSCCO material but is now often disregarded as YBCO is believed to have superior mechanical and magnetic properties.

Besides the higher critical temperature, the main advantage of using YBCO wire over LTS wires is that the upper critical field and critical current density of YBCO is generally higher.

The most important disadvantage of YBCO wire is that the production is more extensive than the production of LTS wires, making it relatively expensive. Two other disadvantages are that YBCO wire is very brittle and exhibits *anisotropic* behavior.

Commercially available YBCO wires are often tapes. YBCO tapes are anisotropic meaning that the critical current density is not only dependent on the magnitude of the magnetic field but also on the direction. This can partly be explained using Figure 3.7. The superconducting material expels all magnetic field causing the field lines to bend around the material. The result is field enhancement at the corners of the superconducting material. The field enhancement for fields perpendicular to the tape is much larger than for parallel fields explaining the higher sensitivity to perpendicular fields.

For the design of a solenoid this means the tapes are oriented parallel to the length of the solenoid and the perpendicular fields must be checked after a design is made.

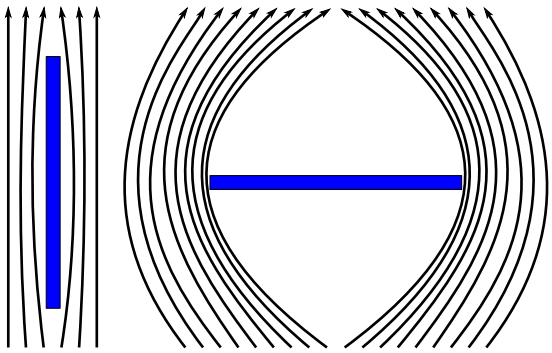

Figure 3.7: Expulsion of magnetic field at different orientations of superconducting tape

3.5.2 MgB_2

A relatively immature but promising material is MgB_2 (magnesium diboride). MgB_2 is a type II superconductor and has a critical temperature of 39 K.

MgB_2 is generally considered to be a low temperature superconductor. The Cooper pairs are believed to be formed by electron-phonon interaction but two separate band gaps are formed in the material making it debatably an LTS or HTS.

The main advantage of MgB_2 is the relatively high critical temperature combined with a relatively simple production method. MgB_2 is also less anisotropic than YBCO.

The main disadvantage is that MgB_2 is relatively immature leading to relatively low critical fields and current densities.

3.5.3 NbTi and Nb_3Sn

Niobium titanium (NbTi) is the most mature available superconducting material. NbTi is a type II superconductor and has a critical temperature of 9 K.

NbTi is most common in practical applications like superconductive magnets, MRI equipment and fusion reactors. The advantages of NbTi are that it is easily produced, the anisotropy is negligible and it exhibits high critical field and current densities.

The main disadvantage lies in the low critical temperature of NbTi requiring an expensive and extensive cooling set-up.

Niobium tin (Nb_3Sn) is a type II superconductor and has a critical temperature of 18 K. Compared to NbTi Nb_3Sn is rather similar but has superior critical characteristics and it is also more expensive.

3.6 Theory conclusions

The superconductive properties stem from the formation of Cooper pairs in materials. Cooper pairs condense into a Bose-Einstein condensate resulting in identical phase and a band gap for the removal of a single Cooper pair.

The main properties of a superconductor are negligible resistivity, the Meissner effect (expulsion of the magnetic field), flux quantization and flux preservation.

Superconductors can be classified according to field behavior, type I and type II. Superconductors can also be classified according to temperature (mechanism of Cooper pair formation), LTS or HTS.

The characteristics of a superconductive material is often represented by a critical surface. The critical surface indicates under what conditions of current (density), magnetic field and temperature the material is superconductive.

For the extent of the research YBCO, MgB_2, NbTi and Nb_3Sn is considered. These materials are commercially available and are mature enough for practical applications.

Chapter 4

High temperature superconducting magnet concepts

Contents

The history and theory of superconductivity have been discussed in Chapter 2 and 3 respectively. This chapter focuses on finding the boundaries of using superconductors at high temperatures (65 or 77 K) to generate magnetic fields.

The goal of this chapter is to find the maximum achievable fields using HTS wire and HTS bulk material. First concepts using HTS tapes are discussed in sections 4.1 to 4.3 after which a design using HTS bulk is evaluated in section 4.4.

4.1 Solenoid magnet

To generate magnetic fields using wires either solenoids or racetrack coils are used in practice (pancake wound coils are also used but are magnetically very similar to solenoids). In the following sections only solenoids are evaluated as the highest magnetic field can be achieved with a solenoid and racetrack coils are evaluated at a later stage.

This section provides the analytical expressions required to maximize the field generated by a superconducting solenoid.

Solenoids concentrate the magnetic field generated by wires inside while the field outside the solenoid often is considered negligible.

Solenoids can be characterized by three parameters namely the inner radius (R_i), the outer radius (R_o) and the length of the solenoid (L). Assuming densely packed windings the solenoid can be modeled as a hollow cylinder as shown in Figure 4.1.

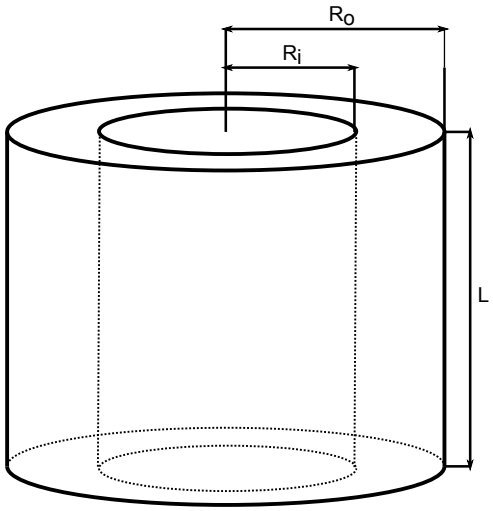

Figure 4.1: Solenoid modeled as a hollow cylinder

The magnetic field generated by a solenoid is dependent of multiple things besides the three geometric parameters. The field is also dependent on the current density flowing in the solenoid, the media (configuration) and the position in the media.

For the design of a superconducting solenoid magnet there are a few positions of interest. First, as the critical current is dependent on the magnetic field inside the solenoid and the solenoid is only as strong as its weakest link, the maximum field inside the solenoid (B_m) is of interest. Second, the point where the magnetic field is desired is of importance. In this case it can be either the field at a certain distance outside of the solenoid (B_x, B_{15} for 15 mm outside the solenoid) or in the center of the solenoid (B_c). These points of interest and a cross-section of the cylinder are shown in Figure 4.2.

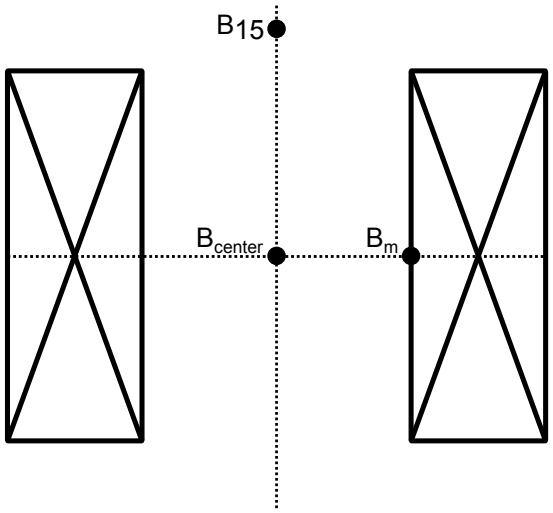

Figure 4.2: Cross-section of a solenoid and points of interest

As the field generated by a solenoid is mainly parallel to the length of the solenoid (Figure 4.1) only these fields are analytically calculated. The perpendicular fields of each of the concepts are evaluated using finite element modeling (*FEM*) at a later stage.

First two geometrical parameters need to be defined, α and β, which represent the ratio of the radii and the ratio between the length and the inner radius respectively. The parameters α and β are given by: [16]

$$\alpha = \frac{R_o}{R_i} \tag{4.1}$$

$$\beta = \frac{L}{2R_i} \tag{4.2}$$

The analytical expressions for the fields (parallel to the length of the solenoid) in the points of interest are given in Equations 4.3-4.5. [16, 17]

$$B_c = \mu_0 J R_i K_0 \tag{4.3}$$

$$B_m = \mu_0 J R_i (K_0 - \frac{1}{2}K_2 + \frac{3}{8}K_4 - \frac{5}{16}K_6 \ldots) \tag{4.4}$$

$$B_x = \frac{\mu_0 J}{2}\left((L+x)\ln\left(\frac{\sqrt{R_o^2+(L+x)^2}+R_o}{\sqrt{R_i^2+(L+x)^2}+R_i}\right) - x\ln\left(\frac{\sqrt{R_o^2+x^2}+R_o}{\sqrt{R_i^2+x^2}+R_i}\right)\right) \tag{4.5}$$

Where

$$K_0 = \beta\ln\left(\frac{\alpha+\sqrt{\alpha^2+\beta^2}}{1+\sqrt{1+\beta^2}}\right) \tag{4.6}$$

$$K_2 = \frac{1}{2\beta}\left(c_1^{\frac{3}{2}} - c_3^{\frac{3}{2}}\right) \tag{4.7}$$

$$K_4 = \frac{1}{24\beta^3}\left(c_1^{\frac{3}{2}}(2+3c_2+15c_2^2) - c_3^{\frac{3}{2}}(2+3c_4+15c_4^2)\right) \tag{4.8}$$

$$K_6 = \frac{1}{240\beta^5}\left(c_1^{\frac{3}{2}}(8+12c_2+15c_2^2-70c_2^3+315c_2^4)) - c_3^{\frac{3}{2}}(8+12c_4+15c_4^2-70c_4^3+315c_4^4)\right) \tag{4.9}$$

And

$$c_1 = \frac{1}{1+\beta^2} \tag{4.10}$$

$$c_2 = \frac{\beta^2}{1+\beta^2} \tag{4.11}$$

$$c_3 = \frac{\alpha^2}{\alpha^2+\beta^2} \tag{4.12}$$

$$c_4 = \frac{\beta^2}{\alpha^2+\beta^2} \tag{4.13}$$

Here μ_0 is the permeability of vacuum and J is the current density inside the solenoid.

Equations 4.3, 4.4 and 4.5 can be written as:

$$B_c = \mu_0 J C_c(\alpha, \beta, D) \tag{4.14}$$

$$B_m = \mu_0 J C_m(\alpha, \beta, D) \tag{4.15}$$

$$B_{15} = \mu_0 J C_{15}(\alpha, \beta, D) \tag{4.16}$$

Where C_c, C_m and C_{15} are geometrical constants for given values of α ,β and D.

4.2 Solenoid magnet: Field outside the magnet

The expressions to calculate the fields generated by a solenoid have been provided in the previous section. This section uses the expressions and the critical characteristics of an HTS wire to design a solenoid (α, β and D) to achieve a maximum field 15 mm outside of the solenoid.

For the design of a solenoid magnet where the required field is outside of the magnet some requirements are of importance. The outer diameter (D) of the solenoid is preferred to be 50 mm and maximally 100 mm. The maximum diameter of the magnets is set to 100 mm to keep them comparable to the permanent magnets used by Philips Innovation Services. A field is to be generated 15 mm outside of the solenoid on the solenoids axis (see B_{15} in Figure 4.2).

For this design the YBCO AP wire of SuperPower is used as its characteristics are excellent compared to the other available HTS wires. The critical engineering current densities for different temperatures and external fields for this wire are show in Figure 4.3. There is a ripple in the characteristics because experimental data is used.

It can be shown that for this AP wire, at 77 and 65 K, each doubling of the parallel magnetic field results in around a factor of 0.7 in critical current density. Consequently in the design it is preferred to double the magnetic field over doubling the current density requirement (even more so at lower temperatures).

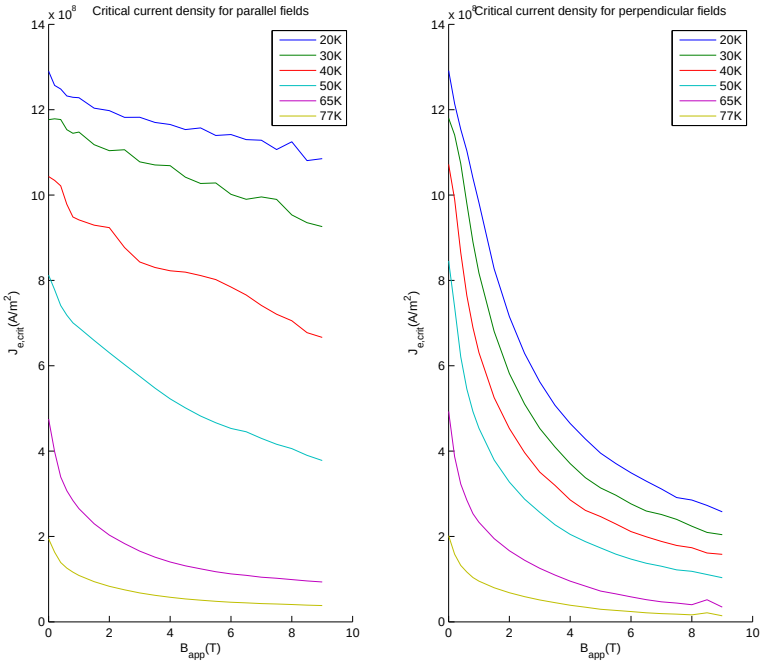

Figure 4.3: Critical characteristics of SuperPower AP HTS wire [18, 19, 20]

As each doubling in magnetic field results in a factor 0.7 in critical current the critical characteristic of the AP wire can be approximated by Equation 4.17.

$$J_{crit} \approx K \frac{1}{\sqrt{B_m}} \tag{4.17}$$

Where K is $1.09 * 10^8$ A/m^2 for 77K and $2.65 * 10^8$ A/m^2 for 65 K.

Using Equations 4.15 and 4.16 one can derive the expression for the current density as function of the maximum field (the load line of the solenoid) and the expression for the field at 15 mm as function of the maximum field. These expressions are given in Equations 4.18 and 4.19.

$$J = \frac{B_m}{\mu_0 C_m} \tag{4.18}$$

$$B_{15} = \frac{B_{15}}{B_m} B_m = \frac{C_{15}}{C_m} B_m \tag{4.19}$$

The maximum operating point of the solenoid can be found by intersecting the load line (Equation 4.18) with the critical characteristic (Equation 4.17). The point of intersection is given by Equation 4.20.

$$B_{m,max} \approx (K \mu_0 C_m)^{\frac{2}{3}} \tag{4.20}$$

Utilizing Equation 4.19 B_{15} at the maximum operating point is then given by Equation 4.21.

$$B_{15,max} \approx \frac{C_{15}(K\mu_0)^{\frac{2}{3}}}{C_m^{\frac{1}{3}}} \tag{4.21}$$

Equation 4.21 shows that, for this YBCO wire at 65 and 77 K, the maximum achievable field at 15 mm outside the solenoid is dependent on the geometrical constants C_{15} and C_m. These constants can be calculated using the Equations 4.4 and 4.5 (with $\mu_0 J = 1$).

4.2.1 Solenoid dimensions: D, α and β

For different diameters of the solenoid, using Equations 4.4 and 4.5 with $\mu_0 J = 1$ and $\alpha = \beta = 3$, C_m and C_{15} are plotted in Figure 4.4.

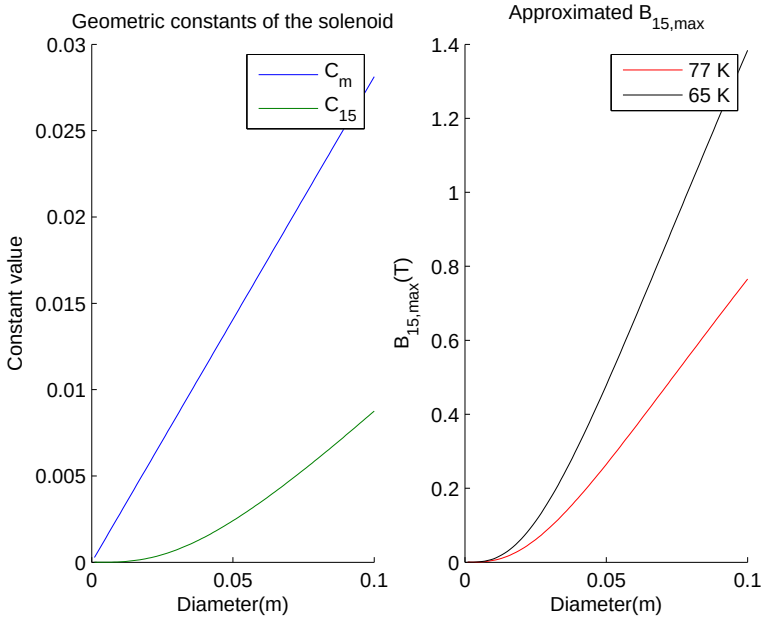

Figure 4.4: Approximated maximum achievable field of the solenoid for various diameters

Figure 4.4 also shows an approximation of the maximum achievable field for each diameter in a separate plot. The maximum achievable field is approximated using Equation 4.21.

The maximum of the achievable field occurs at infinity. As a consequence, for the design of a superconducting solenoid magnet where the required field is outside of the solenoid, it is beneficial for the diameter to be as large as possible (In this case $D = 100$ mm; $R_o = 50$ mm).

After the evaluation of different outer diameters next in consideration is the ratio α (equivalently R_i). In Figure 4.5 C_{15} and C_m are plotted for various values of α with $D = 100$ mm and $\beta = 3$. Figure 4.5 again shows an approximation of the maximum achievable field in a separate plot.

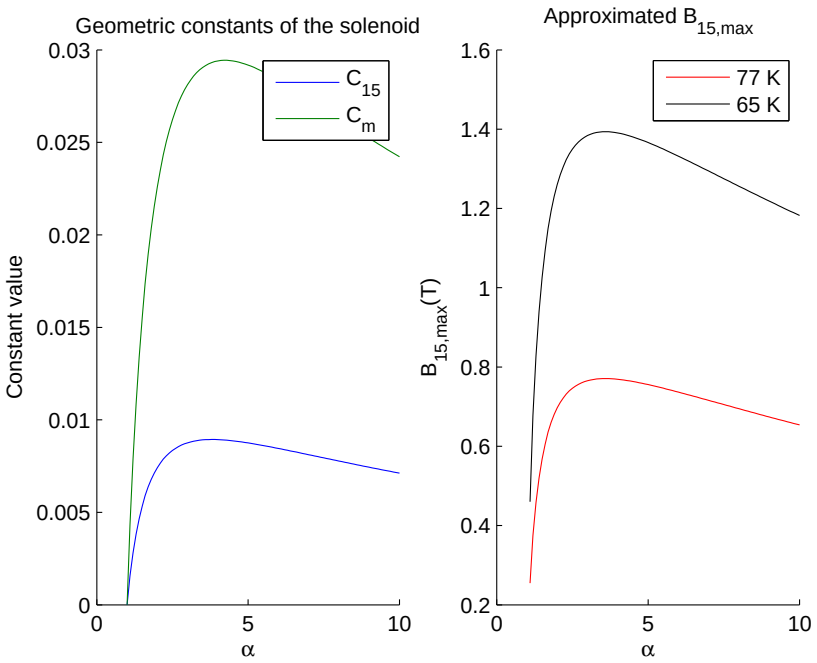

Figure 4.5: Approximated maximum achievable field of the solenoid for various α

The maximum of the achievable field occurs at $\alpha = 3.6$ for $D = 100$ and at $\alpha = 2.8$ for $D = 50$ mm. For this design α is chosen to be 3 (In this case with $D = 100$ mm $R_i = 16\frac{2}{3}$ mm).

Lastly, after determining the outer diameter D and the ratio α, β and with that L can be determined. C_{15} and C_m are calculated for various values of β with $D = 100$ mm and $\alpha = 3$. The results are shown in Figure 4.6. An approximation of the maximum achievable field is also plotted in a separate graph.

The maximum of the achievable field occurs at infinity for both $D = 100$ and $D = 50$. A solenoid with a higher β than 3 is not viable, much additional material is used for minor performance increase.

Identically assessing approximated maximum achievable field at other values of α one can conclude that a solenoid with a $\beta = \alpha$ (consequently $L = D$) is preferable. For this design β is chosen as 3 (In this case for $D = 100$ mm $L = 100$ mm).

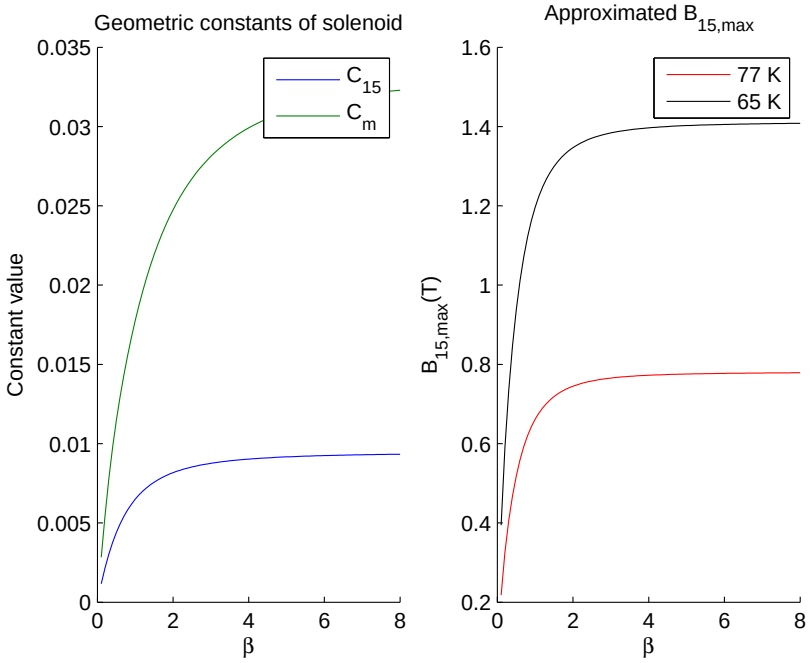

Figure 4.6: Approximated maximum achievable field of the solenoid for various β

4.2.2 Concept with an air core

The values of α (3) and β (3) have been chosen for a solenoid with a diameter D between 50 and 100 mm.

The load line of the solenoid is chosen to be a modified version of Equation 4.18 given in Equation 4.22

$$J = \frac{1}{0.90}\frac{B_m}{\mu_0 C_m} \tag{4.22}$$

A factor of $\frac{1}{0.90}$ is introduced as operating the superconductor on the border of superconductivity is risky (quenches are bound to happen). An operating factor of 90% of the critical current density is chosen.

This factor is chosen as a minimal incorporation of the influence of the perpendicular field, the productional variation in current density and the influence of strain on the critical current density. The factor is appropriate for low external fields but in practical applications this factor can be much lower.

Now that everything has been defined the maximum operating points of the solenoids can be determined. Using Equation 4.22 load lines of the solenoids can be plotted in the left graph of Figure 4.3 for a diameter of 50, 100 and 140 mm. This is shown in Figure 4.7.

From the intersections of the load lines with the critical density characteristics the maximum operating conditions can be determined for multiple temperatures. The operating conditions can be calculated, with the maximum field found at the point of intersection, using Equations 4.18 and 4.19. For 77K and 65K these operating conditions are shown in Table 4.1.

In Table 4.1 the maximum perpendicular field inside the solenoid B_p is also found. This value is not calculated analytically but by means of FEM modeling in Opera.

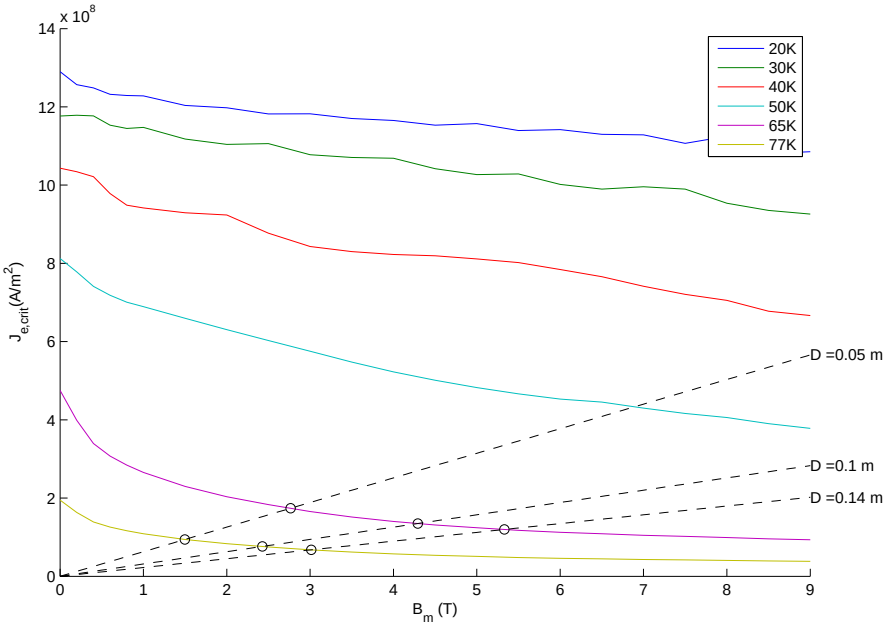

Figure 4.7: Load lines in the critical characteristic

	D = 50 mm		D = 100 mm		D = 140 mm	
	77K	65K	77K	65K	77K	65K
B_m(T)	1.49	2.77	2.43	4.29	3.01	5.33
B_{15}(T)	0.26	0.47	0.76	1.34	1.12	1.98
$J(10^7$ A/m$^2)$	8.48	15.66	6.87	12.15	6.09	10.77
B_p(T)	0.50	0.92	0.81	1.43	1.00	1.77

Table 4.1: Maximum operating conditions of multiple air core solenoids

As a final check for these solenoids the current densities can be checked using the values of B_p and the right graph in Figure 4.3. Doing so one can conclude that the assumption that the field is mostly parallel to the length of the solenoid (and one can temporarily ignore the perpendicular field) is justified. The found critical current densities for the perpendicular fields are much greater than the current densities used in Table 4.1.

4.2.3 Concept with a non-air core

The previous section shows that for a design generating 1T with an air core the maximum magnetic field B_m is at least 2.5 T. When using a core with a relative permeability higher than air this would mean the core would be driven far into saturation. As this is a non-linear process, for designing a solenoid with a core which does not entirely consist of air, analytical expressions do not suffice. FEM is used extensively in this section to compute the fields for different geometries.

Using a 100 mm diameter coil with $\alpha = 3$ and $\beta = 3$ the field at 15 mm distance, the parallel field and the perpendicular field are computed. As core a steel cylindrical core is used. The results of the FEM computations for several radii of the core are shown in Figure 4.8. The current densities used to compute the fields for the solenoids with cores are found in Table 4.1.

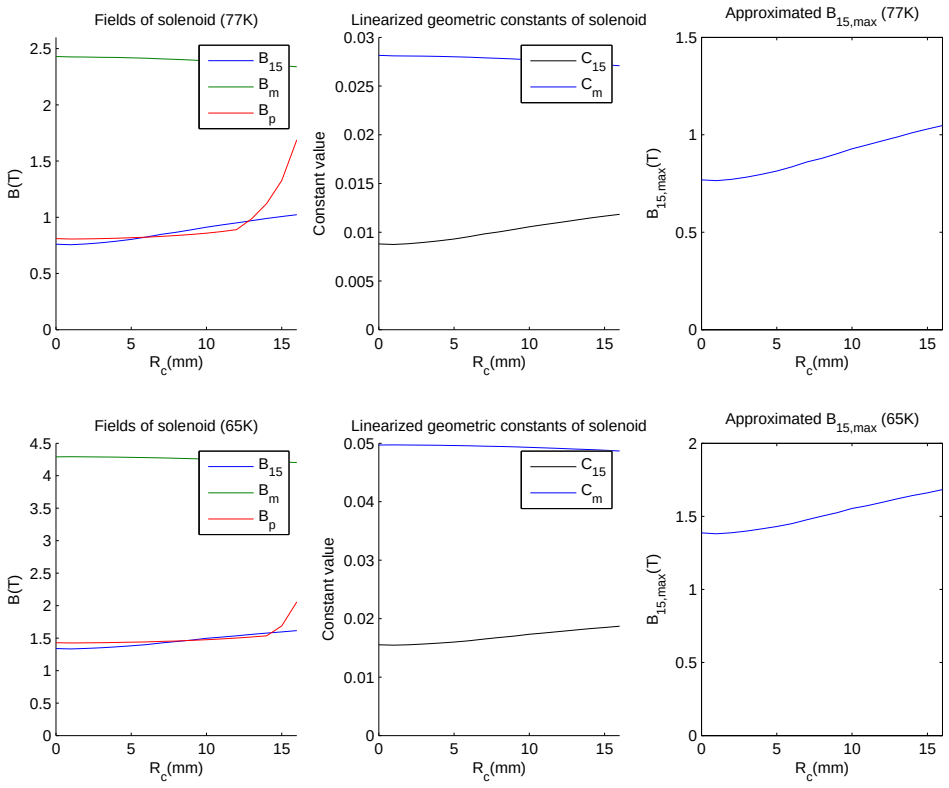

Figure 4.8: Fields and approximate maximum achievable field for various radii of the core

Figure 4.8 also shows linear approximations of C_m and C_{15} and an approximated maximum achievable field in separate plots.

In the previous sections C_m and C_{15} and consequently $B_{15,max}$ were calculated using analytical equations. Because of the non-linearity the maximum achievable field can not be analytically calculated. However a linear approximation of C_m and C_{15} can be made using Equations 4.15 and 4.16 and FEM. Subsequently a linear approximation of $B_{15,max}$ is made using Equation 4.21.

The accuracy of this approximation increases as the current density used in the FEM calculations approaches the actual maximum current density.

The maximum of the achievable field occurs at the maximum radius for both solenoids. However at a radius of 12 mm of the core for the 77K values and at 14 mm for 65K the perpendicular field starts to increase rapidly. As this field can largely influence the critical current density (due to anisotropy) the the radii are chosen to be 12 and 14 mm. The operating conditions of these solenoids with optimized core are found in Table 4.2

As an α of 3 does not leave much space for a core (a third of the outer radius) a solenoid with an α of 2 (and consequently also a β of 2) is also evaluated.

First the operating conditions are determined for a similar air core solenoid using Equations 4.18 and 4.19 analogous to the other solenoids with an air core (seen in Figure 4.7). In a similar manner as for the solenoid with $\alpha = \beta = 3$ the core radius and corresponding operating conditions are determined for 77 and 65 K. All the results are shown in Table 4.2.

	$\alpha = \beta = 3$		$\alpha = \beta = 3$		$\alpha = \beta = 2$		$\alpha = \beta = 2$	
	77K	65K	77K	65K	77K	65K	77K	65K
Core radius	0 mm	0 mm	12 mm	14 mm	0 mm	0 mm	15 mm	16 mm
B_m(T)	2.43	4.29	2.38	4.22	1.97	3.54	1.90	3.47
B_{15}(T)	0.76	1.34	0.95	1.58	0.67	1.21	0.92	1.47
$J(10^7$ A/m$^2)$	6.87	12.15	6.87	12.15	7.55	13.57	7.55	13.57
B_p(T)	0.81	1.43	0.89	1.54	0.81	1.45	0.91	1.55

Table 4.2: Maximum operating conditions of multiple solenoids with core ($D = 100$ mm)

From Table 4.2 it can be seen that using a steel core is beneficial. For the solenoids with $\alpha = \beta = 3$ a steel core increases performance with 18-25% and for $\alpha = \beta = 2$ it is 21-37%. Introducing a steel core also marginally decreases the maximum field inside the solenoid and slightly increases the perpendicular field.

A steel core proves more beneficial at lower fields. Steel behaves as air at fields far past saturation but still gives an initial increase in magnetic field. With increasing magnetic field the initial increase becomes more negligible.

Adopting a design with less optimal α may prove desirable when using a steel core. Comparing the designs with $\alpha = \beta = 3$ and $\alpha = \beta = 2$ the material used is decreased by 33% while only slightly decreasing performance.

4.3 Solenoid magnet: Field inside the magnet

In the previous section a solenoid designed to the field 15 mm outside the solenoid. This section uses the expressions of section 4.1 and the critical characteristics of an HTS wire to design a solenoid (α, β and D) to achieve a maximum field inside the solenoid.

In contrast to the previous section the magnetic field is wanted at the center of the solenoid. The achievable fields at the center are evaluated in a similar fashion as was done for the field outside the solenoid.

In this case there are no requirements set to the diameter or desired field of the solenoid. The maximum achievable fields are determined for solenoids with diameters of 100, 150 and 250 mm. A solution with core is not considered as the field ought to be used for actuating purposes.

The derivation of the maximum achievable field inside the solenoid is analogous to the derivation for the field outside the solenoid. Equation 4.21 is modified to the maximum achievable field inside the solenoid and is given by Equation 4.23.

$$B_{c,max} \approx \frac{C_c (K\mu_0)^{\frac{2}{3}}}{C_m^{\frac{1}{3}}} \tag{4.23}$$

Where K is $1.09 * 10^8$ A/m^2 for 77K and $2.65 * 10^8$ A/m^2 for 65 K.

4.3.1 Solenoid dimensions: D, α and β

For various diameters C_m, C_c and the approximated maximum achievable field (for $\alpha = \beta = 5$) are plotted in Figure 4.9.

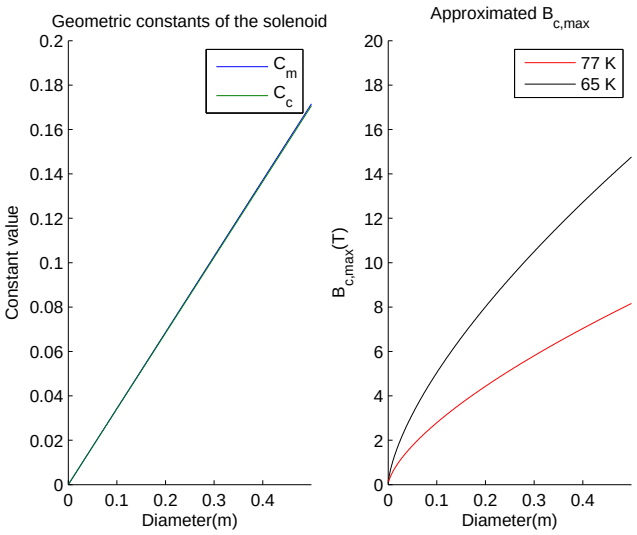

Figure 4.9: Approximated maximum achievable field of the solenoid for various diameters

As with the solenoid designed for field at 15 mm outside the solenoid an increase in diameter results in an increase in maximum achievable field of the solenoid (with constant α and β).

The maximum achievable fields various values of α ($D = 100$ mm, $\beta = 5$) and β ($D = 100$ mm, $\alpha = 5$) are shown in Figure 4.10.

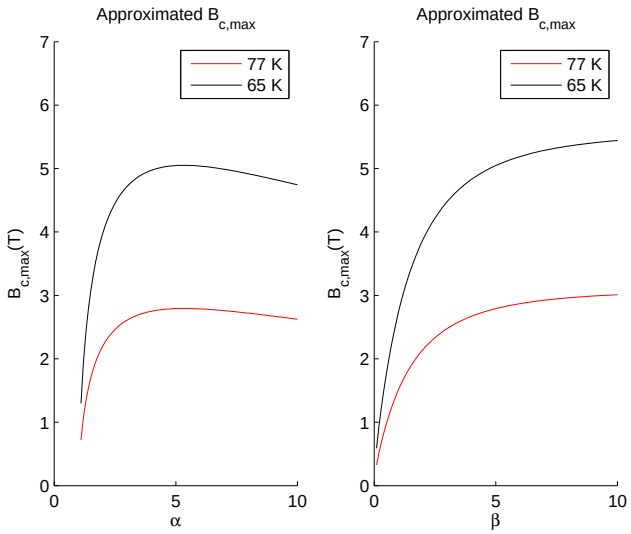

Figure 4.10: Approximated maximum achievable field of the solenoid for various α and β

The maximum of B_c, max occurs at $\alpha = 5.3$ for all diameters. The maximum of B_c, max occurs at β equal to infinity for all diameters.

For this design α is chosen to be 5. This value of α is chosen to calculate the maximum achievable fields while in practical machines α would likely be lower to leave more space for the moving part of the machine.

For the same reasons as in previous section β is chosen to be equal to α. Increasing β to 2α would increase performance by only 6% while doubling the material used.

4.3.2 Magnet concept

Rewriting Equations 4.18 and 4.19 the current density as function of the maximum field and the field in the center as function of the maximum field become:

$$J = \frac{1}{0.90}\frac{B_m}{\mu_0 C_m} \tag{4.24}$$

$$B_c = \frac{B_c}{B_m}B_m = \frac{C_c}{C_m}B_m \tag{4.25}$$

From these equations the load lines can again be plotted. Using the intersections between the load lines and the critical current density characteristic the maximum operation conditions can be calculated. The load lines and the critical current density graphs are shown in Figure 4.11.

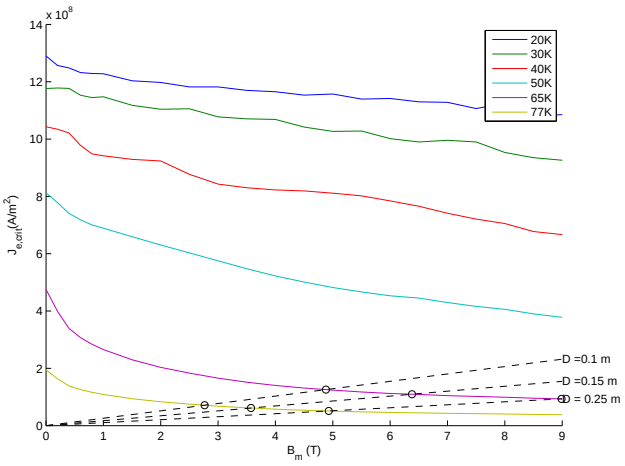

Figure 4.11: Load lines in the critical characteristic

The maximum operation conditions for the solenoids with $\alpha = \beta = 5$ are given in Table 4.3.

	D = 100 mm		D = 150 mm		D = 250 mm	
	77K	65K	77K	65K	77K	65K
B_m(T)	2.76	4.88	3.57	6.38	4.93	9.06
B_c(T)	2.75	4.86	3.56	6.35	4.91	9.02
$J(10^7$ A/m$^2)$	6.41	11.32	5.53	9.87	4.61	8.41
B_p(T)	0.78	1.37	1.00	1.79	1.39	2.54

Table 4.3: Maximum operating conditions of multiple solenoids

4.4 Trapped field magnet

An alternative to a solenoid magnet is a bulk of superconducting material. As explained in Chapter 3 at fields above B_{c1}, in a type II superconductor, regions of normal conduction start to form and flux lines penetrate the superconductor. All the material around the resistive region is superconducting thus the flux penetrating through the bulk is preserved. This means that even if you remove the field that initially created the resistive regions the component of the field that penetrated the material is preserved. Such a magnet is called a Trapped Field Magnet (TFM).

This section researches the maximum achievable fields using these TFM's.

In Re-BCO materials the boundaries of the grains (regions that form a single crystal) are of great importance. Unaligned grains cause low critical currents at the grain boundaries (grain boundary mismatch). [2] Because of this it is preferred to grow TFM's single grained (for superconducting wire special deposition techniques are used to ensure grain alignment [2]).

Single grained trapped field magnets are grown (crystallized) from a seed crystal and their components in powder form. For a single grained trapped field magnet the maximum field that can be trapped can be represented by Equation 4.26. [21]

$$B_{trapped} = A\mu_0 J_c r \tag{4.26}$$

Where A is a geometric constant, J_c is the critical current and r is the radius of a single grain.

From Equation 4.26 it is clear that to improve a trapped field magnet either the critical current or the grain radius should be increased. The maximum grain sizes currently achievable for YBCO, $GdBCO$ and $SmBCO$ materials are 100, 65 and 60 mm respectively. [21]

For YBCO, GdBCO and SmBCO disks the maximum trapped fields that have been achieved are shown in Figure 4.12 (diameters of the disks are stated in the legend). Figure 4.12 also shows the theoretical trapped fields for similar 50 mm single grained disks in a separate plot (calculated using Equation 4.26).

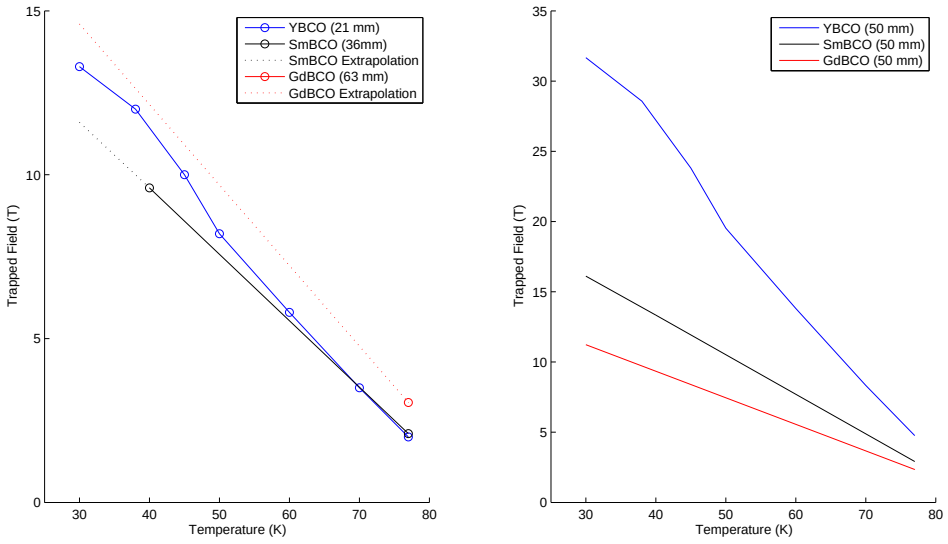

Figure 4.12: Maximum achieved and theoretical fields of TFMs [22, 23, 24]

There are some practical constraints on the graphs shown in Figure 4.12. Firstly the trapped fields presented are under lab conditions. Secondly the bulks used are not necessarily commercially available. Lastly only for GdBCO larger diameters than 30 mm have been achieved without degradation. The degradation is caused by grain boundary mismatch and crack formation during the growth process. [25] As such the presented maximum trapped fields are theoretical maxima and need to be re-evaluated using the manufacturers data when a design is made.

The magnetic field in trapped field magnets is essentially caused by the persistent currents around the resistive regions. As these regions are distributed throughout the magnet it can be modeled as a conductor of identical geometry with a current flowing around the center of the magnet. Both the distributed currents and the model are shown in Figure 4.13.

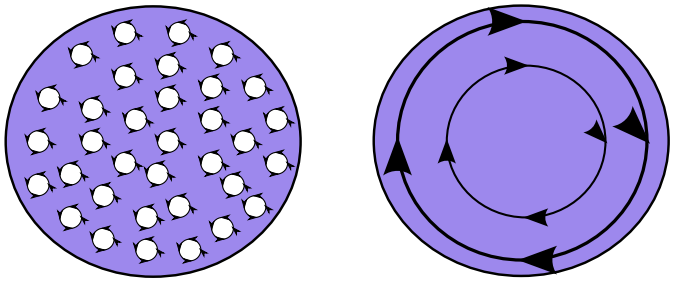

Figure 4.13: Distributed currents and model of a trapped field magnet

Averagely the current density is evenly distributed throughout the geometry leading to either a conical or pyramidal field distribution for a circular and rectangular bulk respectively. These distributions are shown in Figure 4.14.

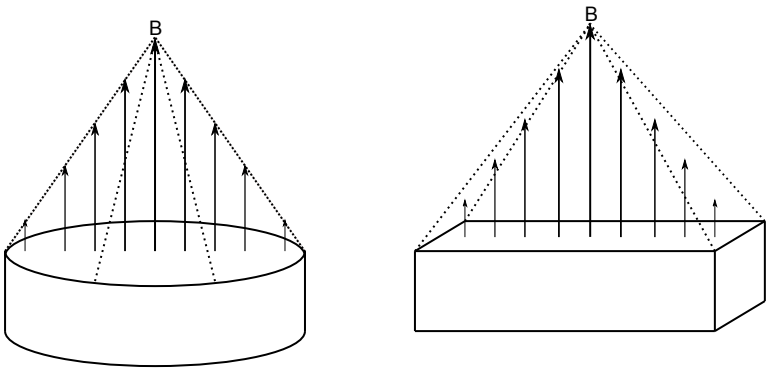

Figure 4.14: Distribution of magnetic field of a trapped field magnet

4.4.1 Trapped field magnet concept

Assuming a circular trapped field magnet with a diameter of 50 mm and a height of 20 mm and evenly distributed current density, one can calculate the field at different points in space. Again the position where the field is desired is at 15 mm above the center of the magnet, but also the field distribution at 15 mm distance from the edges of the magnet is of interest.

Finite element modeling is used to evaluate the fields. The current density is chosen so that it generates 1 Tesla in the center at 0.5 mm from the surface of the magnet (distance of measurements from Figure 4.12). In this way a factor between the field at the surface and at 15 mm can be determined. The results of the simulation are shown in Figure 4.15.

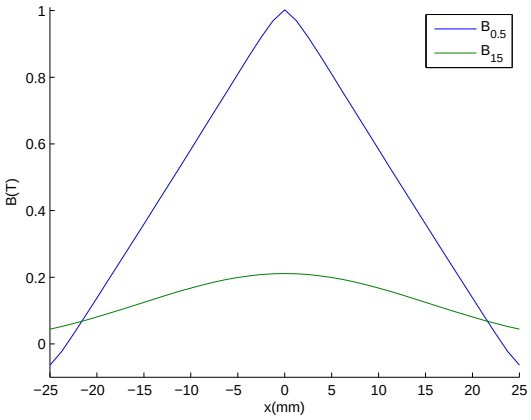

Figure 4.15: Distribution of magnetic field of a 1T trapped field magnet at 15 and 0.5 mm

Using the results from Figure 4.15 we can now determine the maximum fields achievable at 15 mm distances. For the different materials this is plotted in Figure 4.16.

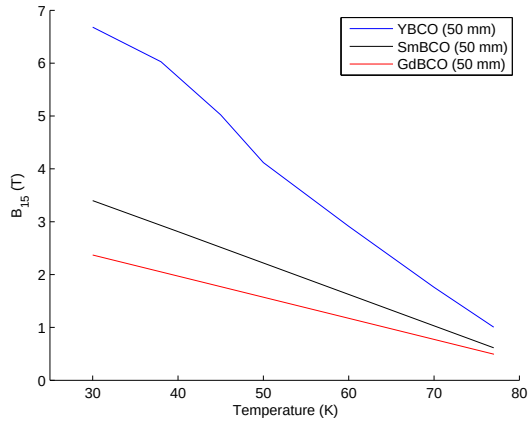

Figure 4.16: Maximum achievable fields of TFM's at 15 mm distance

From this graph it is clear that again at a temperature of 77 K it is fairly difficult to achieve 1T at a 15 mm distance. Decreasing the temperature would increase the possible trapped field considerably.

The final results for 65 and 77 K are also summed up in Table 4.4.

	77K B_{15}(T)	65K B_{15}(T)
YBCO	1.00	2.33
SmBCO	0.62	1.33
GdBCO	0.50	0.97

Table 4.4: Maximum operating conditions of multiple trapped field magnets

4.5 High temperature magnet concepts conclusions

This chapter was aimed at finding the highest achievable magnetic fields at 65 and 77 K using superconductors. Concepts using HTS wire and bulk were considered at these temperatures.

For fields at 15 mm distance a solenoid with $R_o = 50$ mm, $R_i = 16\frac{2}{3}$ mm and $L = 100$ mm was designed. This solenoid was able to achieve fields up to 1.34 T without a steel core and up to 1.58 T with a steel core at 65 K.

For fields inside the solenoid the parameters were chosen to be $R_o = 125$ mm, $R_i = 25$ mm and $L = 250$. This solenoid was able to achieve fields up to 9.02 T at 65K.

Trapped field magnets with a diameter of 50 mm were also considered. Theoretically the fields achievable at 15 mm distance with TFM's are 1.0 T at 77 K and 2.33 T at 65 K. Consideration must given to practical achievability and availability of such TFM's.

Chapter 5

Low temperature superconducting magnet concepts

Contents

In the previous chapter solenoid magnets at 77 and 65 K were discussed using HTS tape and bulk material. The maximum field that could be achieved by the solenoid was highly dependent on the chosen diameter and temperature of the solenoid.

At lower temperatures the performance of the superconducting wires increases significantly. Reducing the temperature to 20 or 4 K also increases the number of applicable superconductive materials. The goal of this chapter is to find the maximum achievable fields at these temperatures.

Although this chapter follows similar reasoning and similar calculations are made, a separate chapter is necessary for low temperatures. This is because multiple materials are considered, the materials have dissimilar characteristics and anisotropic nature is of importance.

In this chapter TFM's are not considered as the Re-BCO bulk material would most likely crack at higher fields than achieved in the previous chapter. In sections 5.1 and 5.2 the low temperature variants of the air core solenoid magnets presented in the previous chapter are discussed. A steel core is not considered as the benefit is considered negligible.

5.1 Solenoid magnet: Field outside the magnet

In the previous chapter a solenoid design was made for to the field 15 mm outside the solenoid. This section uses the expressions of section 4.1 and the critical characteristics of various materials to design a solenoid (α, β and D) to achieve a maximum field 15 mm outside the solenoid. In this section a solenoid is considered at 20 and 4 K. The maximum diameter (D) of the solenoid is again 100 mm.

At temperatures at and below 20 K new materials become interesting besides the YBCO wire discussed in the previous chapter. MgB_2 becomes a viable option at and below 20 K while NbTi and Nb_3Sn become interesting at and below 4 K.

These materials have the advantage of showing low to no anisotropy and can be processed using other (cheaper) manufacturing techniques. In general HTS material can achieve higher current densities than LTS material at the same temperature. HTS material however requires a stabilizer (as it is brittle) leading to a relatively small superconductive area in the wire.

In Figure 5.1 the critical engineering current densities are shown for various materials at 20 and 4 K. It is clear that the HTS wire has the superior critical characteristics at higher magnetic fields while the LTS materials prevail at lower magnetic fields.

Importantly HTS wire is more anisotropic at lower temperatures introducing an additional restraint on operating an HTS magnet at lower temperatures. As a consequence the critical current can be dominated by the perpendicular magnetic field instead of the parallel magnetic field as was the case in the previous chapter.

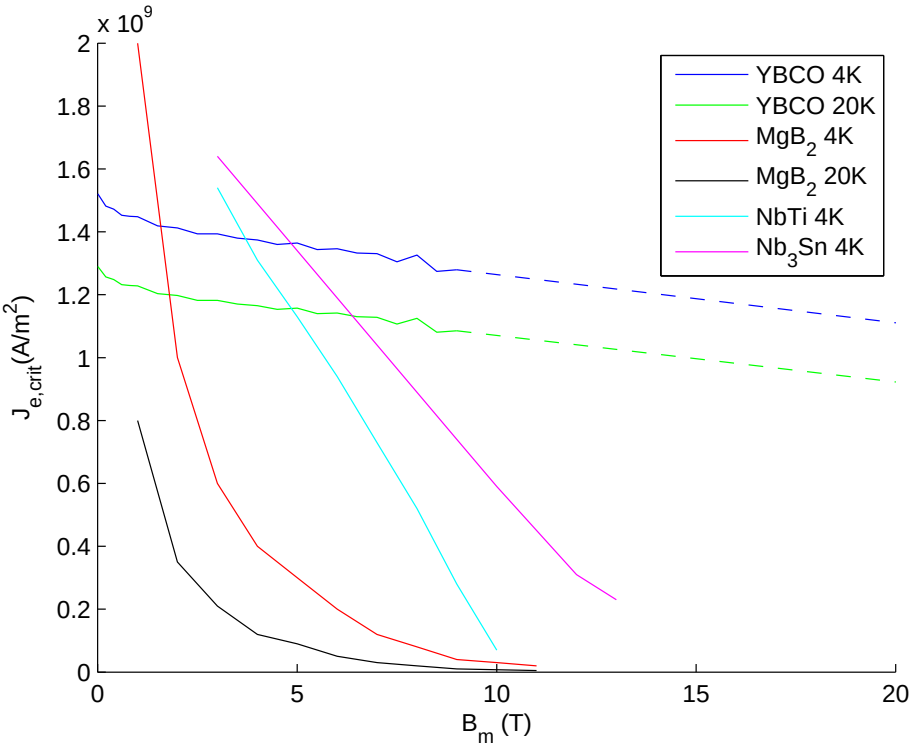

Figure 5.1: Critical engineering current densities of various materials [18, 19, 20, 26, 27, 28, 29, 30]

The critical characteristics of the different materials at 20 and 4 K can be approximated by Equations 5.1-5.4.

$$J_{crit,YBCO} \approx -0.0158 * 10^9 B_m + K \tag{5.1}$$

Where K is $1.23 * 10^9$ A/m^2 for 20 K and $1.42 * 10^9$ A/m^2 for 4 K.

$$J_{crit,MgB2} \approx K \frac{1}{B_m^{1.25}} \tag{5.2}$$

Where K is $0.8 * 10^9$ A/m^2 for 20 K and $2.0 * 10^9$ A/m^2 for 4 K.

$$J_{crit,NbTi} \approx -0.21 * 10^9 B_m + 2.17 * 10^9 \tag{5.3}$$

$$J_{crit,Nb3Sn} \approx -0.148 * 10^9 B_m + 2.08 * 10^9 \tag{5.4}$$

Analogous to the methods shown in the previous chapter the approximation of the maximum achievable field is derived and given in Equations 5.5-5.8.

$$B_{15,max,YBCO} \approx \frac{K\mu_0 C_{15} C_m}{C_m + 0.0158 * 10^9 \mu_0 C_m^2} \tag{5.5}$$

$$B_{15,max,MgB2} \approx \frac{(K\mu_0)^{0.44} C_{15}}{C_m^{0.56}} \tag{5.6}$$

$$B_{15,max,NbTi} \approx \frac{2.17 * 10^9 \mu_0 C_{15} C_m}{C_m + 0.21 * 10^9 \mu_0 C_m^2} \tag{5.7}$$

$$B_{15,max,Nb3Sn} \approx \frac{2.08 * 10^9 \mu_0 C_{15} C_m}{C_m + 0.148 * 10^9 \mu_0 C_m^2} \tag{5.8}$$

For various diameters with $\alpha = 2.5$ and $\beta = 1$ the geometric constants C_m, C_{15} and the maximum achievable fields are shown in Figure 5.2.

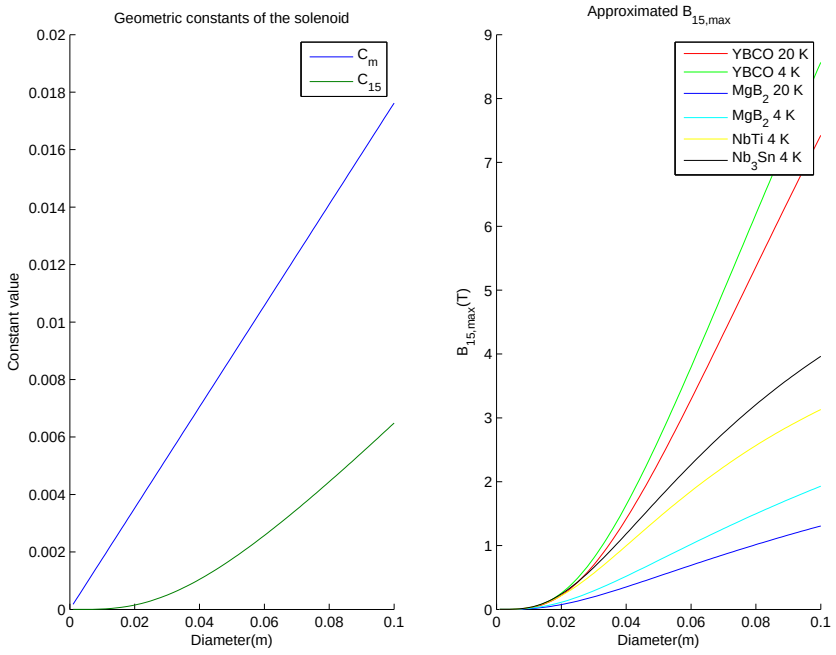

Figure 5.2: Approximated maximum achievable field of the solenoid for various diameters

Identically to the previous chapter the performance increases as the diameter of the solenoid is increased. Consequently the diameter is chosen to be 100 mm.

For various α with $\beta = 1$ and for various β with $\alpha = 2.5$ the maximum achievable field is shown in Figure 5.3.

The optima for the various materials occurs around $\alpha = 2.5$ for all materials. $\alpha = 2.5$ is chosen for this design.

The optima for the various materials are more dispersed but occur around $\beta = 1$ or at infinity. For this design β is chosen to be 1.

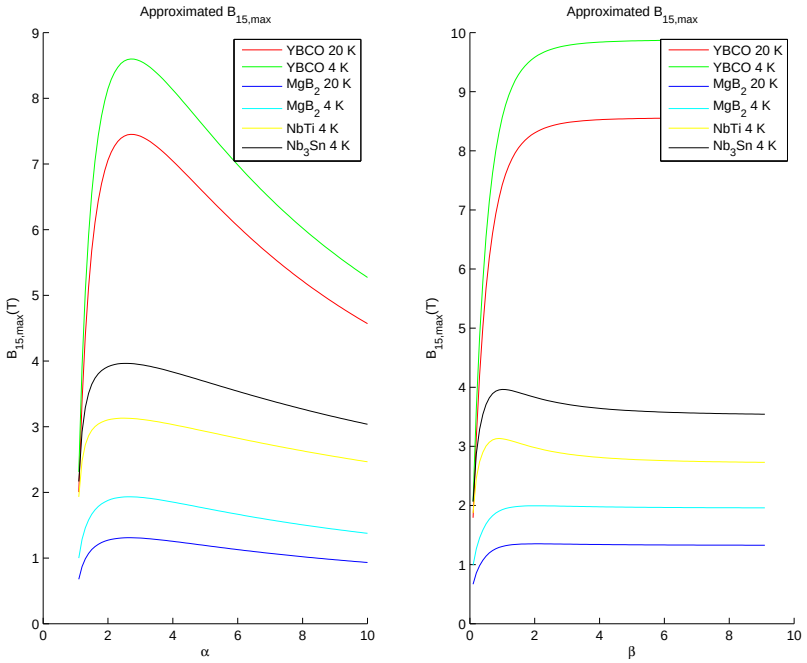

Figure 5.3: Approximated maximum achievable fields for various α and β

The load line can again be plotted using Equation 4.22. For $\alpha = 2.5$ and $\beta = 1$ the load line and the critical characteristic are shown in Figure 5.4.

The intersections between the load line and the critical characteristics indicate the maximum operating conditions. From the maximum field at the point of intersection the field at 15 mm can be calculated using Equation 4.19. The results are shown in Table 5.1.

	YBCO		MgB_2		NbTi	Nb_3Sn
	20K	4K	20K	4K	4K	4K
B_m(T)	9.3	10.8	3.4	5.33	8.4	10.5
B_{15}(T)	3.4	4.0	1.3	2.0	3.1	3.9
$J(10^8$ A/m$^2)$	4.20	4.90	1.55	2.40	3.80	4.73
B_p(T)	4.1	4.8	1.5	2.4	3.7	4.7

Table 5.1: Maximum operating conditions of multiple solenoids

Table 5.1 and Figure 5.4 show a discrepancy for YBCO. The discrepancy is caused by the anisotropy of the material. At the low temperatures the high perpendicular fields, also shown in the table, start to dominate the critical behaviour (see the second graph in Figure 4.3).

The maximum operating conditions for YBCO in Table 5.1 are approximated using FEM calculations and the data found in the right graph of Figure 4.3.

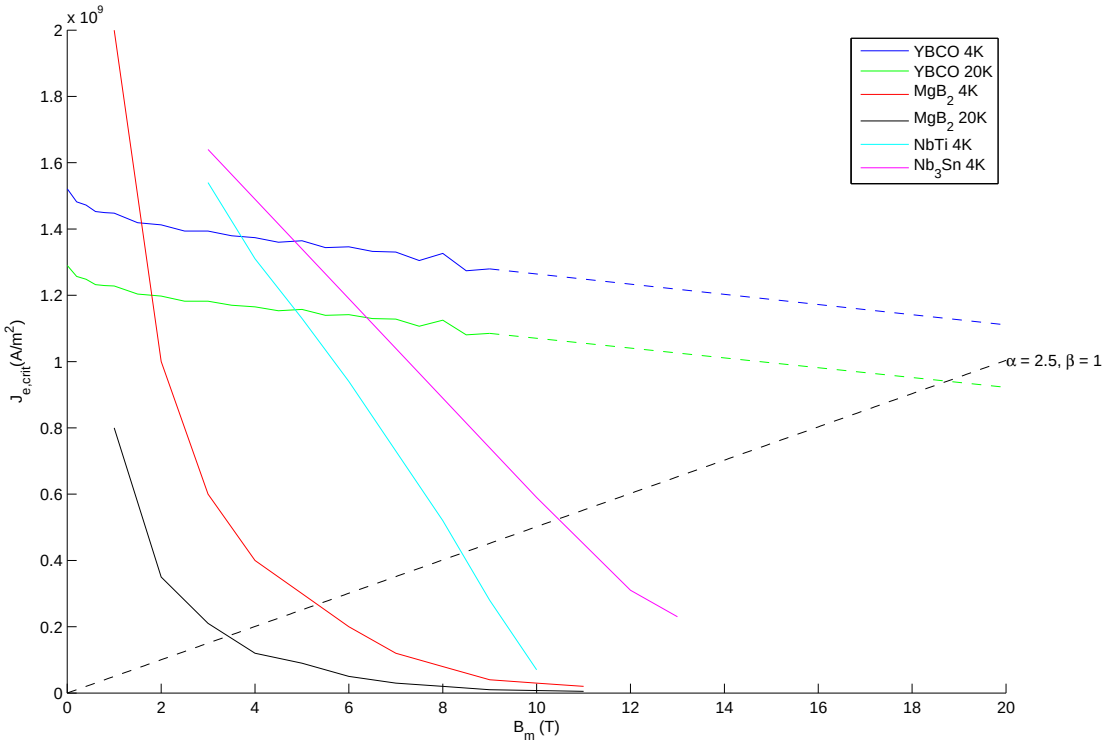

Figure 5.4: Load line of the solenoid in the critical characteristics

5.2 Solenoid magnet: Field inside the magnet

The previous section designed a solenoid for the field 15 mm oustide the solenoid. This section finds a solenoid design (α, β and D) to achieve a maximum field inside the solenoid in a similar fashion. In this section a solenoid with a maximum diameter D of 100 mm is considered at 20 and 4 K using the same materials found in the previous section.

The derivation of the maximum achievable field inside solenoid is analogous to the derivation found in the previous section. The maximum achievable fields inside the solenoid for the various materials are given in Equations 5.9-5.12.

$$B_{c,max,YBCO} \approx \frac{K\mu_0 C_c C_m}{C_m + 0.0158 * 10^9 \mu_0 C_m^2} \tag{5.9}$$

$$B_{c,max,MgB2} \approx \frac{(K\mu_0)^{0.44} C_c}{C_m^{0.56}} \tag{5.10}$$

$$B_{c,max,NbTi} \approx \frac{2.17 * 10^9 \mu_0 C_c C_m}{C_m + 0.21 * 10^9 \mu_0 C_m^2} \tag{5.11}$$

$$B_{c,max,Nb3Sn} \approx \frac{2.08 * 10^9 \mu_0 C_c C_m}{C_m + 0.148 * 10^9 \mu_0 C_m^2} \tag{5.12}$$

For various diameters with $\alpha = 5$ and $\beta = 5$ the field constants C_m, C_c and the maximum achievable field is shown in Figure 5.5.

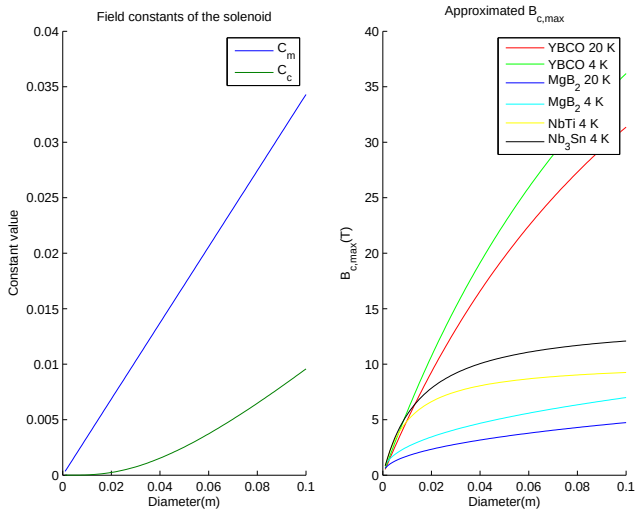

Figure 5.5: Approximated maximum achievable field of the solenoid for various diameters

Again the performance increases as the diameter of the solenoid is increased. This section only focuses on a solenoid with a diameter of 100 mm as that is sufficient to compare the performance with a solenoid operated at higher temperatures.

For various values of α with $\beta = 5$ and for various values of β with $\alpha = 5$ the maximum achievable field is shown in Figure 5.6.

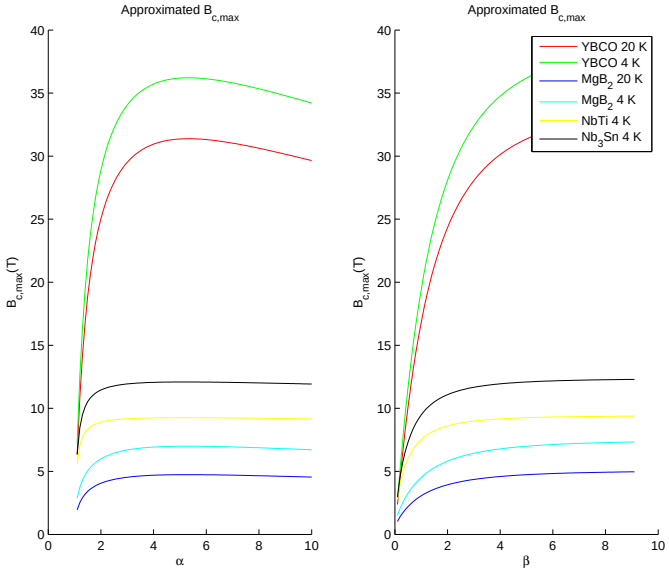

Figure 5.6: Approximated maximum achievable fields for various α and β

The maximum for various α occurs for all materials around $\alpha = 5$. α is chosen to be 5.

The maximum for various β occurs at infinity for all materials. β is chosen to be 5 after which the increase in performance of the solenoid becomes negligible with increasing β.

The load line can again be plotted using Equation 4.24. For $\alpha = 5$ and $\beta = 5$ the load line and the critical characteristic are shown in Figure 5.7

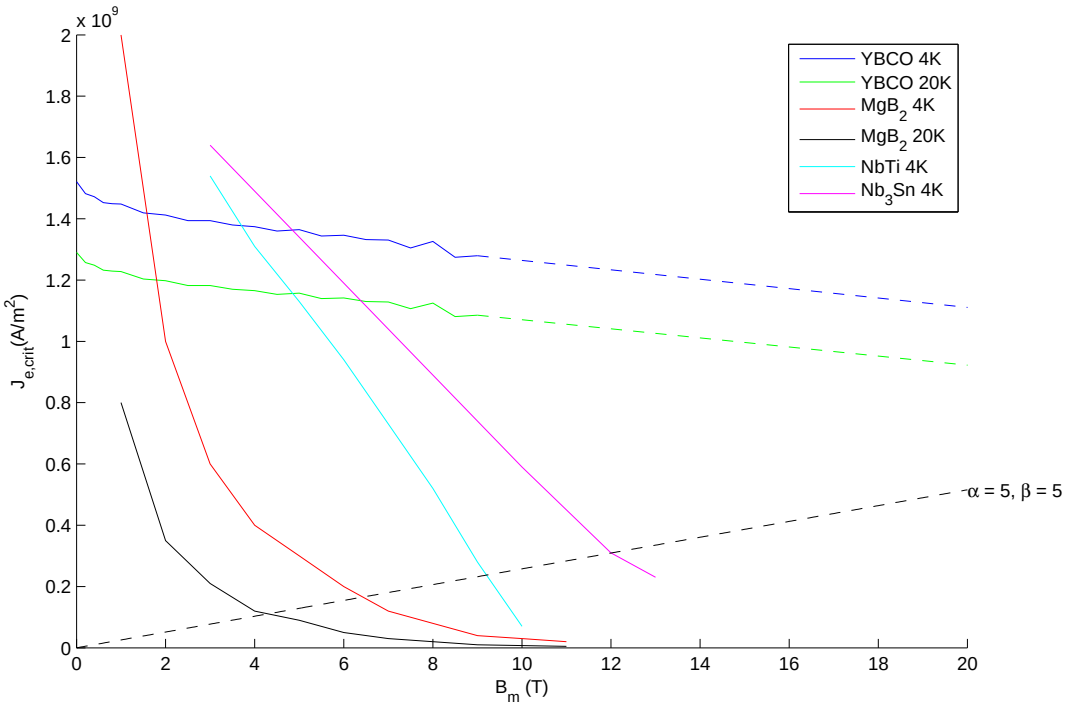

Figure 5.7: Load line of the solenoid in the critical characteristics

Again the maximum operating conditions can be calculated from the intersections of the load line with the critical characteristics. The results are shown in Table 5.2.

For YBCO the maximum operating conditions are approximated using FEM as the perpendicular field again dominates the critical behaviour.

	YBCO		MgB_2		NbTi	Nb_3Sn
	20K	4K	20K	4K	4K	4K
B_m(T)	19.4	22.5	4.3	6.4	9.2	12.0
B_c(T)	19.3	22.3	4.3	6.4	9.2	11.9
$J(10^8$ A/m$^2)$	4.49	5.22	1.00	1.49	2.14	2.79
B_p(T)	3.7	4.3	1.2	1.8	2.6	3.4

Table 5.2: Maximum operating conditions of multiple solenoids

5.3 Low temperature magnet concepts conclusions

This chapter was aimed at finding the highest achievable magnetic fields at 20 and 4 K using superconductors. Concepts using various materials at these temperatures were evaluated.

For the field at 15 mm distance a solenoid with D = 100 mm, R_i = 20 mm and L = 20 mm was designed. This solenoid was able to generate 1.3 - 3.4 T at 20 K and 2.0 - 4.0 T at 4 K depending on the material used.

For the field inside the solenoid the design parameters were D = 100, R_i = 10 mm and L = 100 mm. This solenoid was able to generate 4.3 - 19.3 T at 20 K and 6.4 - 22.3 T at 4 K depending on the material used.

Chapter 6

Thermal concepts

Contents

It has been shown in the previous chapters that a decrease in operating temperature of superconductors greatly benefits the performance. The goal of this chapter is to acquire the information necessary to asses the thermal aspects of designing a superconducting actuator.

The lowest achievable temperature is dependent on the cooling power available and the degree of thermal leakage which are both in turn a function of temperature.

This chapter first discusses the different heat transfer and generation mechanisms in sections 6.1 and 6.2 respectively. Second the different *cryostat* designs are discussed in section 6.3.

6.1 Heat transfer

The cooling power required to keep a stable temperature in the cryostat is a combination of the heat leak and generated heat. With heat leak the transfer of thermal energy from the outside to the inside of the cryostat is meant. This section reviews all the sources of heat leak to be able to evaluate the cooling power needed at a later stage.

Heat transfer can be seen as the transmission of thermal energy from one object to another. The transmission of thermal energy can be conveyed by several processes.

Firstly heat can be transferred due to direct contact of objects of different temperatures. Colliding particles of the objects cause a conduction of thermal energy from one object to another. This heat flow is highly dependent on the thermal gradient, the ability of a material to conduct heat and the contact surface of the objects.

Secondly heat transference can be caused by the physical removal or addition of objects that possess thermal energy, advection. Inside the cryostat (stable cryogenic environment) this mechanism plays no role as it is a closed environment.

Thirdly heat can be transferred in forms of convection. Convection is the transference of heat due to the flow of a fluid or gas which can technically be seen as a combination of conduction,

advection and again conduction. Heat transfer due to convection is not evaluated as it is assumed negligible in vacuum or is prevented otherwise.

Lastly heat can be transferred due to radiation. Every object at a higher temperature than 0 K generates (electromagnetic) thermal radiation. This electromagnetic radiation transfers thermal energy to the surface of incidence.

The thermal insulation is focused on reducing all of these sources of heat transmission. Decreasing the heat flow to the cryostat decreases the cooling power requirement.

6.1.1 Heat conduction

In this chapter two bodies with an insulated distance L between them are considered. This is shown in Figure 6.1. The heat transfer due to conduction can in general be approximated by Equation 6.1. [31]

$$Q_c = \frac{A}{L}\int_{T_1}^{T_2} k(T)\mathrm{d}T \tag{6.1}$$

Where A is the interface surface, L is the distance between the two bodies, k is the thermal conductivity and $T_{1,2}$ are the temperatures of the bodies. Equation 6.1 is valid for solids, liquids and most gasses.

From Equation 6.1 the heat transfer per unit area can be approximated by Equation 6.2.

$$\frac{Q_c}{A} = \frac{(T_2 - T_1)(k(T_1) + k(T_2))}{2L} \tag{6.2}$$

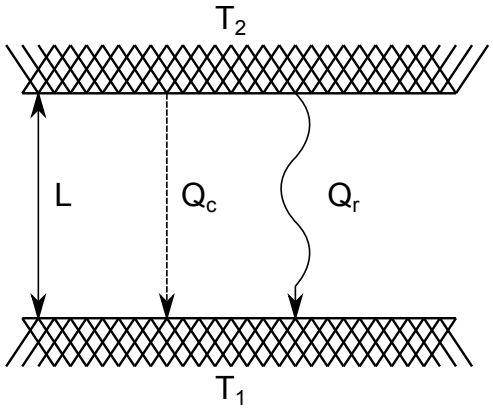

Figure 6.1: Heat transmission between two bodies

Air is commonly used in the thermal insulation of a cryostat. The thermal conductivity of air is low (0.024 $\frac{W}{mK}$ at room temperature) and it is readily available.

Equations 6.1 and 6.2 are valid for air at regular pressures (roughly 10^2-10^6 Pa). Remarkably at these pressures the thermal conductivity is not dependent on the pressure of the gas. This is because the mean-free path a particle can travel without collision increases with decreasing pressure but the particle density also decreases. These two effects counteract each other in terms of number of collisions in the gas.

When the mean-free path (l) of the insulation approaches the insulation dimensions a further increase ceases to influence the thermal conductivity. The mean-free path of a gas can be calculated using Equation 6.3. [32]

$$l = \frac{k_B T}{\sqrt{2}\pi d^2 p} \tag{6.3}$$

Where k_B is the Boltzmann constant, T is the temperature, d is the molecular diameter and p is the pressure.

When $l > 0.1L$ Equation 6.1 is no longer valid. In this case Equation 6.4 is used. Care has to be taken for calculations around $l = 0.1L$ as complicated transition effects occur. [33]

$$\frac{Q_c}{A} = a\frac{(\gamma+1)}{(\gamma-1)}\left(\frac{R^o}{8\pi M\frac{T_1+T_2}{2}}\right)^{\frac{1}{2}} p(T_2 - T_1) \tag{6.4}$$

Where a is the thermal accommodation factor, γ is the specific heat ratio of the gas, M is the molecular weight of the gas and R^o is the molar gas constant.

For an air insulation of 10 mm the heat transfer is calculated for several pressures and temperatures ($T_2 = 293$ K). The results of the calculations are shown in Table 6.1. For the temperatures shown in Table 6.1 pressures lower than 0.1 Pa ensure $l > 10$ mm (Equation 6.3).

The conduction of heat in solids is very similar to the conduction in regular pressurized air. Equations 6.1 and 6.2 are valid for calculations on solid insulation.

Examples of solid insulation materials are G10 epoxy and polyimide. The resulting heat conduction of 10 mm insulation of these materials are shown in Table 6.1.

6.1.2 Heat radiation

The second important source of heat transfer between the cryostat and the outside wall is due to radiation. The energy radiating from a body is given by Equation 6.5. [33]

$$P_r = \sigma\epsilon A T^4 \tag{6.5}$$

Where σ is the Stefan-Boltzmann constant and ϵ is the emissivity of the surface. For the surfaces stainless steel can be chosen which has a low emissivity of around 0.07.

As both bodies emit radiation the heat transfer is given by Equation 6.6. [33]

$$\frac{Q_r}{A} = \sigma\frac{1}{(\frac{1}{\epsilon_1}+\frac{1}{\epsilon_2}-1)}(T_2^4 - T_1^4) \tag{6.6}$$

Assuming two bodies with at least on the surface stainless steel the heat transfer is calculated for 77, 65 and 20 K (T_2 is 293 K). The results are shown in Table 6.1.

	Q_c/A (W/m^2)			Q_c/A (kW/m^2)		Q_r/A (W/m^2)
T_1	10^2 Pa	10^{-1} Pa	10^{-2} Pa	G10 epoxy	Polyimide	Stainless steel
77 K	336.6	37.9	3.8	9.2	3.3	15.1
65 K	342.3	38.9	3.9	9.5	3.4	15.1
20 K	349.8	42.6	4.3	10.0	3.4	15.2

Table 6.1: Heat conduction and radiation of 10 mm material in various conditions

6.2 Joule heating

Another important heat mechanism in cryostats is Joule heating. Heat is generated by the current flowing in the magnet windings. Although we have assumed the resistance of a superconductor to be absolutely zero and this assumption is valid for most electrical evaluations the very small resistances can have an impact on heat management.

The electric field inside a superconductor can be approximated by the so-called power law given in Equation 6.7. [34]

$$E = E_0 \left(\frac{J}{J_c} \right)^n \tag{6.7}$$

Where E_0 is the critical electrical field, J is the current density, J_c is the critical current density and n is the power factor which is usually above 20 for high quality superconductors.

Conventionally a material is considered superconducting when the electric field $E < E_0$ (where $E_0 = 10^{-4}$ V/m).

Using Equation 6.7 the heat generated by the superconducting material is derived and given in Equation 6.8.

$$Q_J = \iiint J E_0 \left(\frac{J}{J_c} \right)^n \mathrm{d}V \tag{6.8}$$

Where V is the volume of the coils superconducting wire.

6.3 Cryostat designs

A cryostat is the encapsulating "box" isolating the low temperature sections from the room temperature environment. When designing a cryostat there are many considerations to be taken. An important consideration is the cryogen (low temperature cooling liquid; most commonly liquid nitrogen, liquid helium or gaseous helium). The choice is mostly dependent on the temperature requirement and the availability of cryogens.

Secondly it has to be chosen if an open or closed loop system is used. An open loop system requires the constant inflow of the cryogens while warm gas is exhausted or collected. The advantage of a closed loop system is that it does not require a (replenishment of the) cryogen.

This section discusses the various types of cryostats to be able to make a choice of the total cryogenic system at a later stage.

6.3.1 Open loop cryostats

Open loop cryostats require the constant inflow of cryogen. Two common open loop cryostats are the bath cryostat and the continuous flow cryostat.

In a bath cryostat the superconducting magnet is simply submerged in a limited amount of cryogen. The operation time of a bath cryostat is very limited as the cryogen evaporates transferring heat to the magnet and counteracting the heat leak. The evaporated gas is exhausted or collected via a relief valve but not re-used. The temperature of the magnet can somewhat be controlled by reducing the pressure inside the cryostat thus lowering the boiling temperature of the cryogen. A cryogenic system with a bath cryostat is initially relatively cheap but can be rather expensive in continuous operation.

An example of a bath cryostat with a relief valve and a connection valve for a pressure pump is shown in Figure 6.2.

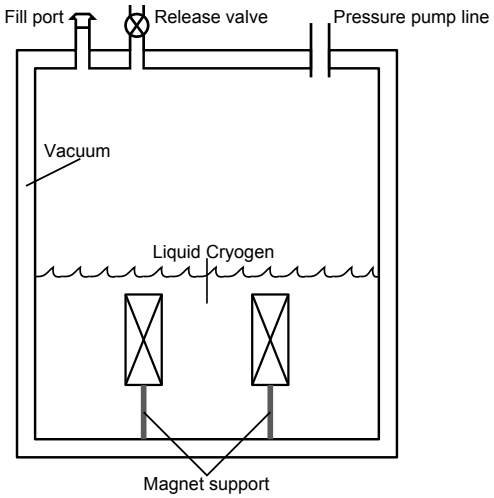

Figure 6.2: Bath cryostat

A continuous flow cryostat is similar to the bath cryostat in the sense that the cryogen is evaporated and released. The continuous flow cryostat on the other hand replenishes the cryogen from a cryogenic container (Dewar). This cryostat is thus not limited in operation time as much as the bath cryostat.

The flow of the cryogen is moderated to regulate the desired temperature of the magnet. This is a huge advantage over a bath cryostat where the temperature of the magnet is fixed to the evaporation temperature of the cryogen.

An example of a continuous flow cryostat is shown in Figure 6.3.

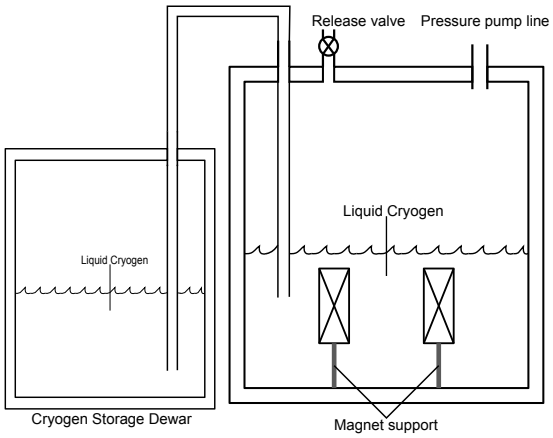

Figure 6.3: Continuous flow cryostat

6.3.2 Closed loop cryostats

Closed loop cryostats do not require the replenishment of the cryogen even for continuous operation. Two common closed loop cryostats are the conduction cooled cryostat and a crycooler system.

A conduction cooled cryostat makes use of a cryorefrigerators cold head to transfer heat from the magnet to outside of the cryostat. Two major advantages of this design are that no cryogen is necessary and no inner cryostat wall is required. On the other hand the initial cost is quite high as cryorefrigerators are relatively expensive.

Most cryorefrigerators operate on the Gifford-McMahon(GM), Stirling or Pulse-tube principles which all use compression and expansion to cool their cold heads. These cryorefrigerators are fairly inefficient as they remove heat at extremely low temperatures and do not even approach the Carnot efficiency.

An example of a conduction cooled cryostat is shown in Figure 6.4.

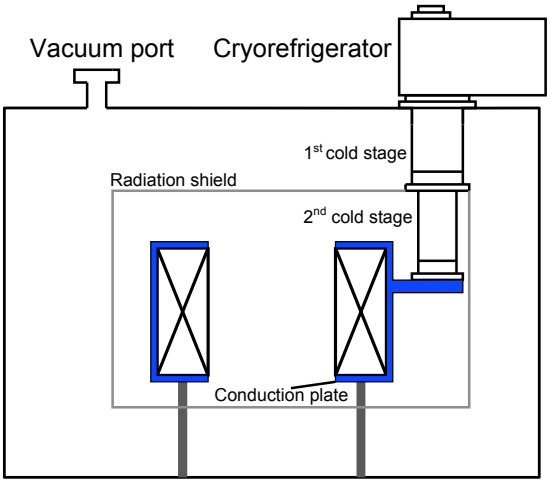

Figure 6.4: Conduction cooled cryostat

A cryocooler makes use of a cryorefrigerator to condense or cool the exhaust gasses recovered from the cryostat. The main advantage of a cryocooler over every alternative is the ability to control the temperature with relative ease and very low temperatures can be achieved.

An example of a cryocooler system and is shown in Figure 6.5.

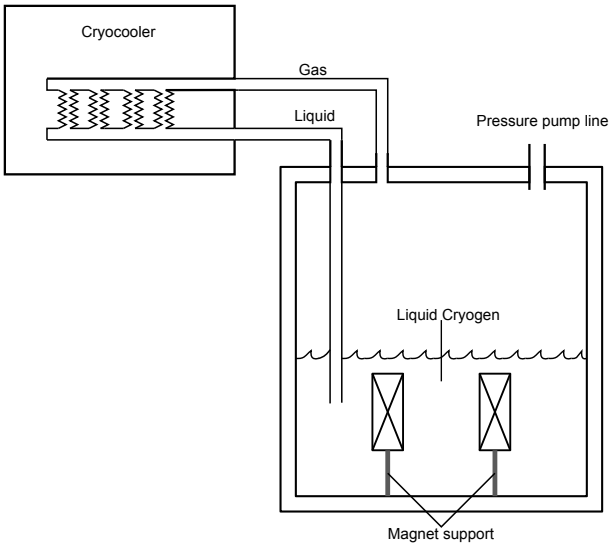

Figure 6.5: Cryocooler system

6.4 Thermal concepts conclusions

The goal of this chapter was to acquire the knowledge to assess the thermal aspects of a superconducting machine.

The different heat transference mechanisms were evaluated at cryogenic temperatures to be able to do heat leak calculations at a later stage. In cryogenic environments the most important mechanisms are conduction and radiation where conduction is dominant up to very low pressures. Calculations were made to be able to assess the heat leak of the actual system at a later stage.

Another important mechanism is Joule heating. Joule heating accounts for the (small) resistive losses in the superconductor.

Various cryostats were discussed including open (bath and continuous flow) and closed loop (conduction cooled and cryocooler) systems.

Chapter 7
Linear machine concepts

Contents

Now that the various magnet and cryostat concepts are discussed multiple concepts of superconducting linear machines are provided. The goal of this chapter is to provide several design options for a superconducting linear actuator. In all concepts some form of superconductive material is used.

First conventional machines (DC, SM and a SRM) are redesigned using superconductors in section 7.1. Second more unconventional machines are designed that aim for more novel superconducting machine designs in section 7.2. Figure 7.1 represents a legend for the various machine design figures.

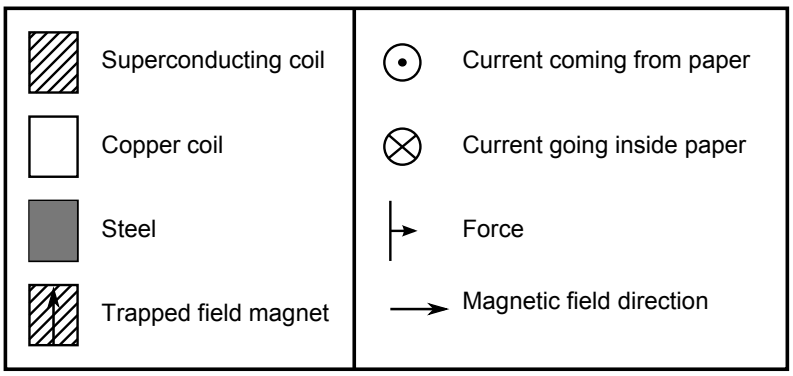

Figure 7.1: Legend for different machine designs

7.1 Conventional linear machines

This section discusses superconducting variations to the linear machines that are widely commercially available. Variations on DC, synchronous and synchronous reluctance machines are discussed.

The first machine to be discussed is the DC machine. Superconductive material is introduced into the DC machine by replacing the field windings by a superconductive coil or a trapped field magnet. This is shown in Figure 7.2.

The armature is in this case a simple direct current operated coil which is to be mechanically commutated. Besides the horizontal force depicted in Figure 7.2 there is also an alternating vertical force present. The vertical force can either be used or compensated using an additional coil or mechanical support.

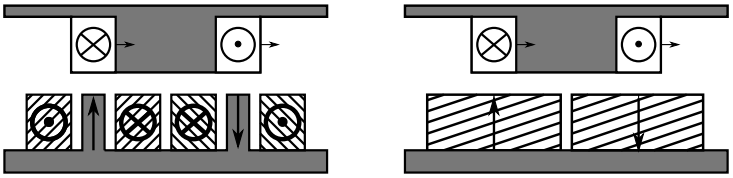

Figure 7.2: Superconducting Linear DC Machine (SLDCM)

Secondly a synchronous machine is shown in Figure 7.3. The field windings are again replaced by a superconducting coil or trapped field magnets.

The difference with the DC machine lies in the armature which in this case consists of three phase windings. In this case the vertical force is automatically compensated but an additional vertical force can be generated by additional windings or a superposition of a current on the armature.

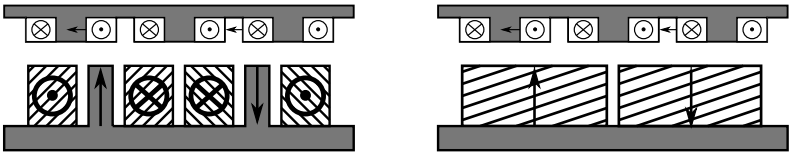

Figure 7.3: Superconducting Linear Synchronous Machine (SLSM)

An induction machine is not viable. The induction machine operates on the resistance in the short-circuited construction. As the superconductors have no resistance no torque would be generated.

The last of the conventional machines is the synchronous reluctance machine. In a superconducting synchronous reluctance machine bulk superconducting material is used to increase the reluctance of the machine in certain positions. This machines makes use of the fact that superconducting material expels magnetic field.

The phases can either be switched to make a stepped motor or operated in three phase to create a continuous motion. The synchronous reluctance superconducting motor is shown in Figure 7.4.

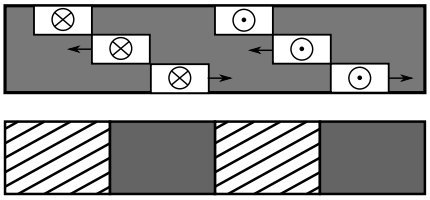

Figure 7.4: Superconducting Synchronous Reluctance Machine (SSRM)

7.2 Unconventional linear machines

Limiting the design possibilities to the conventional machine could possibly limit the machine performance. This section is focused on less conventional machine designs.

A less conventional design for a machine is a superconducting levitation machine shown in Figure 7.5. This machine makes a vertical movement and is horizontally unstable. Stability can be achieved by either mechanical support or by suspending this machine upside down and reversing polarity of the superconducting magnets (This would require mechanical support when the machine is off).

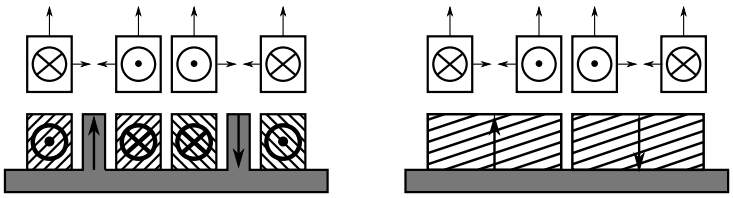

Figure 7.5: Superconducting Levitation Machine (SLM)

Another novel design is the superconducting homopolar machine shown in Figure 7.6. This machine is named superconducting homopolar machine as it has borrowed characteristics of a homopolar machine (the armature does not requires commutation).

The lower part of the superconducting homopolar machines armature, where the current is coming from the paper, is a conducting plane connected to the top part by brush contacts. Only the top part moves while the brush contacts slide over the bottom plane.

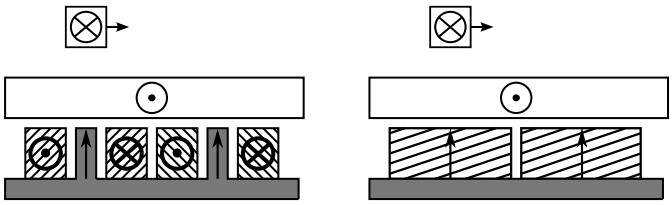

Figure 7.6: Superconducting Homopolar Machine (SHM)

When using a superconducting material, which is not anisotropic, another possible design is using a superconducting voice coil machine shown in Figure 7.7. Using opposite magnets with opposite polarity strongly increases the magnetic field at the position of the armature. On the other hand this also causes the field perpendicular to the superconducting material to increase.

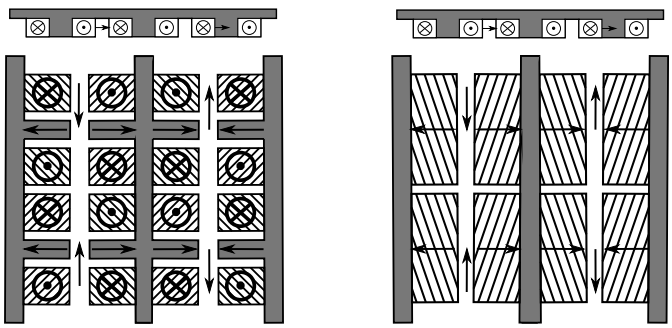

Figure 7.7: Superconducting Voice Coil Machine (SVCM)

As seen in the previous chapters it is beneficial for a machine to use the magnetic field inside the solenoid instead of a distance outside the solenoid. Utilizing the field at the center of the solenoid requires an unusually shaped configuration. Two possible configurations of such a machine are shown in Figures 7.8 and 7.9.

These two unconventional machines only facilitate short-stroke operation. The maximum stroke length of both these machines is limited by the bore radius of the solenoids.

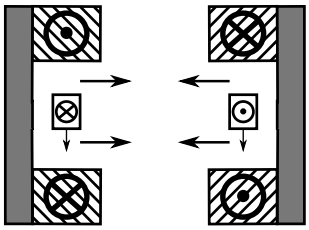

Figure 7.8: Superconducting Short Stroke Machine (SSSM)

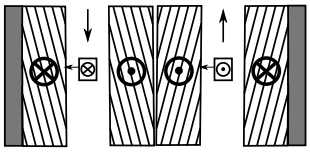

Figure 7.9: Superconducting Bedstead Machine (SBM)

The last of the unconventional machines is the transverse flux machine shown in Figure 7.10. The transverse flux machine's armature moves parallel to the current of the copper coil (colored red for convenience of understanding the figure). Building a transverse flux machine has some difficulty as the steel has to be specially shaped. The advantage of these machines is their high power density.

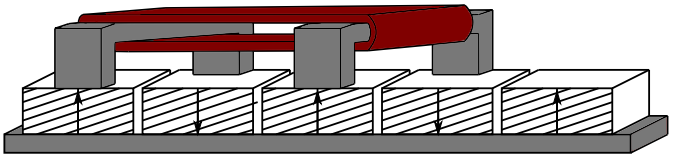

Figure 7.10: Superconducting Transverse Flux Machine (STFM)

7.3 Linear machine concepts conclusions

The goal of this chapter was to provide several machine designs. At a later stage a design choice of one of these machines is made.

The conventional machines (DC, synchronous and synchronous reluctance machines) were redesigned using superconductors. An important aspect when making an actual (mechanical) design are the vertical forces that can be generated by the machines.

Also some unconventional designs were made. Machines with an unconventional operation (levitation and homopolar machine), magnet usage (voice coil machine) and mechanical design (short stroke, bedstead and transverse flux machine) were introduced.

In the next chapter an optimal choice for the linear actuator consistent with the design requirements is made.

Chapter 8

Actuator design

Contents

In the introduction some initial design boundaries were set. AC operation of superconductors is not considered and in this design the weight and the volume of the stator are not of much importance.

The goal of this chapter is to evaluate the various possibilities and arrive at a basic actuator design. First choices of actuator topology, superconductive magnet and cryostat type are made in section 8.1. Second more specific design choices are made in section 8.2. Last the stator and armature coils are designed in sections 8.3 and 8.4 respectively.

8.1 General design choices

The previous chapters presented various concepts for superconductive magnets, cryostats and actuator designs. In this section a design choice is made for each of these components of the linear actuator.

8.1.1 Actuator topology

Chapter 7 discussed 10 possible actuator topologies. Every topology has its strengths and weaknesses and is more or less suitable for certain applications. In this section the topology most suitable for this design is chosen.

An induction machine topology is incompatible with this design. In the introduction it was mentioned AC operation of superconductors will not be considered. Therefore an induction machine topology can not be considered.

A synchronous reluctance topology is illogical for this design. A superconducting synchronous reluctance actuator offers an increase in performance over a switched reluctance actuator that uses iron. However the forces generated by a superconducting actuator with magnetized superconducting material is an order of magnitude higher.

The levitation machine is very suitable for applications where position of the mover is to be regulated with accuracy. Depending on the current flowing in the armature the mover would remain at a certain distance from the magnets.

As the distance between the armature and magnets is increased the force that can be generated quickly decreases. Large stroke lengths are therefore difficult to achieve making it incompatible with this design.

A homopolar actuator is a rather simple topology. The magnets of a homopolar topology are magnetized in the same direction. As a consequence the field perpendicular to the length of the magnets is decreased. This topology is therefore attractive to use with anisotropic superconductors.

On the other hand it is difficult to design a homopolar motor with an armature that has more than one turn. Also brush contacts are necessary which increase the complexity of the actuator. A homopolar topology is therefore considered to be unsuitable for this design.

A voice coil topology is used when the magnetic field is to be increased and the magnet dimensions are of less importance. This is the case in this design if the superconducting magnets are in the stator.

However the voice coil topology greatly increase the magnetic field perpendicular to the length of the magnet. Because anisotropic materials are considered for the superconducting magnets this topology is not suitable for this design.

The short stroke and bedstead actuators seem as attractive topologies because these actuators use the field inside the superconductive coil. Utilizing the fields inside the coils is beneficial as much higher fields can be achieved inside than outside a coil.

However for this application the required stroke length is 40 cm. Assuming $\alpha = 5$ this would result in a minimum diameter of 2 meters of each magnet (Equation 4.1). A short stroke or bedstead topology is therefore incompatible with this design.

The main advantage of a transverse flux topology generally is the high power density. Magnetic fields generated by superconducting magnets are generally high enough to drive the iron far past saturation. The inability to control the flux lines with iron defeats the purpose of such a topology.

The remaining suitable topologies of a superconducting actuator are a synchronous actuator and a DC actuator. Fact is these topologies are fairly similar. The main difference is that a DC machine is mechanically commutated and only has 1 phase.

The synchronous actuator is chosen as the most suitable topology because this topology generates a constant horizontal force and eliminates vertical forces. Additionally a synchronous actuator does not use mechanical commutation.

8.1.2 Superconducting magnet

The actuator topology was chosen to be a synchronous actuator in the previous section.

Chapter 4 and 5 discussed the three superconductive magnet concepts for high and low temperatures. In this section the most suitable superconductive magnet is chosen.

As it is decided a synchronous actuator is used for this design it is impossible to use the field generated by the field inside a coil magnet.

Figure 4.16 shows the fields that are theoretically achievable at 15 mm from the magnet with trapped field magnets. The performance of commercially available YBCO TFM's is not close to these theoretically achievable fields (with current technology). The achievable fields of these TFM's are about a factor 6 lower than in Figure 4.16. [35] This makes the increase in field compared to the 0.7 T of the permanent magnets only marginal (even at lower temperatures).

Also, using trapped field magnets would require magnetization after each warm up of the superconductors. Additionally the magnetization must happen at fields about twice the trapped field. These fields can only be generated by a superconducting coil.

Trapped field magnets are therefore very unpractical besides only marginally increasing performance. The only viable option for this design are coil magnets. More specifically coil magnets where the field outside of the coil is used.

8.1.3 Cryostat type

Chapter 6 showed several concepts of cryostats. Every type of cryostat has its strengths and weaknesses and is more or less suitable for certain applications. In this section a suitable cryostat type is chosen.

For a continuously operated actuator the only viable option is a closed loop system. If an open loop system would have been chosen the actuator would have to be interrupted at intervals to replenish the cryogen. Open loop systems are ideal for testing purposes (as closed loop systems are more expensive) but are not suitable for continuously operated applications.

A cryocooler system requires two cryostat walls as the superconducting magnet is submerged in a cryogen isolated from the outside by vaccuum (Figure 6.5). In the conduction cooled system the superconducting magnet is in the vaccuum thus requiring only one wall (Figure 6.4). Having only one wall reduces the gap between the superconducting magnet and the armature.

Another advantage of a conduction cooled system is that it is cheaper than a cryocooler system. At 65 K a cryorefrigerator costs about 150 $/W of cooling power while the cryocooler system costs about 450 $/W. At 25 K a cryorefrigerator costs about 430 $/W of cooling power while the cryocooler system costs about 1200 $/W. [36]

Additionally a conduction cooled system is cryogenless and less bulky. Therefore for this design a conduction cooled system is chosen.

8.2 Specific design choices

A general design of the superconducting linear actuator was chosen in the previous section. A synchronous actuator with superconducting coils cooled by a cryorefrigerator via conduction cooling is used.

This section makes some more specific design choices such as the operating temperature and the materials used.

8.2.1 Operating temperature and superconducting materials

One of the most influential choices of a superconductive actuator is the choice of operating temperature. Common design choices for temperatures are 77, 65, 20 and 4 K.

The fields achieved with a 100 mm solenoid at 77 and 65 K are 0.76 and 1.34 T respectively. These fields are not substantially higher than the 0.7 T of the permanent magnets to justify the use of expensive superconducting material. Therefore 77 and 65 K are not considered to be viable for this design.

Operating at 4 K requires a pulse tube refrigerator. The cooling power of these pulse tube refrigerators is very limited (to about 40 W). This cooling power limitation puts high demands on the heat management of the system (see Chapter 6).

Additionally these pulse tube refrigerators use two stages to cool down the target. This means that an extra encapsulated environment must be created which would further increase the gap between the armature and the superconducting magnets.

These arguments lead up to the conclusion an operating temperature of 20 K is the most suitable choice for this design. Additionally the superconducting materials considered for this design are YBCO and MgB_2. YBCO and MgB_2 are the only viable materials at this temperature.

8.2.2 Cryostat design

Another important choice is to either include or exclude the armature in the cryostat. Including the armature in the cryostat has the advantages of only needing one cooling system and low armature wire resistance.

Including the armature in the cryostat also has several disadvantages. First some form of force transfer element is needed to transfer the force from the cryogenic environment to the room temperature environment. This transfer element would greatly increase the complexity of the system and add additional weight to the mover.

Second including the armature in the cryostat introduces a new heat source to the cryostat as the armature is not lossless. The resistivity of copper is $2.8 * 10^{-11}\Omega$m at 20 K. Using the armature of the reference permanent magnet synchronous actuator (found in the next chapter) the heat production of one coil can be approximated. At maximum current density the losses of three armature coils would be around 25 W.

The extra complexity and the heat generated by the armature lead to the the conclusion that for this design only the superconductive magnets are chosen to be inside the cryostat.

Another important design aspect of the cryostat is the stainless steel wall thickness. The deflection (bending) of a plate under pressure can be approximated by Equation 8.1. [37]

$$w_{max} < \frac{5}{32}\frac{Pl^4}{Et^3} \tag{8.1}$$

Where w is the deflection, P is the pressure, l is the length of the beam (plate), E is the Young's modulus and t is the thickness of the plate.

For a length of 200 mm this would require a thickness of 5 mm to limit the deflection to 1 mm. The minimal cryostat wall thickness is therefore chosen to be 5 mm.

8.2.3 Armature

For the armature a couple of choices have to be made. First the armature is either chosen to be in the stator or in the mover. Second the armature winding configuration has to be chosen.

The main advantage of having the armature in the stator is that the number of required superconducting magnets is strongly decreased (at the very least 2 poles).

However putting the armature in the stator introduces several difficulties. The weight of the mover would be increased as the superconducting magnets are generally bulkier than the armature windings and the weight of the cryostat would be added to the mover. Additionally the coupling between the cryorefrigerator and its compressor would be required to withstand the forces and movement of the cryostat.

Therefore for this design it is chosen to put the armature on the mover and keep the superconductive magnets stationary.

There are many ways to wind the armature coils. Generally a distinction is made between distributed and concentrated windings. The main advantage of distributed windings is that the space harmonics are much lower compared to concentrated windings.

On the other hand the end windings of distributed winding are much longer and bent. This increases the copper losses, the weight of the mover and complicates the cooling of the armature windings. Additionally the forces generated by concentrated winding armatures are generally slightly higher.

As space harmonics can also be countered by using an EM shield (if necessary) the choice of this design is concentrated windings.

8.2.4 Stator

The magnetic field produced by an armature contains space harmonics. These space harmonics result in AC magnetic fields at the superconducting coils inducing AC currents in the coils. AC currents flowing through the superconducting coils accommodate a loss mechanism through hysteresis (and causes heat generation).

The AC fields produced by the armature can be blocked by an electromagnetic shield. A conducting plate can be placed between the stator and the mover. Eddie currents would be generated in the plate partly screening the stator from the AC magnetic fields.

But as AC mechanisms are beyond the scope of this thesis the loss mechanism can not be analyzed. An electromagnetic shield is thus not considered in this design. Although the cryostat wall partly fulfils a screening role it is recommended that these mechanisms are analyzed before an actual actuator is manufactured.

8.2.5 Air gap

Up until now the total "air" gap (the gap between the stator and rotor) was assumed to be 15 mm. A minimal gap is preferred as the magnetic field at the armature is increased with decreasing gap.

A 2 mm space is necessary for the cooling plates of the armature and 2 mm for mechanical clearance between the cryostat wall and the armature cooling plates resulting in a 4 mm air gap. The cryostat wall thickness was determined to be 5 mm which resulted in a maximum deflection of 1 mm. An additional 2 mm clearance between the cryostat wall and the stator is chosen for this actuator. The total gap between the stator and the rotor is therefore 12 mm.

8.3 Stator design

In the previous sections the general design of the superconducting actuator was chosen. In the stator superconducting coils are used to generate magnetic field. This section focuses on the design of these superconducting coils and the back iron.

Racetrack coils are versatile coils as the depth (d) of the magnets can arbitrarily be chosen. Also one racetrack coil is generally cheaper and generates a more homogeneous field over the depth than multiple solenoids. For these reasons, even though solenoids generally generate higher fields, racetrack coils are used.

A model of a racetrack coil is shown in Figure 8.1. A racetrack coil that generates a magnetic field 12 mm outside the racetrack coil is designed in this section.

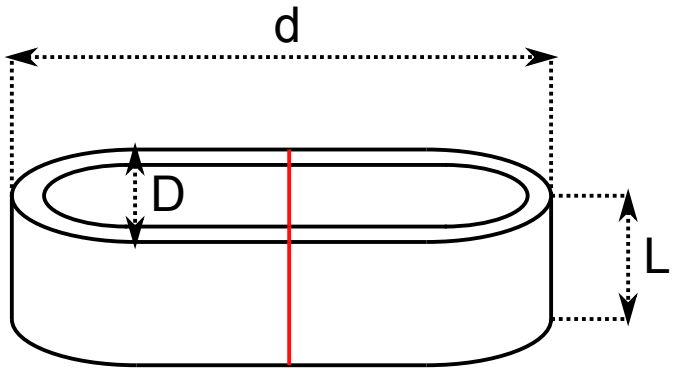

Figure 8.1: Model of a racetrack coil

The cross-section (the red line in Figure 8.1) and the positions of the fields of interest from the racetrack coil are shown in Figure 8.2. The same schematic is used as a model for the racetrack coil in 2D FEM calculations.

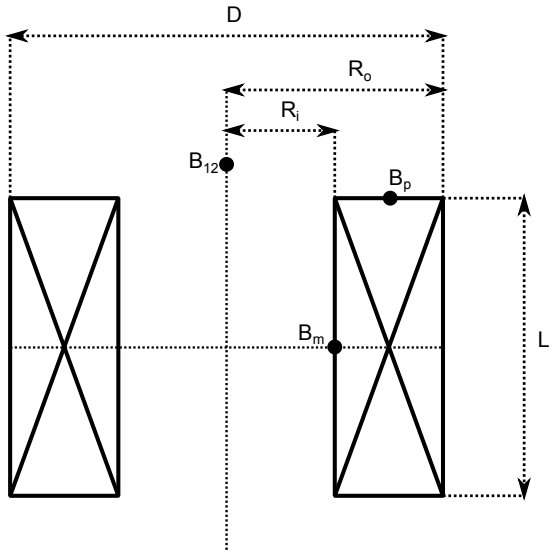

Figure 8.2: Cross-section and 2D FEM model of a racetrack coil

As no analytical calculations are made geometric parameters need not be used. But for the purpose of continuity of this thesis and comparability with the solenoids α and β are used.

The geometric parameters α and β are defined by Equations 8.2 and 8.3.

$$\alpha = \frac{R_o}{R_i} \tag{8.2}$$

$$\beta = \frac{L}{2R_i} \tag{8.3}$$

The critical current characteristics for YBCO and MgB_2 wire at 20 K can be approximated by Equations 8.4 and 8.5 respectively (estimated from Figures 4.3 and 5.1). Here the YBCO wire is dependent on the perpendicular field while the less anisotropic MgB_2 wire is dependent on the maximum field (see Chapter 5).

$$J_{crit,YBCO} \approx 9.82 * 10^8 \frac{1}{\sqrt{B_p}} \tag{8.4}$$

$$J_{crit,MgB2} \approx 8.0 * 10^8 \frac{1}{B_m^{1.25}} \tag{8.5}$$

Similarly to Chapter 4 and 5 the maximum achievable field can be approximated using linear equations. A linear approximation of the fields generated by the racetrack coil is made according to Equations 8.6 to 8.8.

$$B_m = \mu_0 J C_m \tag{8.6}$$

$$B_{12} = \mu_0 J C_{12} \tag{8.7}$$

$$B_p = \mu_0 J C_p \tag{8.8}$$

The geometric constants C_m ,C_{12} and C_p are not determined using analytical expressions but by FEM calculations. This way the effect of both linear variations (α, β, D) and non-linear variations can be evaluated.

The approximated maximum achievable fields are derived in a similar fashion as in Chapter 4 and are given by Equations 8.9 and 8.10.

$$B_{12,max,YBCO} \approx \frac{(9.82 * 10^8 * \mu_0)^{\frac{2}{3}} C_{12}}{C_p^{\frac{1}{3}}} \tag{8.9}$$

$$B_{12,max,MgB2} \approx \frac{(8.0 * 10^8 * \mu_0)^{0.44} C_{12}}{C_m^{0.56}} \tag{8.10}$$

When making a design for the actuator the cost of the superconducting magnet becomes important. To be able to evaluate the cost effects of design choices the volume of the racetrack coils needs to be evaluated. The volume of a racetrack coil is given by Equation 8.11.

$$V_{racetrack} = \pi L(R_o^2 - R_i^2) + 2L(R_o - R_i)(d - 2R_o) \tag{8.11}$$

Equation 8.11 can be modified to calculate the volume from the geometric parameters (D, α and β) the result is Equation 8.12.

$$V_{racetrack} = \frac{1}{4}\pi D^3 \beta \left(\frac{1}{\alpha} - \frac{1}{\alpha^3}\right) + D^2 \beta (d - D)\left(\frac{1}{\alpha} - \frac{1}{\alpha^2}\right) \tag{8.12}$$

The goal of making a design for the superconducting racetrack coils is finding a balance between limiting the volume of the coil and maximizing the achievable field.

First various diameters for the superconducting racetrack coil are evaluated. For various diameters while $\alpha = 5$ and $\beta = 1$ the geometric constants C_m, C_{15} and C_p are determined. Subsequently the maximum achievable fields and the total volume of the racetrack coils in the stator are approximated. The results are shown in Figure 8.3.

The total volume of the racetrack coils is estimated by assuming a depth (d) of 500 mm (which is necessary for higher diameters). The total volume is calculated by determining the number of required poles and multiplying that by the volume of one racetrack coil.

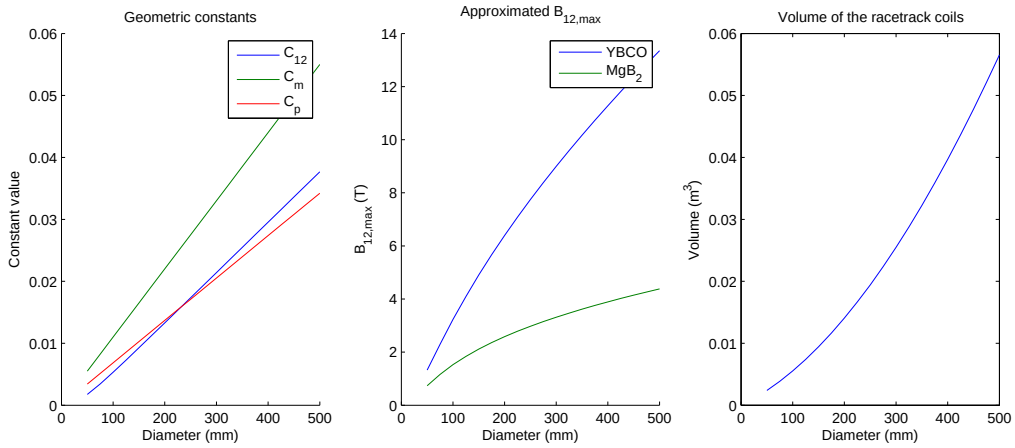

Figure 8.3: Approximation of the maximum achievable field and volume for various diameters

As the diameter of the superconducting coils 100 mm is chosen. At diameters lower than 100 mm the achievable field is relatively low and would not provide a significant improvement over permanent magnets. Diameters higher than 100 mm are not chosen either because the superconducting magnets become even more expensive. For example a diameter of 200 mm would increase the achievable field by about 85% while increasing the volume (cost) of the racetrack coils by 160% compared to the 100 mm coils.

Second the geometric constant α is evaluated. For various α while $\beta = 1$, $d = 200$ mm and $D = 100$ mm the constants C_m, C_{15} and C_p are determined. After this the maximum achievable fields and the volume of one racetrack coil is approximated. The results are shown in Figure 8.4.

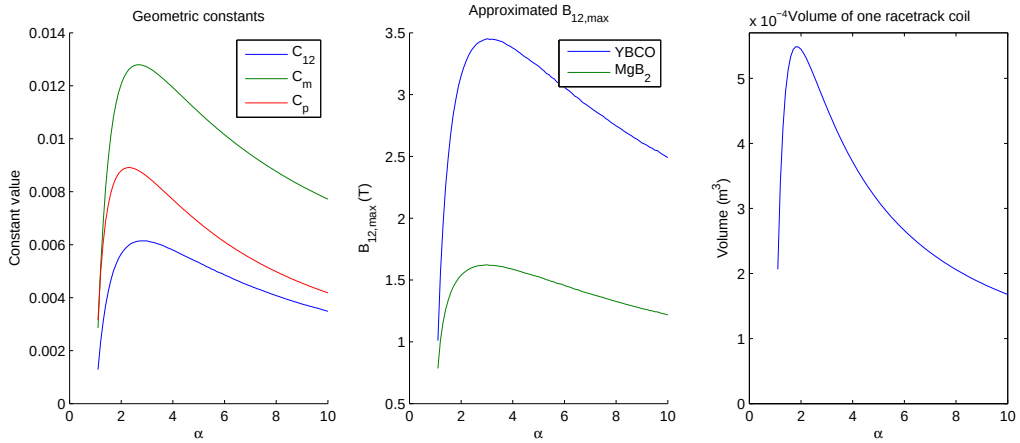

Figure 8.4: Approximation of the maximum achievable field and volume for various α

α is chosen to be 5 for the superconducting racetrack coils. The field peaks at an α of around 2.5 but the volume of the coil peaks as well. At an α of 5 the maximum achievable field has only decreased by about 10% while the volume (cost) has decreased by about 65% compared to an α of 2.5. An even higher α is not viable as, with $\alpha = 5$ and a diameter of 100 mm, the inner radius is already near the minimum bend diameter of the YBCO wire.

Last the geometric constant β is evaluated. For various β while $\alpha = 5$, $d = 100$ mm and $D = 100$ mm the constants C_m, C_{15} and C_p are calculated. The maximum achievable fields and the volume of one racetrack coil are approximated. The results are shown in Figure 8.5.

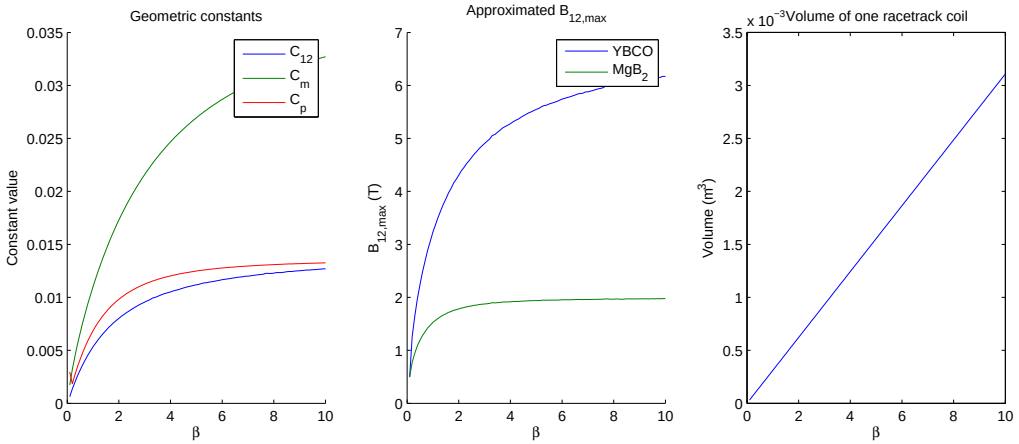

Figure 8.5: Approximation of the maximum achievable field and volume for various β

β is chosen to be 1 for the superconducting racetrack coils. At a β lower than 1 the field is deemed to be insignificantly higher than fields generated by permanent magnets. A beta higher than 1 is not viable as much additional material is used for only marginal performance increase (especially for MgB_2 wire).

Besides the coil dimensions there are two more parameters of the stator namely the gap between coil magnets g_m and the length of the back iron L_{bi}. These parameters are shown in Figure 8.6.

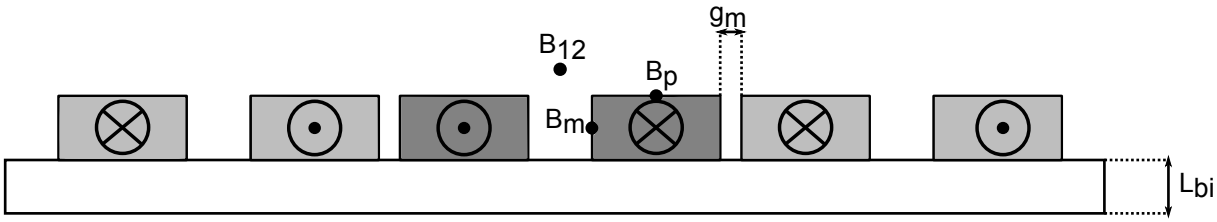

Figure 8.6: Stator schematic and 2D FEM model

The parameters g_m and L_{bi} do not have linear effects on the actuator. A linear approximation can be made by calculating C_m, C_{15} and C_p using FEM at a current density close to the operating point (to increase accuracy). With the geometric constants the maximum achievable fields can be approximated using Equations 8.9 and 8.10. For the computation racetrack coils with $D = 100$ mm, $\alpha = 5$, $\beta = 1$ carrying a current density of 440 A/mm^2 are used. The geometric constants and the maximum achievable fields are shown for various g_m and L_{bi} in Figure 8.7.

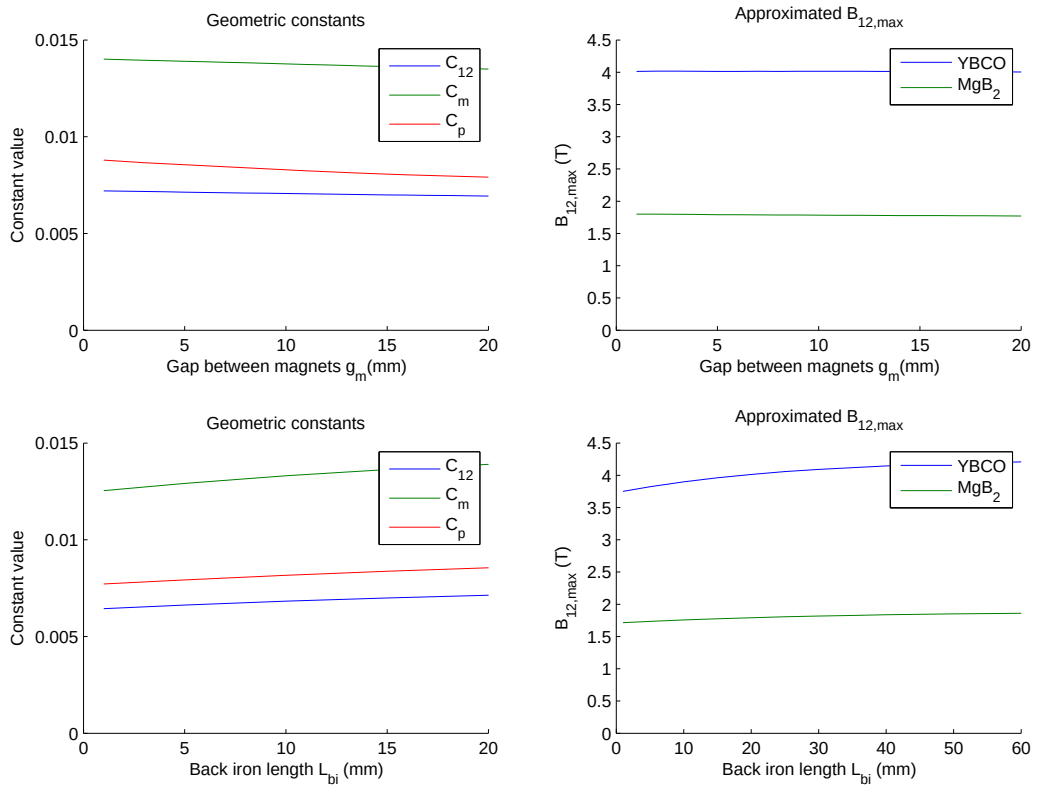

Figure 8.7: Approximation of maximum achievable fields for various g_m and L_{bi}

According to Figure 8.7 g_m can more or less arbitrarily be chosen. The gap between the magnet poles (racetrack coils) g_m is chosen to be 5 mm.

The back iron length L_{bi} is chosen to be 20 mm. At larger lengths of the back iron the increase in field is minimal while the total dimensions and weight of the cryostat are increased. Increasing the dimensions of the cryostat increases the heat leak which is highly unwanted.

The depth of the superconducting coils can somewhat be chosen arbitrarily. But at depths of the racetrack coil close to the diameter D the racetrack starts to behave like a solenoid. In this case the 2D FEM models (Figure 8.2) used to determine the maximum achievable fields are not valid. The depth is chosen to be 200 mm to ensure the approximations remain valid.

The specifications of the superconducting coil magnets are summed up in Table 8.1.

Magnet specifications	
Magnet length	20 mm
Magnet width	100 mm
Magnet inner radius	10 mm
Magnet depth	200 mm
Gap between poles	5 mm
Back iron length	20 mm

Table 8.1: Magnet specifications

8.4 Armature coil design

A stator design has been made in the previous section. This section focuses on designing the armature (mover) of the actuator.

In the next chapter the superconducting actuator is compared with a high performance permanent magnet synchronous motor. The specifications of the stator and mover of the PM actuator are shown in Table 8.2.

Stator specifications	
Magnet length	15 mm
Magnet width	40 mm
Magnet inner radius	-
Magnet depth	200 mm
Gap between poles	4 mm
Back iron length	20 mm
Mover specifications	
Armature pole pair span	2 pole pairs
Armature length	15 mm
Armature width	50 mm
Armature inner radius	5 mm
Armature depth	200 mm
Gap between armature poles	$8\frac{2}{3}$ mm

Table 8.2: Permanent magnet actuator specifications

For several reasons the armature of the superconducting actuator is chosen to be a scaled version of the permanent magnet actuators armature. First, scaling the armature increases comparability between the two actuators. Second, the optimization of an armature involves extensive thermal and mechanical engineering beyond the scope of this thesis. Last, the optimization of an armature differs per application and for this thesis no definite application is specified.

The remaining design choice is the armature pole pair span. The armature pole pair span is the number of pole pairs that the three-phase armature envelops. An armature pole pair span of one pole pair means the three-phase armature has a total width equal to the width of two poles. Only pole pair spans of one, two and three pole pairs are evaluated because a larger span than three would not result in a higher generated force.

For each of these armature pole pair spans a scaled version of the permanent magnet armature is used. The specifications of these armatures are shown in 8.3.

Armature pole pair span (pole pairs)	1	2	3
Phase length (mm)	15	15	15
Phase width (mm)	60	120	180
Phase inner radius (mm)	6	12	18
Phase depth (mm)	200	200	200
Gap between Phases (mm)	10	20	30

Table 8.3: Specifications of the armatures for several armature spans

The armature spans is evaluated according to the force per unit mass (their acceleration). 2D FEM is used to compute the forces on the armature. The force is calculated by integrating $B \times J$ over the armature to get the Lorentz force. The result is the force per mm of depth (N/mm). The 2D model and the axes (x, y and z) used are shown in Figure 8.8.

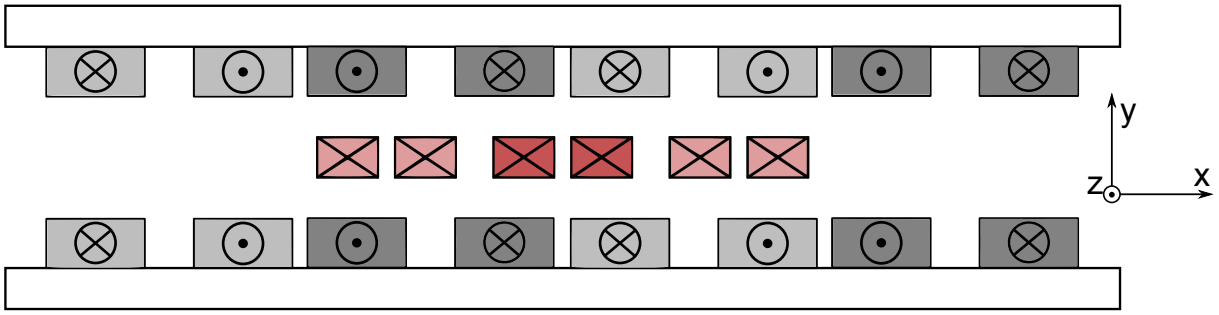

Figure 8.8: 2D FEM model of the superconducting linear actuator

Not the entire racetrack coil is similar to the model as a racetrack has half of a hollow cylinder at each end. To estimate the total force of the actuator an effective armature depth d_{eff} has to be introduced. The effective armature depth is assumed to be composed of the depth of the beams and 50% of the depth of the two half hollow cylinders. The effective depth d_{eff} is shown in a top view of the armature coil in Figure 8.9.

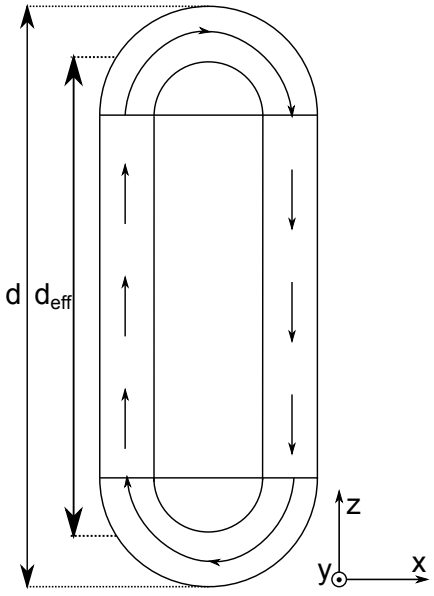

Figure 8.9: Top view of an armature coil and the current flowing in the armature

A current density of 50 A/mm^2 is used for the armature. This current density is assumed to be the maximum current density for water cooled copper.

The magnets used have specifications found in Table 8.1 and carry a current density of 440 A/mm^2 (which is assumed to be close to the operating point of YBCO coils).

Equation 8.11, a fill factor of 70% and a copper mass density of 8960 kg/m^3 is used to compute the volume and subsequently the mass of the mover.

Using the 2D FEM computation, the effective depth and the mass of the armature the force per mass unit can be calculated. The force per unit mass for each of the pole spans is shown in Figure 8.10.

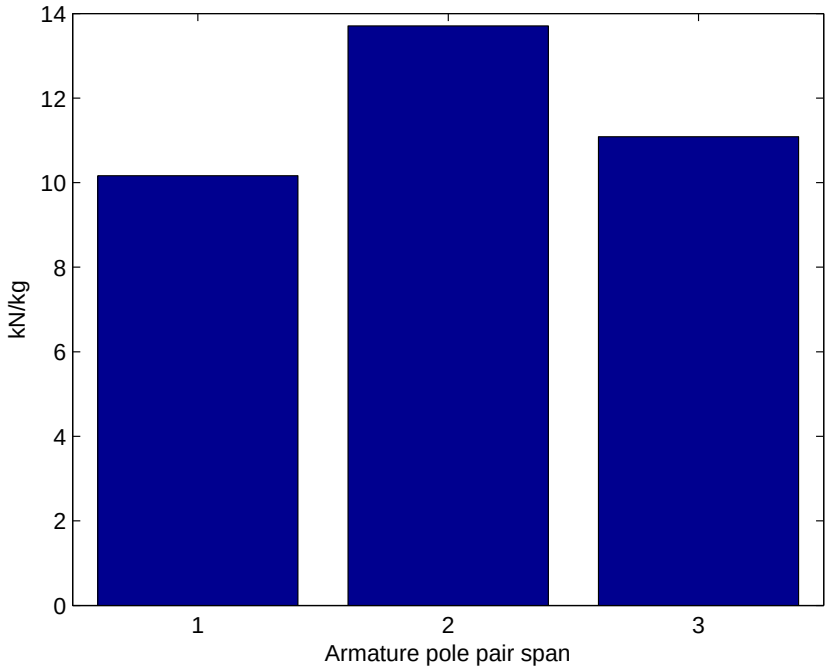

Figure 8.10: Force per unit mass for various pole spans

From Figure 8.10 it can be seen that the largest force density (N/kg) can be generated with a pole pair span of 2. But for a span of 2, assuming a required stroke length of 40 cm, the number of magnet poles used increases from 6 (for a span of 1) to 8. This means the cost increases by 33% which is similar to the increase in force density. For this design a pole pair span of 2 is chosen as this increases comparability with the permanent magnet actuator.

The results from Figure 8.10 must not be taken as an absolute. The force density is calculated solely by the mass of the copper in the armature. Practically the total mass of the total mover is about 4 to 6 times higher.

The complete specifications of the armature are summed up in Table 8.4.

Armature specifications	
Armature span	2
Phase length	15 mm
Phase width	120 mm
Phase inner radius	12 mm
Phase depth	200 mm
Gap between Phases	20 mm

Table 8.4: Armature specifications

8.5 Actuator design conclusions

In this chapter many design choices were made. The superconducting linear actuator is a synchronous machine with superconducting racetrack coil magnets in the stator and the armature windings in the mover. As armature three phase concentrated windings are used.

The operating temperature of superconducting magnets is 20 K. A cryorefrigerator is used to cool the superconducting magnets by means of conduction cooling. The encapsulating cryostat has a stainless steel wall of at least 5 mm thick to limit the deflection to 1 mm. The resulting total gap between the magnets and the armature is 12 mm.

As superconductive magnets both YBCO and MgB_2 racetrack coils are considered. These racetrack magnet coils have a diameter of 100 mm, an inner radius of 10 mm and a length of 20 mm. The depth of the racetrack coils is chosen to be 200 mm.

In the armature copper racetrack coils are used. The following chapter compares the superconducting synchronous actuator with a high performance actuator permanent magnet actuator. Therefore the armature of the superconducting machine is a scaled version of the permanent magnet actuators armature. The armature spans over 2 pole pairs and has a diameter of 120 mm, an inner radius of 12 mm and a length of 15 mm.

The electromechanical specifications of the stator and the armature were determined. These specifications are summed up in Table 8.5.

Stator specifications	
Magnet length	20 mm
Magnet width	100 mm
Magnet inner radius	10 mm
Magnet depth	200 mm
Gap between poles	5 mm
Back iron length	20 mm
Mover specifications	
Armature span	2 pole pairs
Armature length	15 mm
Armature width	120 mm
Armature inner radius	12 mm
Armature depth	200 mm
Gap between armature poles	20 mm

Table 8.5: Superconducting machine electromagnetic specifications

Chapter 9

Actuator analysis

Contents

In the previous chapter an electromechanical design was given for the superconducting linear actuator. Chapter 6 discussed the several heat leak and generation sources in detail.

This chapter focuses on evaluating the superconducting linear actuator. First the electromechanical performance is analyzed in section 9.1. Second the thermal feasibility of the actuator is evaluated in section 9.2. Last the costs of the superconducting linear actuator are estimated in section 9.3.

9.1 Electromechanical analysis

In this section the electromechanical performance of the superconducting linear actuator designed in the previous chapter is evaluated.

To be able to evaluate the designed actuators performance a reference actuator is necessary. As reference an existing high performance permanent magnet linear actuator is used. First the electromechanical performance of the PM linear actuator is evaluated. Second the performance of the SC (superconducting) linear actuator is analyzed. Last the SC linear actuator is compared to the permanent magnet actuator.

9.1.1 Permanent magnet synchronous actuator

To properly evaluate the SC linear actuator a reference permanent magnet synchronous linear actuator is used. This permanent magnet actuator is a high performance long-stroke actuator used in a wafer stage. The specific purpose of this actuator is not disclosed due to confidentiality. Also the exact specifications of the actuator are slightly modified for similar reasons.

The specifications of both the permanent magnet and the superconducting actuator are shown in Table 9.1.

	PM actuator	SC actuator
Stator specifications		
Magnet length	15 mm	20 mm
Magnet width	40 mm	100 mm
Magnet inner radius	-	10 mm
Magnet depth	200 mm	200 mm
Gap between poles	4 mm	5 mm
Back iron length	20 mm	20 mm
Mover specifications		
Armature span	2 pole pairs	2 pole pairs
Armature length	15 mm	15 mm
Armature width	50 mm	120 mm
Armature inner radius	5 mm	12 mm
Armature depth	200 mm	200 mm
Gap between armature poles	$8\frac{2}{3}$ mm	20 mm
Air gap specifications		
Mechanical clearance	2 mm	2 mm
Armature cooling plate	2 mm	2 mm
Cryostat wall thickness	-	5 mm
Cryostat clearance	-	3 mm
Total gap	4 mm	12 mm

Table 9.1: Actuator specifications

A permanent magnet actuator with the specifications found in in Table 9.1 is used. The magnets used are neodymium magnets. FEM modeling is used to compute the forces on the armature similarly to the actuators from the previous chapter. The current density in the armature coils is again 50 A/mm^2. The FEM model of the permanent magnet actuator is shown in Figure 9.1.

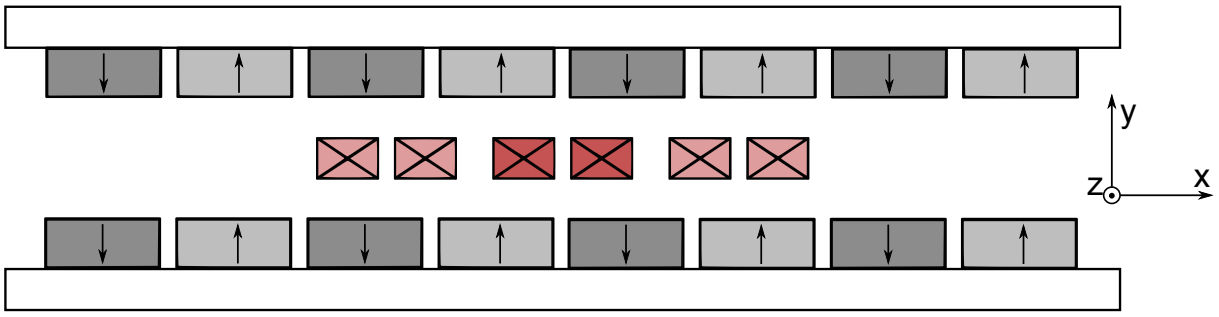

Figure 9.1: 2D FEM model of the permanent magnet linear actuator

The forces are calculated for several permanent magnet actuator designs. A single sided (only stator magnets on one side of the armature) design with and without iron is evaluated. Besides a single sided design a double sided and a double sided Halbach configuration are considered.

To calculate the total force the effective depth of the racetrack coils is again assumed to be the sum of the depth of the beams and 50% of the hollow cyllinder halves. The volume and consequently weight of the armature is calculated using Equation 8.11.

The maximum field in the armature B_a and the force (N/mm) are determined by 2D FEM calculations. The total force is determined by multiplying the force (N/mm) by the effective depth. Subsequently the force density is calculated by dividing the total force by the mass of the copper. Additionally the motor constant is determined ($N/\sqrt{W}$). The results are given in Table 9.2.

	No iron	Single sided	Double sided	Halbach
B_a (T)	0.31	0.45	0.66	0.75
F (N/mm)	8.7	11.9	24.7	25.6
F (kN)	1.30	1.79	3.71	3.84
N/kg	586	802	1665	1725
$N/\sqrt{W}$	15.1	20.7	43.0	44.5

Table 9.2: Permanent magnet synchronous actuator operating conditions

With Table 9.2 a reference for the superconducting linear actuator has been created. The maximum achievable field with permanent magnets is around 0.75 T. At those fields a force density of about 1.7 kN/kg can be generated in the actuator.

9.1.2 Superconducting synchronous actuator

Now that a reference has been created the performance of a superconducting linear actuator is evaluated. The specifications of the actuator can be found in Table 9.1. The 2D FEM model for the superconducting linear actuator is shown in Figure 9.2.

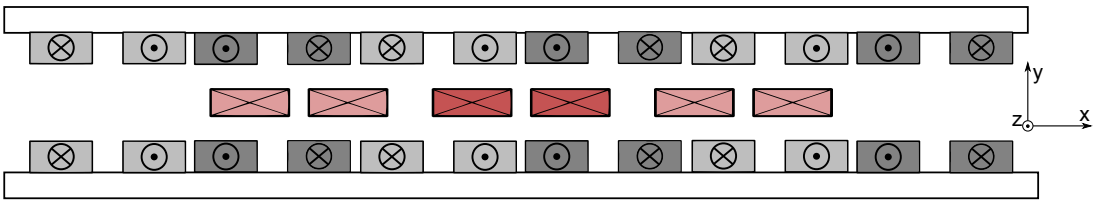

Figure 9.2: 2D FEM model of the superconducting linear actuator

Similar to the permanent magnet actuator the superconducting actuator is evaluated for several configurations. A single sided actuator without a back-iron, a single sided actuator with a back-iron and a double sided actuator with a back-iron are evaluated.

First the operation point of the magnets needs to be determined for each of the configurations. As a safety factor 90% of the critical current density is used. This factor is chosen as a minimal incorporation of the influence of the external fields, the productional variation in current density and the influence of strain on the critical current density. The factor is appropriate for low external fields but in practical applications this factor can be much lower.

The operation point is determined using FEM simulations using an iterative process. First, an initial guess is done for the current density at the 90% operation point. Second, using the FEM model the fields B_m and B_p are determined. Third, from Figures 4.3 or 5.1 the actual critical current density is determined. Last, the current density is revised and the steps can be repeated until the 90% operation point is reached.

The maximum field in the armature B_a, B_m, B_p and the force per mm are calculated at the 90% operation point. Subsequently the total force, the force density and the motor constant ($N/\sqrt{W}$) are determined.

For YBCO and MgB_2 magnets the results are shown in Tables 9.3 and 9.4 respectively.

	No iron	Single sided	Double sided
B_a (T)	3.3	3.5	6.1
B_m (T)	6.4	6.9	8.5
B_p (T)	4.0	4.2	3.9
J (10^8 A/m^2)	4.1	3.9	4.2
F (N/mm)	213.1	229.8	491.4
F (kN)	29.8	32.2	68.8
kN/kg	5.70	6.15	13.15
$N/\sqrt{W}$	225.1	243.2	519.6

Table 9.3: YBCO superconducting synchronous actuator operating conditions (20K)

	No iron	Single sided	Double sided
B_a (T)	1.4	1.6	2.4
B_m (T)	2.9	3.3	3.5
J (10^8 A/m^2)	1.8	1.5	1.4
F (N/mm)	93.6	103.1	196.8
F (kN)	13.1	14.4	27.6
kN/kg	2.50	2.76	5.27
$N/\sqrt{W}$	98.9	108.8	208.5

Table 9.4: MgB_2 superconducting synchronous actuator operating conditions (20K)

9.1.3 Actuator comparison

The permanent magnet and superconducting actuators are compared on three attributes. The actuators are evaluated on magnetic field generated at the armature, the force density and the ripple in the force distribution. To increase comparability the double sided variant of both actuators are compared.

The permanent magnet actuator maximally generates a field at the armature of 0.66 T which results a force density of 1.67 kN/kg.

The superconducting actuator maximally generates a field of 6.1 T for YBCO and 2.4 T for MgB_2 at the armature. These actuators achieve force densities of 13.15 and 5.27 kN/kg respectively.

This means the magnetic field of the superconducting field is increased by roughly a factor 9 or 4 for YBCO and MgB_2 respectively. On the other hand the force density is increased by roughly a factor 8 or 3 for YBCO and MgB_2 respectively.

These observations can lead to the false conclusion that the force generated is not entirely linear with respect to the armature field (as the armatures are comparable). But the cause of this discrepancy between the armature field and the force density is mainly because of the stator configuration.

Two things have changed compared to the permanent magnet stator. The first is the field generated at the surface of the magnets. The field distribution of a solenoid is dissimilar to the field distribution of a permanent magnet. Second the gap between the stator and the armature differs significantly.

These two changes have a large influence on the field distribution at the armature coils. Using the 2D FEM models shown in Figures 9.1 and 9.2 the field distribution along the x-axis for one pole pair length is computed. The field distributions and their harmonics of the permanent magnet actuator at 4 mm from the stator and of the superconducting actuator at 12 mm from the stator are shown in Figure 9.3.

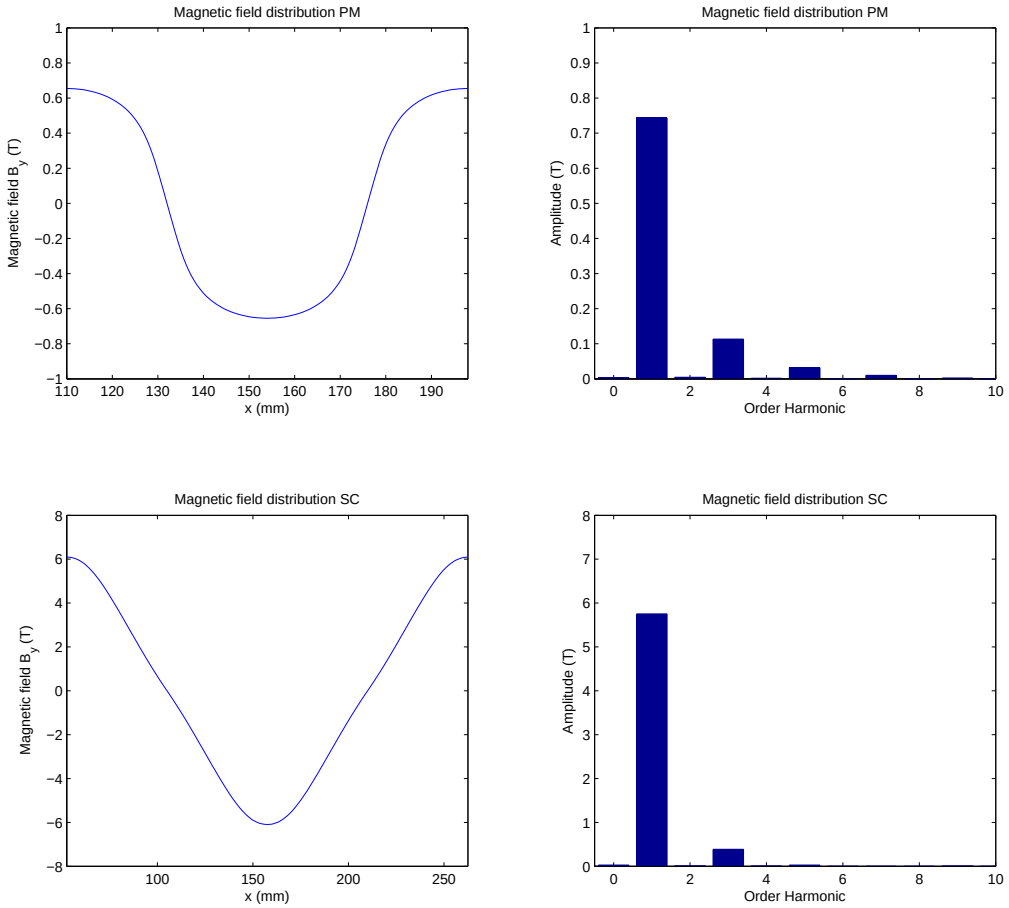

Figure 9.3: Field distribution and their harmonics of PM and SC actuators

The field distribution of the superconducting actuator has a near sinusoidal shape (THD of 6,7%). This is caused by the nature of the coil and the large air gap.

The field distribution of a permanent magnet actuator has a broader peak and is less sinusoidal (THD of 15.9%). Because of the broader peak the permanent magnet actuator generates a slightly larger force density for a certain maximum field than the superconducting actuator.

The shape of the field distribution of the superconducting does not only cause the relative generated force be slightly lower. A beneficial effect is that the ripple on the force distribution benefits from the more sinusoidal distribution. By force distribution the force over different positions of the armature is meant. The force ripple is mainly caused the harmonics of the field generated by the stator.

The armature of both the permanent magnet and superconducting actuators is swept along the length of one pole pair. In intermediate steps the force in both x and y directions are calculated by FEM modelling (Figures 9.1 and 9.2). The result is the force distribution along a pole pair length which is shown in Figure 9.4.

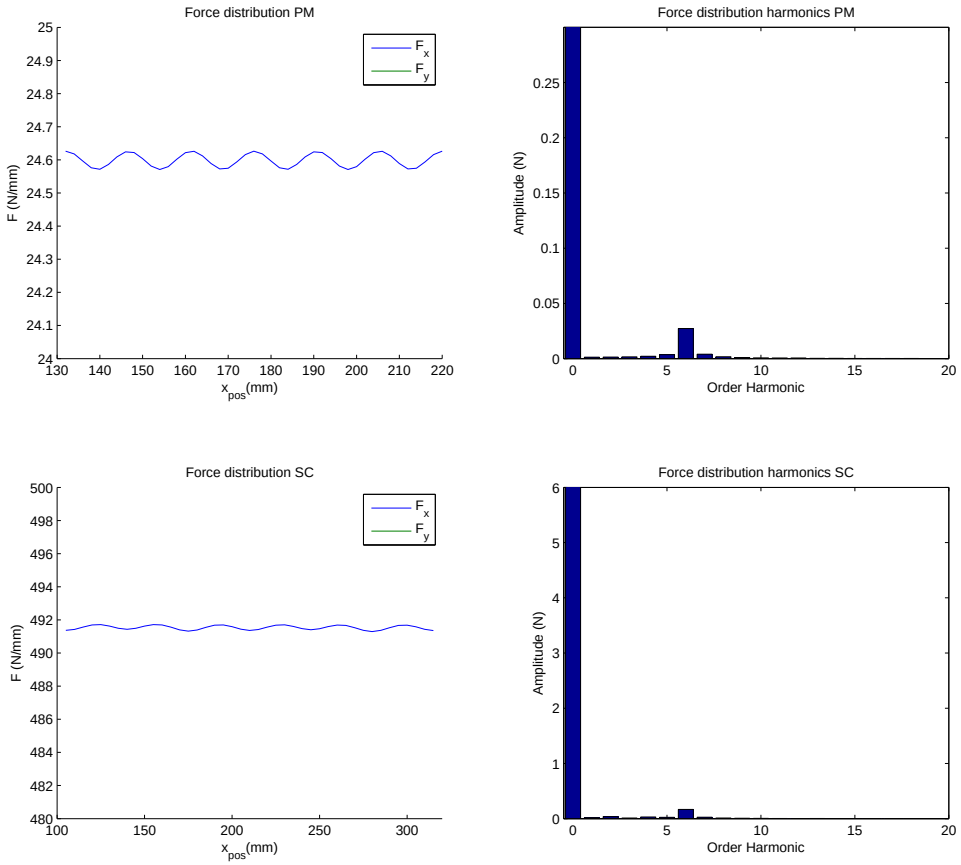

Figure 9.4: Force distribution and their harmonics of PM and SC actuators

The main ripple in the force is caused by the 6^{th} harmonic. The force ripple of the permanent magnet actuator is about 0.11% of the average force (0.0273 N/mm). The force ripple of the superconducting actuator is about 0.034% of the average force (0.168 N/mm).

9.2 Thermal analysis

In the previous section the electromechanical performance of the actuator was analyzed. This section focuses on the thermal feasibility of the actuator. A basic cryostat design is made in this section under several thermal and mechanical assumptions. The extensive thermal and mechanical engineering required to make a thorough cryostat design are beyond the scope of this thesis.

The cryostat design is first presented after which the heat sources in the cryostat are computed. For the computation of the heat sources the equations of Chapter 6 are used.

9.2.1 Cryostat design

To determine the dimensions of the cryostat the dimensions of the stator, the suspension of the stator and the dimensions of the cryorefrigerator are required.

For the actuator a stroke length of 40 cm was chosen. Additionally the armature pole pair span was chosen to be 2. Therefore the required number of magnet poles of this actuator is 8. These 8 magnet poles including the back iron have a width of 860 mm.

The 8 magnet poles are bolted on the back iron. Employing polyimide the stator is suspended from the cryostat. Polyimide is used on all sides of the back iron to ensure rigidity to forces in all directions.

The suspension adds 80 mm to the total width and on both sides the cryostat wall thickness is 5 mm resulting total width of the cryostat of 950 mm.

As cryorefrigerator the AL325 of Cryomech is used. This cryorefrigerator has a cooling power of 75 W at 20 K and is the highest performing (single stage) cryorefrigerator at 20 K available from Cryomech.

The length (excluding connection pipe) of the cryorefrigerator is 165 mm. Including the length of the back iron (20 mm), the magnet poles (20 mm), the gap (3 mm), 2 mm of additional clearance and the wall thicknesses (10 mm) the total length of the cryostat is chosen to be 220 mm.

The depth of the cryostat is comprised of the magnet depth (200 mm), the suspensions (80 mm) and wall thicknesses (10 mm). Resulting is a total depth of the cryostat of 290 mm.

The dimensions of the cryostat design are summed up in Table 9.5.

Cryostat dimensions	
Cryostat length	220 mm
Cryostat width	950 mm
Cryostat depth	290 mm
Cryostat specifications	
Cryostat wall thickness	5 mm
Stator suspension width	40 mm

Table 9.5: Cryostat dimensions and specifications

A graphical representation of the cryostat and the stator is shown in Figure 9.5. Here the blue color indicates polyimide and dark orange represents a material used for heat conduction between the cryorefrigerator and the stator.

For this design the suspension is assumed to be able to withstand the forces on the stator. Additionally the temperature throughout the stator is assumed to be single valued. In practice extensive mechanical and thermal analysis and design are necessary to ensure the validity of these assumptions. These analyses are however beyond the scope of this thesis.

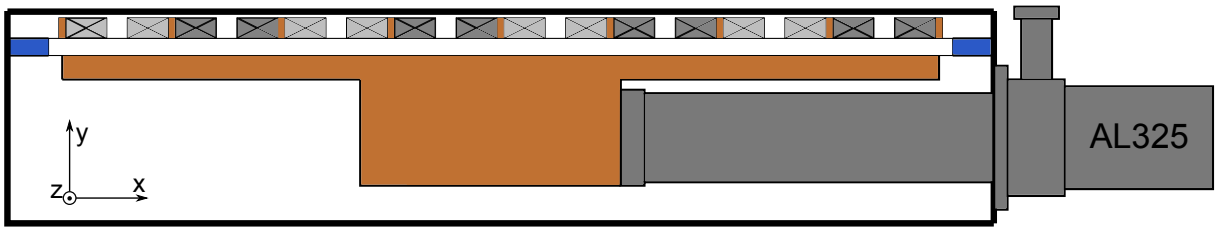

Figure 9.5: Graphical representation of a cross section of the cryostat

9.2.2 Heat leakage

For the cryostat shown in Figure 9.5 the heat leakage and heat generation are determined. First, the heat conduction through the vacuum and suspension is calculated. Second, the heat transfer through radiation is evaluated. Third, the heat transfer and generation of the current leads are taken into account. Last, the Joule heating in the superconducting material is estimated.

The total surface of the cryostat is 1.6766 m^2. In the cryostat a pressure of 10^{-2} Pa is maintained. Consequently the conduction through the vacuum is 7.2 W (Table 6.1).

From Table 6.1 a conduction of 3.4 kW/m^2 is found for a polyimide insulation with an isolation thickness of 10 mm. This leads to a conduction of 850 W/m^2 for the suspension. The total cross section surface of the suspension is 0.0496 m^2. Consequently the conduction through the polyimide suspension is 42.2 W.

The heat transferred by means of radiation is 15.2 W/m^2 (Table 6.1) and the surface of the cryostat of 1.6766 m^2. Therefore the heat transferred through radiation is 25.3 W.

Regular copper current leads can't be used for this cryostat. These current leads would introduce a heat source of about 30 W. In stead vapor cooled current leads need to be used. Using vapor cooled current leads a heat source of about 1 W/kA can be achieved. [38] The heat of two current leads carrying 1016.4 A of current results in a heat leak/generation of 2.0 W.

For the determination of the Joule heating Equation 6.8 is used. The factor $\frac{J}{J_c}$ can not be evaluated on each node of the FEM model. Therefore to assess the Joule heating an approximation is necessary.

The Joule heating is assumed to be negligible when $\frac{J}{J_c}$ reduces below 0.8 (at which the contribution has dropped by a factor 40 compared to 0.9 for n = 30). This factor occurs at a field of about 3.5 T (while 0.9 occurs at 3.9 T). Figure 9.6 represents the field distribution (of B_x) inside one racetrack coil.

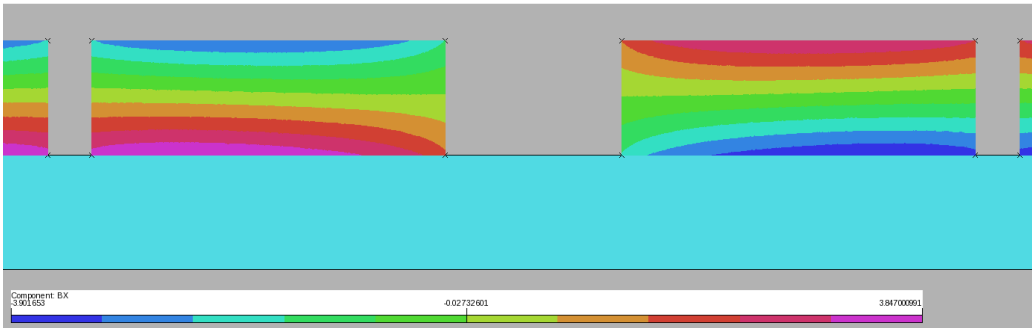

Figure 9.6: Field distribution inside a racetrack coil

From Figure 9.6 the Joule heating is approximated. The approximation is done by taking 20% of the volume and in that region $\frac{J}{J_c} = 0.9$. The n-value of superconductor is assumed to be 30 which is valid for high quality superconductors. Equation 6.8 is rewritten to Equation 9.1.

$$Q_J = \iiint JE_0\left(\frac{J}{J_c}\right)^n \mathrm{d}V = 4.3 * 10^8 * 10^{-4} * 0.9^{30} * 0.2 * V \tag{9.1}$$

The total volume of the superconductive material is 2.797*10^{-3} m^3. This leads to a heat generation of 1.0 W.

All the heat leakage and generation sources and the total heat load is shown in Table 9.6. The heat load is slightly lower than the available cooling power of 75 W. This leads to the conclusion such a design is feasible.

Vacuum conduction	4.4 W
Polyimide conduction	42.2 W
Radiation	25.3 W
Current leads	2.0 W
Joule heating	1.0 W
Total	74.9 W

Table 9.6: Heat leakage and generation

9.3 Cost analysis

In the previous section the electromechanical performance and the thermal feasibility were discussed. This section focuses on making a rough estimate on the costs of the superconducting actuator. Only the material costs of the actuators are evaluated as this gives a ballpark figure and the various other costs are nearly impossible to properly estimate.

First the cost of the permanent magnet machine is determined as a reference. The exact cost and its deduction of the permanent magnet actuator are not used due to confidentiality. A general estimation of the material cost is made using general concepts.

A double sided permanent magnet actuator (shown in Table 9.1) requiring a stroke of 40 cm would need 14 magnets on each side. The total volume of 28 magnets would be $3.36 * 10^{-3}$ m^3. The mass density of 7007 kg/m^3 and a price of 150 \$/kg is assumed for Neodymium magnets. Consequently the material cost of two of such permanent plates would be around \$3500.

Additionally a back iron, mechanical processing and magnetization is necessary. The total cost of the double sided permanent magnet stators is assumed to be \$4000.

Second the cost of the superconducting racetrack coils is estimated. In total 16 racetrack coils are used for a stroke of 40 cm. The total volume of these racetrack coils is $4.97 * 10^{-3}$ m^3.

For the YBCO wire the AP wire of SuperPower is used. The price for this wire is roughly 120 \$/m. As the wire has a cross section of $2.42 * 10^{-6}$ m^3 the cost can also be expressed as $4.96 * 10^7$ \$/m^3.

For the MgB_2 wire a wire of HyperTech is used. The price for this wire is roughly 9 \$/m. The cross section of this wire is 0.81*10^{-6} m^3. Expressing the cost in respect to volume results in a wire cost of 1.11*10^7 \$/m^3.

Additionally for the superconducting actuators two AL325 cryorefrigerator of CryoMech are used which cost about $45,000 each.

With this information the material cost of the stators can be calculated. The material costs of the stator and the cryorefrigerators are shown in Table 9.7. Additionally the cost per N/kg is shown.

	Double sided PM	**SC YBCO**	**SC MgB_2**
Electromechanical performance			
B_a (T)	0.66	6.1	2.4
Force density (kN/kg)	1.665	13.15	5.27
Cost estimate			
Material ($)	3500	246,000	55,200
Cooling ($)	-	90,000	90,000
Total ($)	4000	336,000	145,200
Performance cost ($/(N/kg))	2.4	25.6	27.6

Table 9.7: Cost estimate of PM and SC 40 cm stroke actuators

From Table 9.7 it is clear the superconducting stators are more expensive than permanent magnet stators per N/kg. On the other hand the maximum achievable field and force density are much lower for permanent magnet actuators.

This leads to the conclusion that up to certain force densities it is recommended to use permanent magnet stators. However if the force density requirement exceeds the maximum performance of permanent magnets superconducting magnets can be used. Superconducting magnet stators are therefore suitable for niche applications where the requirements exceed those of permanent magnet actuators.

The technological developments of superconductors lead to a steady decline of the price. Over time superconductors would become feasible for an increasing amount of applications.

9.4 Actuator analysis conclusions

This chapter first analyzed the electromechanical performance. The maximum magnetic field generated by a permanent magnet machine is about 0,75 T. This machine achieves a force density of about 1.7 kN/kg. The maximum magnetic field achievable with a stator containing YBCO superconducting magnets is about 6.1 T at which a force density of 13.15 kN/kg is achieved. The force densities are calculated using only the copper mass.

Second a cryostat design was presented and the thermal feasibility of this design was evaluated. The heat load of the cryostat design is mainly comprised of the conduction through the polyimide suspension and the heat transfer due to radiation. The total heat load is slightly lower than the cooling power available. Although only basic thermal calculations were pursued the calculations show that such an actuator design is feasible.

Last the material cost of a superconducting machine are compared to the material cost of a permanent magnet machine. It is concluded that using superconducting magnets in linear actuators fills a gap in niche applications. For designs where the performance of permanent magnets does not suffice superconducting magnets can be used. Roughly the material cost of superconducting actuators is 10 times higher per N/kg than permanent magnet machines.

Chapter 10

Conclusions and recommendations

Contents

In this chapter the conclusions of the research project are presented. The results of the thesis will be summarized and compared to the earlier stated thesis goals in section 10.1. In section 10.2 an overview of the scientific contributions of this project are given. The chapter is is concluded with section 10.3 where recommendations for future research are given.

10.1 Conclusions

Philips Innovation Services Mechantronics Technologies department designs high precision linear synchronous actuators. The acceleration demands for these actuators rise continuously. Currently the acceleration is limited by the maximum achievable current density in the copper armature and the magnetic field generated by the permanent magnets. This thesis researched the possibilities to replace the permanent magnets with superconductors.

The goals of this thesis were to determine the achievable fields using commercially available superconductors, make a basic design of a superconducting linear actuator and evaluate the electromechanical, thermal and commercial feasibility of the designed superconducting linear actuator.

For various temperatures, materials and conditions the achievable fields using commercially available superconductors were determined. First YBCO superconductors at high temperatures (77 and 65 K) were considered. To generate a magnetic field at high temperatures either wires or bulk superconductors can be used.

Coil magnets were designed to generate a field either inside and outside the coil. At 65 K a field of 1.58 T could be generated 15 mm outside a coil. Inside a coil a field of 9.0 T can be achieved at 65 K.

Additionally bulk magnets were considered. Theoretically these bulk magnets can achieve fields of 2.33 T at 15 mm distance from the magnet (at 65K). However the magnets that can achieve fields of these magnets are not commercially available. Commercially available superconducting bulk magnets can achieve fields of about a factor 6 lower.

Second YBCO, MgB_2, NbTi and Nb_3Sn superconductors at low temperatures (20 and 4 K) were reviewed. The achievable fields at these temperatures were considerably higher. Superconducting bulk magnets were not further considered.

Coil magnets were designed to generated a field inside or outside the coil. These coil magnets were able to generate fields of 1.3 - 3.4 T at 20 K and 2.0 - 4.0 T at 4 K 15 mm outside a coil depending on the superconductor used. Inside a coil fields of 4.3 - 19.3 T at 20 K and 6.4 - 22.3 T at 4 K can be generated depending on the superconductor used.

A basic design was made for a superconducting linear actuator. Several design options were presented including cryostat and actuator topology designs. The design chosen is arguably optimal under the scope of this thesis.

The superconducting synchronous linear actuator was chosen as topology. As magnets superconducting coils are used in the stator to generate a field outside the coil. The operating temperature of the magnets is 20 K. Furthermore MgB_2 and YBCO wires are considered for the coil magnets.

The superconducting coils are cooled by a cryorefrigerator via conduction cooling. The wall of the cryostat was designed to be 5 mm resulting in a total gap between the magnets and the armature of 12 mm.

The armature of the superconducting actuator was chosen to be in the mover. As armature a copper three phase armature with concentrated windings is used.

Additionally the stator and armature coils were designed. The specifications of these racetrack coils can be found in Table 9.1.

The superconducting linear actuator was evaluated on electromechanical performance, thermal feasibility and cost. To evaluate the superconducting linear actuator a reference high performance permanent magnet actuator was presented. This actuator achieved a magnetic field of 0.66 T at the armature. Additionally the force density generated by this actuator is 1.665 kN/kg.

The magnetic field at the armature achieved by YBCO superconducting magnets in the stator was 6.1 T. Moreover the force density generated by this actuator is 13.15 kN/kg. This means the magnetic field a factor 9 higher and the force density is a factor 8 higher. Additionally the force ripple of the superconducting actuator is much lower.

The thermal feasibility of the superconducting actuator was shown. The heat load of a basic design was slightly lower than the cooling power provided by the cryorefrigerator.

Cost wise the superconducting actuator is roughly a factor 10 more expensive per N/kg. Therefore it is preferable to use permanent magnet actuators up to a certain force density. Superconducting actuators can be used for niche markets where the performance demands are high and the cost is less important.

Concluding, using a superconducting synchronous actuator can increase the force density significantly. However the use of superconductors is costly and is therefore only feasible for niche markets.

10.2 Summary of contributions

The following scientific contributions are made in this thesis:

- **A method was developed to approximate the maximum achievable field of superconducting coils from their critical characteristics.**

  This method was used to design and evaluate superconducting coils in the thesis. The method can further be employed to optimize superconducting coil designs according to design specifications.

- **For several commercially available materials at various temperatures the achievable fields were determined outside and inside the magnets.**

  This information can be used in further calculations. However as time progresses these achievable fields must be updated with advances in superconducting technologies.

- **A superconducting linear actuator was designed using superconducting coil magnets.**

  The thesis showed various design options for the linear actuator. Logical deduction showed an arguably optimal design for a superconducting linear actuator.

- **The feasibility of a superconducting linear actuator was shown.**

  The feasibility of the superconducting linear actuator was shown. However this is only in certain (niche) conditions. Further research can be done with confidence in the feasibility.

10.3 Recommendations

Based on the results and scope of this thesis, the following recommendations for further research are given:

- **The AC behavior of superconductors requires thorough evaluation.**

  Throughout the thesis the AC behavior of superconductors was not evaluated. Thorough evaluation of the AC behavior is necessary for:

  - The evaluation of the employment of superconductors in the armature of a linear actuator which was not considered in this thesis.
  - The evaluation of losses induced in the coil magnets. Space harmonics and other possible AC magnetic fields induces AC currents which introduces losses.

- **Thermal and mechanical analyses are recommended.**

  Extensive thermal and mechanical analyses were omitted from the thesis. More comprehensive analyses are necessary for:

  - The optimization of the armature. In the thesis an existing armature has been used with proved dimensions. Thermal and mechanical analyses would enable the optimization of the armature.
  - The optimization of the cryostat. The cryostat was designed and shown to be feasible. However the heat load can be further decreased by analyzing and optimizing the design.

- **Dynamic analysis of the actuator and its environment is called for.**

  Previously it was mentioned that AC magnetic fields induce AC currents in the magnet coils. Additional unexpected magnetic, thermal and/or mechanical distortions can be present due to the environment or dynamic operation. A complete (experimental) assessment of these dynamic effects is necessary for:

  - The evaluation of the losses induced in the magnet coils. The losses in the magnet coils can introduce a new heat source in the cryostat.
  - The safety margin 90% of the critical current was chosen as operational current density. This margin must be reassessed to the distortions preventing a quench in the magnet coils.

- **Experimental proof is necessary.**

  For the entirety of the thesis only theoretical evaluations of the behavior and effects of superconductors have been evaluated. The validity of the theories, methods and results needs experimental proof.

- **The cost of superconducting wire is prone to change.**

  The main disadvantage of superconductors is the costs. However most superconductors are not fully matured and not all superconducting materials are discovered. The price of superconducting materials has been declining over the years. As the prices of superconductors change so can the feasibility.

Bibliography

[1] Dirk van Delft, *Freezing Physics* Heike Kamerlingh Onnes and the quest for cold. KNAW, Amsterdam, 2007.

[2] Martin N. Wilson, *100 Years of Superconductivity and 50 Years of Superconducting Magnets.* IEEE transactions on applied superconductivity, vol. 22, no. 3, june 2012.

[3] *Nobel Lectures.* Physics 1901-1921 Elsevier Publishing Company, Amsterdam, june 2012.

[4] Dirk van Delft, *Little cup of helium, big science.* AIP, Physics Today, 2008.

[5] National Research Council, *The Impact of Selling the Federal Helium Reserve.* TNAP, Washington DC, 2000.

[6] Dirk van Delft and Peter Kes, *The discovery of superconductivity.* AIP, Physics Today, 2010.

[7] H.K. Onnes, *On the Sudden Rate at Whitch the Resistance of Mercury Disappears.* Communications from the Physical Laboratory at the University of Leiden, Leiden, 1911.

[8] W. Meissner and R. Ochsenfeld , *Ein neuer Effekt bei Eintritt der Supraleitfahigkeit.* Die Naturwissenschaften 21, Berlin, 1933.

[9] F. London , *Superfluids Vol 1, Macroscopic Theory of Superconductivity.* John Wiley & Sons inc., New York, 1950.

[10] J. Bardeen, L.N. Cooper, J. R. Schrieffer , *Theory of Superconductivity.* University of Illanois, Urbana, 1957.

[11] T.P. Sheahen , *Introduction to High-Temperature Superconductivity.* Plenum, New York, 1994.

[12] C. Timm , *Theory of Superconductivity.* TU Dresden, Dresden, 2011.

[13] L.N. Cooper , *Bound Electron Pairs in a Degenerate Fermi Gas.* The Physical Review, Urbana, 1956.

[14] P.J. Ford and G.A. Saunders , *The Rise of the Superconductors.* CRC Press, 2004.

[15] N.B. Kopnin , *Theory of Superconductivity.* Aalto University, 2010.

[16] Z.X. Feng , *Optimization of superconducting solenoid core.* IEEE Transactions on magnetics Vol.24 NO.2, Beijing, 1988.

[17] D.B. Montgomery and J. Terrell , *Some useful information for the design of air-core solenoids.* AFC, 1961.

[18] SuperPower inc , *Field dependence of Ic at 20 - 65K 2011 SuperPower AP wire.* University of Houston, 2011.

[19] SuperPower inc , *SuperPower 2G HTS Wire Specifications*. SuperPower inc, New York, 2012.

[20] SuperPower inc , *Insulated 2G HTS Wire*. SuperPower inc, New York, 2012.

[21] J.R. Hull and M. Murakami , *Applications of Bulk High-Temperature Superconductors*. IEEE, 2004.

[22] R. Gonzalez-Arrabal, M. Eisterer, H. W. Weber, G. Fuchs and P. Verges , *Very high trapped fields in neutron irradiated and reinforced YBa2Cu3O7 melt-textured superconductors*. Applied Physics Letters, 2002.

[23] S. Nariki, N. Sakai and M. Murakami , *Melt-processed GdBaCuO superconductor with trapped field of 3 T at 77 K*. ISTEC, Shinonome, 2004.

[24] S. Nariki, N. Sakai and M. Murakami , *Melt-processed SmBaCuO superconductors trapping strong magnetic field*. Nagoya University, Nagoya, 1998.

[25] D.M. Friedman , *New Research on YBCO Superconductors*. Nova, New York, 2008.

[26] D.K. Park , *MgB_2 for MRI Magnets: Test Coils and Superconducting Joints Results*. IEEE Transactions on applied superconductivity Vol. 22 No. 3, 2012.

[27] G.Z. Li , *Critical Current Density and Current Transfer Length of Multifilamentary MgB_2 Strands of Various Design*. IEEE Transactions on applied superconductivity Vol. 22 No. 3, 2012.

[28] Z.Q. Ma and Y.C. Liu , *Low-temperature synthesis of MgB2 superconductors*. International Materials Reviews Vol. 56 No. 5/6, 2011.

[29] Bruker EST, *NbTi wire data sheet*. Bruker EAS, 2013.

[30] Supercon Inc, http://www.supercon-wire.com/products_nb3sn.html, *High Field Nb3Sn (Bronze Route) Superconducting Wire*. Supercon Inc, Accessed: January 2013.

[31] K. A. Gavhane , *Heat Transfer*. Pragati Books, Mumbai, 2008.

[32] R. Chang , *Physical Chemistry for the biosciences*. University Science Books, 2004.

[33] T.F. Irvine Jr. and J.P. Hartnett , *Advances in Heat Transfer Volume 9*. Academic press, London, 1973.

[34] D.M.J. Taylor and D.P. Hampshire , *Relationship between the n-value and critical current in Nb3Sn superconducting wires exhibiting intrinsic and extrinsic behaviour*. IOP, Durham, 2005.

[35] *Personal inequiries with Theva (Ceraco) and ATZ*. 2013, http://www.theva.com/ & http://www.atz-gmbh.com/.

[36] Cryomech, *Cryorefrigerator pricing 2012*. November 2012, http://www.cryomech.com/.

[37] C. Hauviller , *Design rules for vacuum chambers*. CERN, Geneva, 2005.

[38] V.I. Datskov, V. Bartenev and J.A. Demko , *Practical design and manufacturing of cryogenic high current leads*. JINR, Dubna, 2009.

Appendix A

FEM models

In this Appendix various different 2D FEM models are shown and their solutions. For all models 2D Opera is used to solve the model. As solutions the field magnitude (|B|) and magnetic potential lines are drawn.

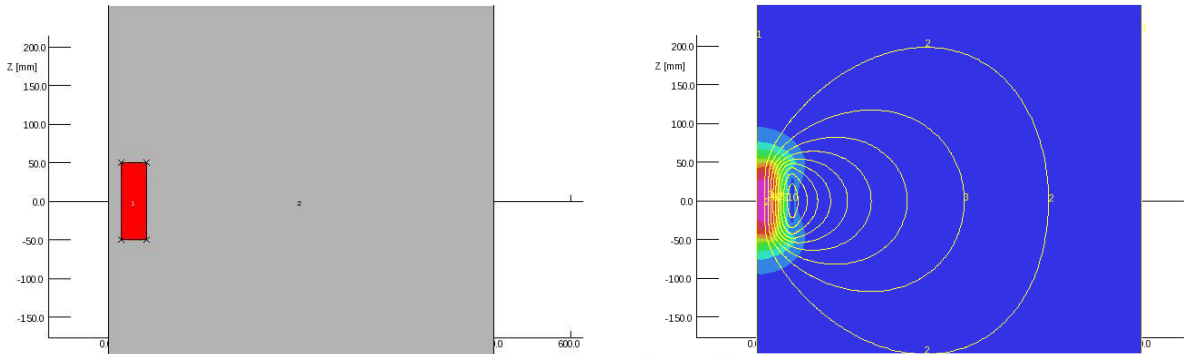

Figure A.1: Axisymmetric solenoid model (2D FEM Opera)

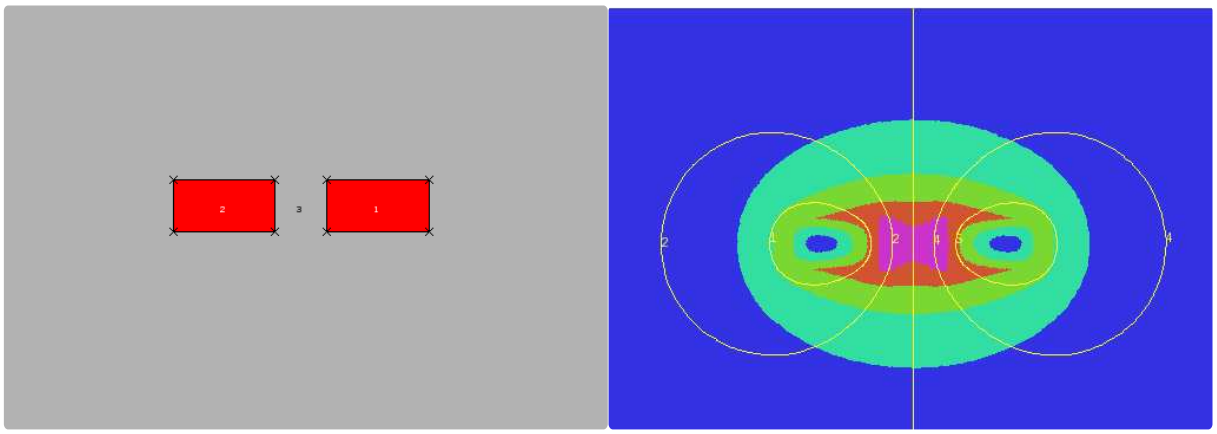

Figure A.2: Plane symmetric racetrack model (2D FEM Opera)

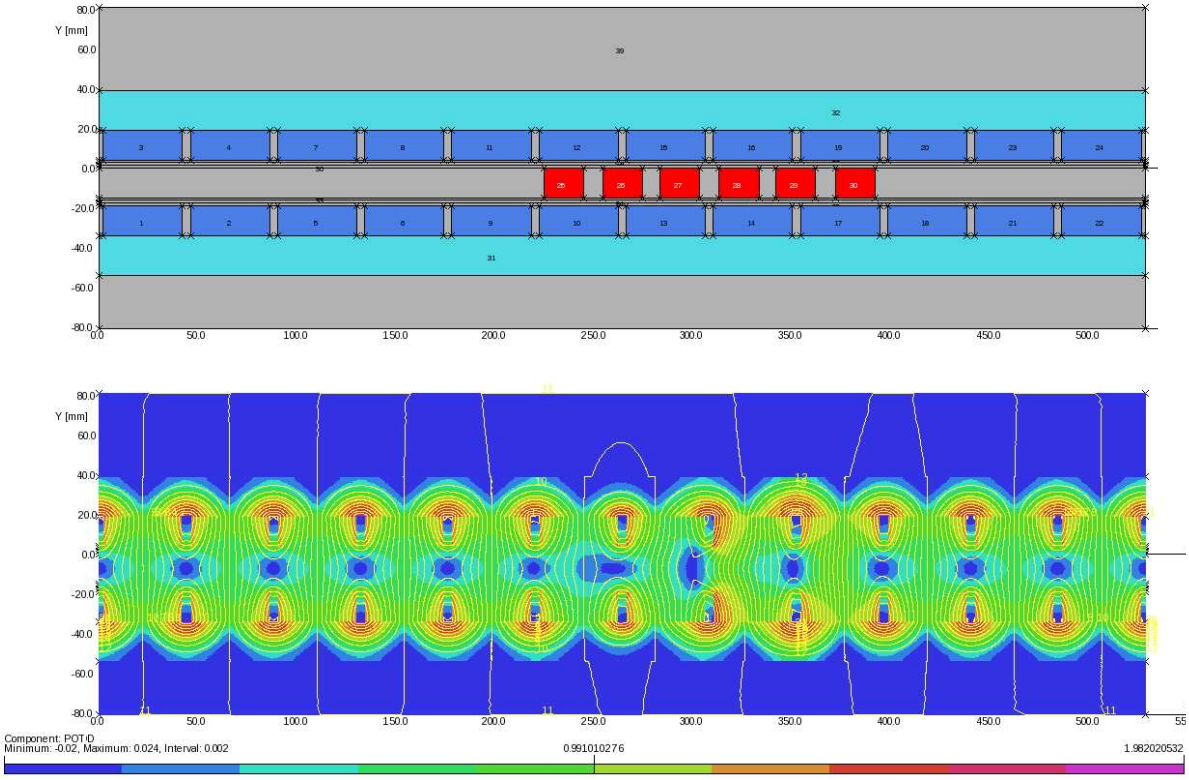

Figure A.3: Plane symmetric PM synchronous actuator model (2D FEM Opera)

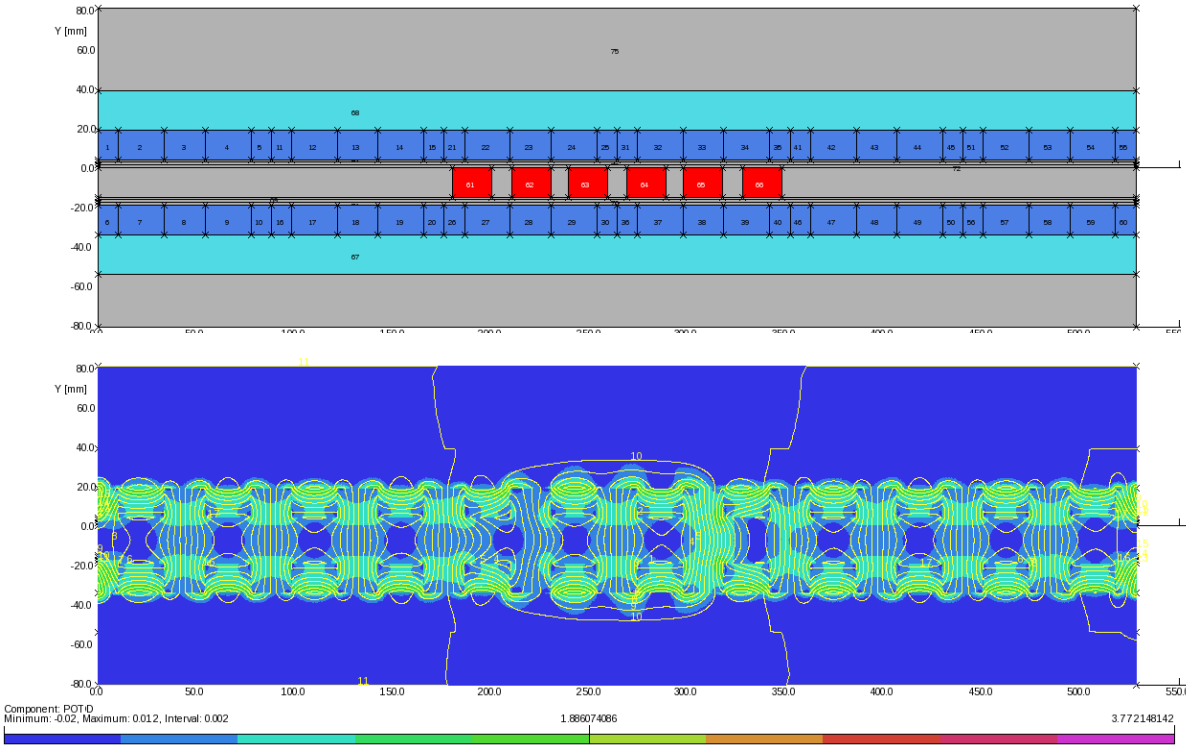

Figure A.4: Plane symmetric Halbach synchronous actuator model (2D FEM Opera)

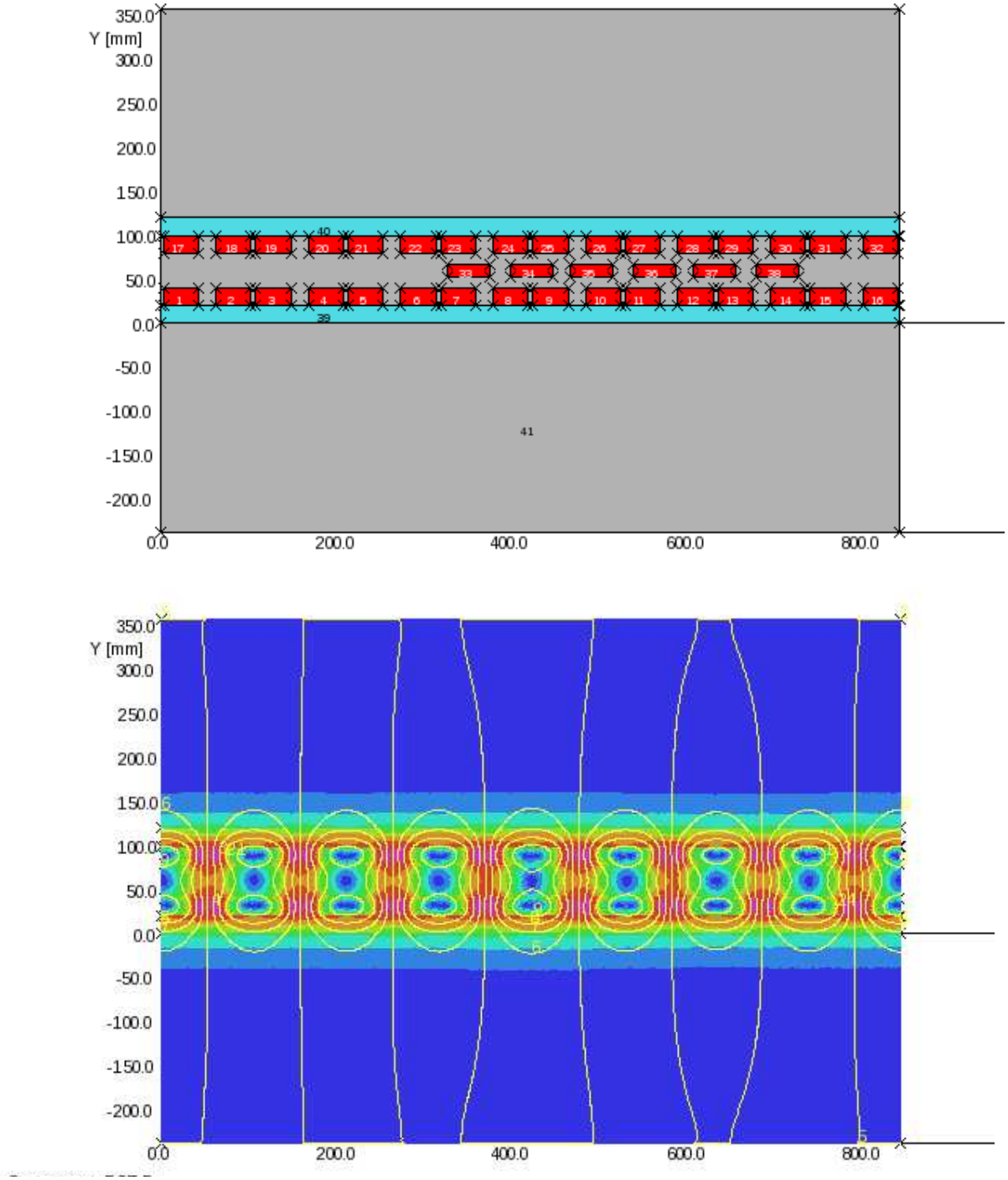

Figure A.5: Plane symmetric SC synchronous actuator model (2D FEM Opera)

Appendix B

Paper: Feasibility Study of a Superconducting Linear Actuator

Feasibility Study of a Superconducting Linear Actuator

Nils H. van der Blij*

University of Technology, Delft
May 15, 2013

Abstract

The acceleration of high precision systems is limited by the magnetic field at the armature and the current density in the armature. Permanent magnets can achieve fields at the armature up to 0.7 T. To increase the performance superconducting coils are considered as replacements for the permanent magnets. A method is provided to approximate the achievable fields of superconducting coils. A superconducting actuator using racetrack coils at 20 K is designed. The superconducting actuator achieves a magnetic field of 9 times and a force density 8 times higher than that of a reference high performance permanent magnet actuator. Additionally the thermal and commercial feasibility of such an actuator is shown.

Index Terms *- Superconductor, linear actuator, magnetic field*

The design of high precision linear synchronous actuators for assembly equipment, wafer scanners, inspection equipment and many other applications is one of the competences of Philips Innovation Services' Mechatronics Technologies department.

The acceleration requirements of the linear actuators continually rise with a higher throughput demand of high precision systems. By Newtons second law the acceleration is proportional to the force density (N/kg) or equivalently, for a fixed armature design, the force.

The force generated in these linear actuators can be simplified to be dependent on both the magnetic field at the armature and the current density flowing in the armature.

The current density of the copper armature is dependent on the cooling of these windings. Generally water is used to cool the copper windings. Using an extensive water cooling system a maximum current density of 50 A/mm^2 can be achieved.

Employing permanent magnets in the stator limits the magnetic field achievable at the armature. The field achievable at the surface of a permanent magnet is around 1.5 T. Mainly due to the air gap the field achievable at the armature is realistically around 0.7 T.

An alternative for permanent magnets is superconductors. Superconductors have no resistance and can carry high current densities.

In this paper a linear actuator with superconducting coils magnets is evaluated. First, a method to approximate the achievable fields of superconducting coils is discussed. Second, the method is applied to design a racetrack coil at 20 K. Third, the design choices of a superconducting actuator are discussed. Finally, the electromechanical, thermal and commercial feasibility of the actuator are evaluated.

I. Approximation method

The current density a superconducting wire can carry is dependent on the magnetic field. This dependency is given by its critical characteristics.

The critical characteristics of YBCO and MgB_2 wire at 20 K are shown in Figure 1.

*In collaboration with Philips Innovation Services

YBCO material is anisotropic meaning the material is not only dependent on the magnitude but also of the orientation of the field.

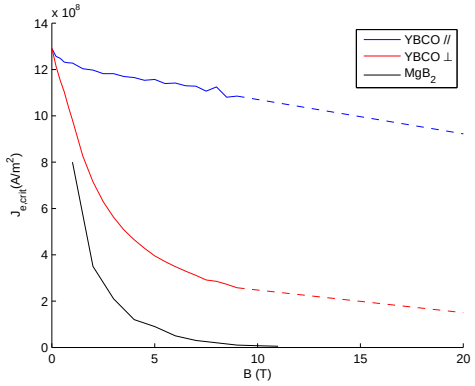

Figure 1: Critical engineering current densities of SuperPower AP YBCO and HyperTech MgB_2 wires [1, 2, 3, 4, 5, 6]

It is assumed that for a coil the following Equations are valid:

$$B_m = \mu_0 J C_m \tag{1}$$

$$B_p = \mu_0 J C_p \tag{2}$$

$$B_x = \mu_0 J C_x \tag{3}$$

Where B_m is the maximum parallel field and B_p the maximum perpendicular field inside and to the length of the coil. B_x is the magnetic field at a arbitrary position on the axis of the coil. A suitable position of B_x can be chosen arbitrarily.

C_m, C_p and C_x are geometrical constants for a given geometry of the coil. These constants can be determined analytically or by finite element modeling.

Equations 1 to 3 lead to the load lines of the coil which are given in Equation 4.

$$J = \frac{100}{S}\frac{B_m}{\mu_0 C_m} \quad , \quad J = \frac{100}{S}\frac{B_p}{\mu_0 C_p} \tag{4}$$

Where S is a safety factor (in %) to ensure the superconductors do not quench.

Additionally the relation between B_x and B_p or B_m is given in Equation 5.

$$B_x = \frac{C_x}{C_m} B_m \quad , \quad B_x = \frac{C_x}{C_p} B_p \tag{5}$$

Equations 6 to 8 approximate the critical characteristics of the superconducting wires.

$$J_{crit,YBCO//} \approx (-0.0158 B_m + 1.23) \times 10^9 \tag{6}$$

$$J_{crit,YBCO\perp} \approx 9.82 \times 10^8 \frac{1}{\sqrt{B_p}} \tag{7}$$

$$J_{crit,MgB2} \approx 0.8 \times 10^9 \frac{1}{B_m^{1.25}} \tag{8}$$

The magnetic field at intersection of the load lines (Equation 4) and the critical current densities (Equations 6-8) indicates the maximum B_m or B_p.

Furthermore, the maximum achievable fields can be determined from these intersections using Equation 5. These maximum achievable fields are shown in Equations 9-11.

$$B_{x,max,YBCO} \approx \frac{S}{100} \frac{1.23 \times 10^9 \mu_0 C_x C_m}{C_m + 0.0158 \times 10^9 \mu_0 C_m^2} \tag{9}$$

$$B_{x,max,YBCO} \approx \frac{S}{100} \frac{(9.82 * 10^8 * \mu_0)^{\frac{2}{3}} C_x}{C_p^{\frac{1}{3}}} \tag{10}$$

$$B_{x,max,MgB2} \approx \frac{S}{100} \frac{(0.8 \times 10^9 \mu_0)^{0.44} C_x}{C_m^{0.56}} \tag{11}$$

For the YBCO material the actual maximum achievable field B_x is the lowest of the two computations. The MgB_2 wire only requires one computation as this materials anisotropy is negligible.

The method, provided in this section, of the computation of the maximum achievable field can be utilized for any temperature, material and coil. However the critical current characteristic of the material has to be known.

For YBCO and MgB_2 coils at 20 K the computation of the geometric constants C_m, C_p and C_x remains for the actual determination of the achievable fields.

II. Racetrack Coil at 20 K

For a superconducting linear synchronous actuator racetrack coils at 20 K are used in the stator. Using the method of the previous section these coils are designed.

For different dimensions of the racetrack coil the maximum achievable fields and volume (cost) are determined. To determine C_m, C_p and C_x Opera 2D (FEM) is used. The FEM model is shown in Figure 2.

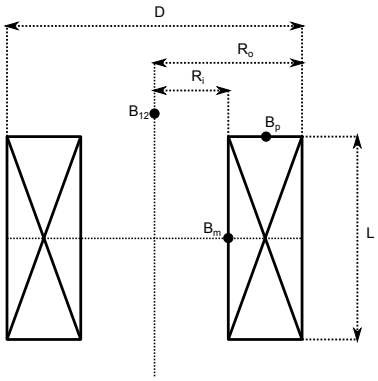

Figure 2: 2D FEM model of a racetrack coil

For this model α and β are defined as:

$$\alpha = \frac{R_o}{R_i} \quad , \quad \beta = \frac{L}{2R_i} \tag{12}$$

For several diameters of the racetrack coil the maximum achievable field 12 mm outside the coil is shown in Figure 3 (S = 100%).

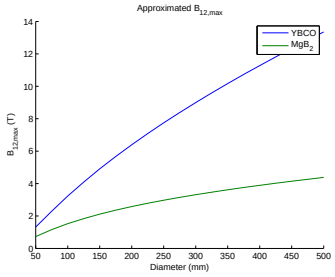

Figure 3: $B_{12,max}$ where $\alpha = 5$, $\beta = 1$

As diameter 100 mm is chosen. At diameters lower than 100 mm the achievable field would not provide a significant improvement over permanent magnets. A diameter of 200 mm would increase the achievable field by about 85% while increasing the volume (cost) of the racetrack coils by 160% compared to the 100 mm coils (assuming a total depth of the coil of 500 mm).

Second, α is evaluated. The achievable field for several α is shown in Figure 4.

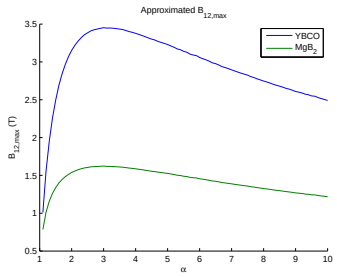

Figure 4: $B_{12,max}$ where $D = 100$, $\beta = 1$

α is chosen to be 5 for the superconducting racetrack coils. At an α of 5 the maximum achievable field has only decreased by about 10% while the volume (cost) has decreased by about 65% compared to an α of 2.5. An even higher α is not viable as the inner radius is already near the minimum bend diameter of most superconducting wires.

Last, β is evaluated. Figure 5 shows the achievable field for various β.

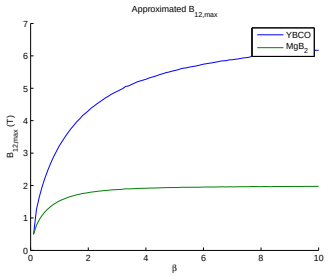

Figure 5: $B_{12,max}$ where $D = 100$, $\alpha = 5$

β is chosen to be 1 for the superconducting racetrack coils. At a β lower than 1 the field is deemed to be insignificantly higher than fields generated by permanent magnets. A beta higher than 1 is not viable as much additional material is used for only marginal performance increase.

III. Actuator design choices

In the previous section a racetrack coil magnet was designed. This section will discuss the various design choices that were made for the superconducting actuator.

As topology a synchronous actuator is chosen. The advantage of a synchronous actuator is that it generates a constant horizontal force and no vertical force if commutated properly.

To generate the magnetic field superconducting racetrack coils are used. The main merit of racetrack coils is that the depth of the actuator can be chosen arbitrarily.

A cryorefrigerator is used to cool the magnets down to 20 K. Superconducting coils at 77 or 65 K would not be able to generate sufficiently high magnetic fields. Operating at 4 K would require a pulse-tube refrigerator which has very limited cooling power.

At 20 K only MgB_2 and YBCO materials are mature and cheap enough to be viable.

The cryostat is chosen to only envelop the superconducting magnets. Including armature in the cryostat would introduce a new source of heat. Additionally such a design would require a torque transference element.

The superconducting magnets are chosen to be in the stator. The weight of the bulky superconducting coils and a cryostat in the mover would decrease the force density.

In the following section the superconducting actuator will be compared to an existing permanent magnet actuator. To increase comparability the armature of the superconducting actuator is chosen to be a scaled version of the permanent magnet actuators mover.

In the stator the superconducting racetrack coils designed in the previous section are used. The complete specifications of the superconducting actuator are shown in Table 1.

Equation 5 found in [7] was used to determine the cryostat wall thickness to limit the deflection to 1 mm.

	PM actuator	SC actuator
Stator specifications		
Magnet length	15 mm	20 mm
Magnet width	40 mm	100 mm
Magnet inner radius	-	10 mm
Magnet depth	200 mm	200 mm
Gap between poles	4 mm	5 mm
Back iron length	20 mm	20 mm
Mover specifications		
Armature span	2 pole pairs	2 pole pairs
Armature length	15 mm	15 mm
Armature width	50 mm	120 mm
Armature inner radius	5 mm	12 mm
Armature depth	200 mm	200 mm
Gap armature poles	$8\frac{2}{3}$ mm	20 mm
Air gap specifications		
Mechanical clearance	2 mm	2 mm
Armature cooling plate	2 mm	2 mm
Cryostat wall thickness	-	5 mm
Cryostat clearance	-	3 mm
Total gap	4 mm	12 mm

Table 1: Operating points of superconducting coils

For both actuators a 2D FEM model is made according to the specifications.

The reference permanent magnet actuator is a high performance actuator. The FEM model of this actuator is shown in Figure 6.

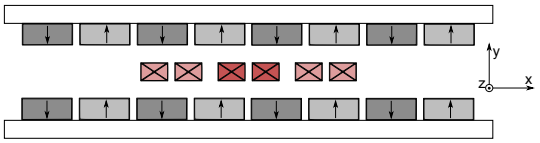

Figure 6: 2D FEM model of the permanent magnet linear actuator

The 2D FEM model of the superconducting actuator is shown in Figure 7.

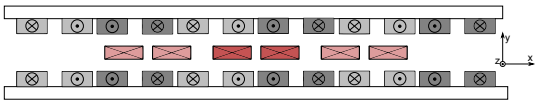

Figure 7: 2D FEM model of the superconducting linear actuator

To compute the forces on the armatures 2D FEM modeling in Opera2D is used. The forces are calculated by integrating the Lorentz force over the armature windings.

IV. Actuator evaluation

IV.1 Electromechanical analysis

The previous section showed the 2D FEM models of both the reference and the superconducting actuator. These actuators will be compared according to magnetic field at the armature, force density and force ripple.

For the racetrack coils a 90% safety factor is used. This factor is chosen as a minimal incorporation of the influence of the perpendicular field, the productional variation in current density and the influence of strain on the critical current density. The factor is appropriate for low external fields but in practical applications this factor can be much lower.

The force density is calculated for only the copper mass. Practically the mass of the mover can be 4 to 6 times higher. However for the comparison the copper mass is sufficient.

The magnetic fields and the force density of the superconducting and permanent magnet actuator are shown in Table 2.

	YBCO	MgB_2	PM
B_a (T)	6.1	2.4	0.66
B_m (T)	8.5	3.5	-
B_p (T)	3.9	1.3	-
J (10^8 A/m^2)	4.2	1.4	-
kN/kg	13.15	5.27	1.67

Table 2: Magnetic fields and force densities of various actuators

The magnetic field achievable at the armature (B_a) is about 9 times higher for the superconducting actuator. However the force density of the superconducting actuator is only 8 times higher.

Additionally the magnetic field distribution at the armature contains less harmonics than the field generated by permanent magnets. The field distributions at the armature and their harmonics are shown in Figure 8.

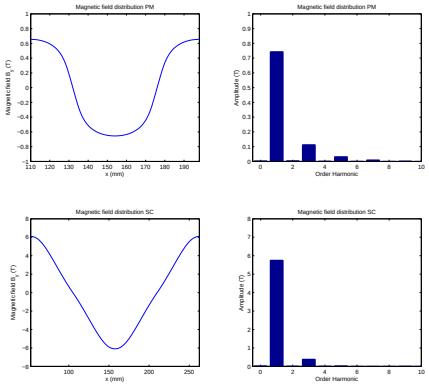

Figure 8: Magnetic field distribution of the linear actuators

The total harmonic distortion for the superconducting actuator is 6.7%. This is an improvement on the permanent magnet actuator which has a THD of around 16%.

The harmonics in the field distribution are the main cause of the force ripple in the synchronous actuator. The reduction of this ripple is an important objective in the design process. The force distributions for different positions of the armature are shown in Figure 9.

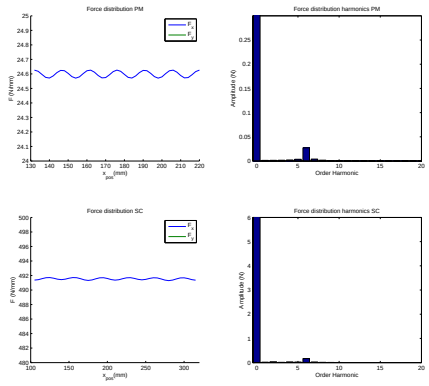

Figure 9: Force distribution and its harmonics of the linear actuators

The ripple in the force distribution is 0.034% of the average force for the superconducting actuator. This is a great improvement compared to a ripple of 0.11% of the average force for the permanent magnet actuator.

IV.2 Thermal analysis

To assess the thermal feasibility of the superconducting linear actuator a cryostat is designed. Only a basic cryostat design is made. The general dimensions of the cryostat are shown in Table 3.

Cryostat dimensions	
Cryostat length	220 mm
Cryostat width	950 mm
Cryostat depth	290 mm

Table 3: Cryostat dimensions

The superconducting magnets are bolted to the back iron and the back iron is suspended from the cryostat using 40 mm of polyimide on all sides.

As cryorefrigerator an AL325 of CryoMech is used. This cryorefrigerator has a cooling power of 75 W at 20 K.

A cross section of the cryostat is shown in Figure 10. Here the blue color indicates polyimide and dark orange represents a material used for heat conduction between the cryorefrigerator and the stator.

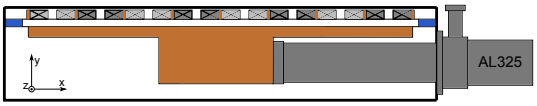

Figure 10: Graphical representation of a cross section of the cryostat

The stator is isolated from the 293 K environment by a vacuum (10^{-2} Pa) and the polyimide insulation.

Besides the conduction through the insulation the radiation, conduction through current leads and Joule heating also contribute to the heat load.

All the heat load sources are summed up in Table 4.

Vacuum conduction	4.4 W
Polyimide conduction	42.2 W
Radiation	25.3 W
Current leads	2.0 W
Joule heating	1.0 W
Total heat load	74.9 W

Table 4: Heat leakage and generation

IV.3 Cost analysis

To evaluate the commercial feasibility of the superconducting actuator the costs are evaluated for a 40 cm stroke actuator.

The permanent magnet actuator has 14 magnets on each side. The total volume of 28 magnets would be $3.36 * 10^{-3}$ m^3. The mass density of 7007 kg/m^3 and a price of 150 \$/kg is assumed for Neodymium magnets. Consequently the material cost of two of such permanent plates would be around \$3500.

The total cost including processing of the double sided permanent magnet stators is assumed to be \$4000.

In total 16 racetrack coils are used for the superconducting actuator. The total volume of these racetrack coils is $4.97 * 10^{-3}$ m^3.

For the YBCO wire the AP wire of SuperPower is used. The price for this wire is roughly 120 \$/m. As the wire has a cross section of $2.42 * 10^{-6}$ m^3 the cost can also be expressed as $4.96 * 10^{7}$ \$/m^3.

For the MgB_2 wire a wire of HyperTech is used. The price for this wire is roughly 9 \$/m. The cross section of this wire is $0.81{*}10^{-6}$ m^3. Expressing the cost in respect to volume results in a wire cost of $1.11{*}10^{7}$ \$/m^3.

Additionally for the superconducting actuators two AL325 cryorefrigerator of CryoMech are used which cost about \$45,000 each.

The material costs of the stator and the cryorefrigerators are shown in Table 5. Additionally the cost per N/kg is shown.

	PM	**YBCO**	**MgB_2**
Electromechanical			
B_a (T)	0.66	6.1	2.4
kN/kg	1.665	13.15	5.27
Cost estimate			
Material (\$)	3500	246,000	55,200
Cooling (\$)	-	90,000	90,000
Total (\$)	4000	336,000	145,200
\$/(N/kg)	2.4	25.6	27.6

Table 5: Cost estimate of PM and SC actuators

V. Conclusions and recommendations

This paper presented a method to approximate the achievable fields for any temperature, material and coil.

Moreover, this method was used to design a superconducting racetrack coil. The coil has a diameter of 100 mm, an inner radius of 10 mm and a length of 20 mm.

The designed racetrack coil was employed in a superconducting synchronous actuator. Using YBCO wire, the double sided design generated a magnetic field of 6.1 T at the armature (with a safety factor of 90%). Additionally the THD of the magnetic field at the armature and consequently the force ripple is strongly reduced by employing these superconducting coils.

The force density (N/kg) generated by the superconducting actuator is 8 times higher than that of the permanent magnet actuator. However the price per N/kg is also about 10 times higher.

A cryostat was designed for the superconducting actuator. This cryostat showed the thermal feasibility of the actuator as the heat load is slightly lower than the cooling power.

Concluding, the superconducting linear actuator can be feasible. Superconducting coils have the ability significantly increase the magnetic field at the armature and the force density. However in practice superconductors are to expensive for most applications. Superconductors are most suited for niche applications where performance demand is high and the cost of the magnets is less important.

More elaborate explanations of the equations and the methods used can be found in [8]. Readers interested in the achievable fields of other materials and at other temperatures are also recommended to read the thesis.

For future research a couple of recommendations are given. First, it is recommended to analyze the AC behavior of superconductors. Second, thorough thermal and mechanical analysis is recommended to optimize the heat load of the cryostat. Third, dynamic analysis of the actuator is recommended to assess the validity of the safety factor. Last, the acquirement of experimental proof is recommended before the production of an actuator.

To conclude this paper it is emphasized that developments in superconducting materials are fast paced. Higher current densities and cheaper wires are achieved on a yearly basis. As time progresses cheaper superconducting actuators with higher performance will be possible.

References

[1] SuperPower inc , *Field dependence of Ic at 20 - 65K 2011 SuperPower AP wire*. University of Houston, 2011.

[2] SuperPower inc , *SuperPower 2G HTS Wire Specifications*. SuperPower inc, New York, 2012.

[3] SuperPower inc , *Insulated 2G HTS Wire*. SuperPower inc, New York, 2012.

[4] D.K. Park , *MgB_2 for MRI Magnets: Test Coils and Superconducting Joints Results*. IEEE Transactions on applied superconductivity Vol. 22 No. 3, 2012.

[5] G.Z. Li , *Critical Current Density and Current Transfer Length of Multifilamentary MgB_2 Strands of Various Design*. IEEE Transactions on applied superconductivity Vol. 22 No. 3, 2012.

[6] Z.Q. Ma and Y.C. Liu , *Low-temperature synthesis of MgB2 superconductors*. International Materials Reviews Vol. 56 No. 5/6, 2011.

[7] C. Hauviller , *Design rules for vacuum chambers*. CERN, Geneva, 2005.

[8] N.H. van der Blij, *Feasibility Study of a Superconducting Linear Actuator*. TU Delft, May 2013.